ADVANCED OPTICAL MATERIALS
www.advopticalmat.de

Recent Advances in PDMS Optical Waveguides: Properties, Fabrication, and Applications

Camila A. Zimmermann, Koffi N. Amouzou, and Bora Ung**

Poly(dimethylsiloxane) (PDMS) has emerged as a promising polymer for fabricating optical waveguides. Its optical transparency, stretchability, flexibility, biocompatibility, and facile processing are a complement to common optical materials that are more brittle and stiff such as fused silica, polystyrene (PS), and poly(methyl methacrylate) (PMMA). Although PDMS is not a new material, with its first synthesis dating back to the early twentieth century, recent decades have seen an increased effort to expand its use in optical waveguides beyond conventional rubber applications. This review compiles established concepts and new advancements in PDMS science to shed light on limitations and new opportunities to better harness PDMS' potential for optical waveguiding. With the materials science tetrahedron in mind (structure, properties, processing, and performance), this review explores the state-of-the-art in PDMS waveguide technology and exposes relevant basic concepts pertaining to its physicochemical properties. The goal is to equip the photonics community with knowledge to further expand PDMS waveguide technology. The review covers three main topics: PDMS' key properties (chemical, optical, thermal, and mechanical, besides biological and environmental aspects); PDMS waveguide fabrication techniques (processing, refractive index tuning, and post-processing); and its applications. The review concludes with a discussion of current challenges and future prospects.

1. Introduction

The optical waveguide market has been valued at USD 8.41 billion in 2019 and is expected to grow at a compound annual growth rate of 6.7% until 2027.[1] Despite silica-based optical waveguides making up 32.7% of this market in 2019, polymer optical waveguides (POWGs) are also considered an important material platform for the fabrication of integrated optoelectronic circuits.[1] According to the Integrated Photonic Systems Roadmap – International (IPSR-I) program on polymer materials, the commercialization of POWGs is expected to continuously grow and gradually displace existing glass, semiconductor and board-based technologies over the next decade.[2] POWGs, prepared from optically transparent polymers, have gained great interest over the years since they combine the advantages of optical signal processing such as fast response time, good sensitivity, reliability, and a set of desired material properties. They are lightweight, cheap, easy to shape, and depending on the choice of the polymer may present high stretchability, flexibility, and biocompatibility. All important features for applications in wearable devices for motion detection,[3–7] healthcare monitoring,[8–10] soft robotic actuation,[11] therapeutical light delivery,[12,13] and data communication,[14] to cite a few.

In sensing applications, for example, the typical stretchable sensors based on changes in electrical response profit from well-known materials and sensing mechanisms. On the other hand, they require complex manufacturing processes in an attempt to combine materials with dissimilar properties. They are also sensitive to electromagnetic interference and may be considered an electrical hazard due to current leakage. Moreover, the range of stretchability and flexibility is often limited by the integrity of the electrical circuit.[11,15] In this sense, optical signals are not limited by the integrity of a conductive path, which can also be dramatically disrupted by corrosion or a dynamic regime such as body motion. Although traditional silica optical fibers offer lower light attenuation compared to polymer alternatives,[16,17] they require very high processing temperatures (approx. 2000 °C),[18] and are not biocompatible.[19] Their stiffness and brittleness make them incompatible with long-term applications that involve a wide range of mechanical deformation and hinder their use in biomedical applications, be it attached to the skin or implanted in the body. The mechanical incompatibility of silica fibers with biological tissues may cause severe reactions and have unfortunate consequences on breakage causing unwanted tissue damage as this material is neither resorbable nor easy to recover by explantation.[19–21]

C. A. Zimmermann, K. N. Amouzou, B. Ung
Department of Electrical Engineering
École de Technologie Supérieure
Université du Québec
1100 Notre-Dame Street West, Montreal, QC H3C 1K3, Canada
E-mail: camila-aparecida.zimmermann.1@ens.etsmtl.ca; bora.ung@etsmtl.ca

The ORCID identification number(s) for the author(s) of this article can be found under https://doi.org/10.1002/adom.202401975

DOI: 10.1002/adom.202401975

Polystyrene (PS) and poly(methyl methacrylate) (PMMA) are prominent polymeric materials employed in the fabrication of optical waveguides, thanks to their high availability, cost-effectiveness, and optical transparency.[17,22,23] As thermoplastics, PS and PMMA optical fibers can be readily produced via industrial melt processing techniques, such as extrusion and thermal drawing, at processing temperatures ranging from 180 to 260 °C.[17,23] Room-temperature processing of these polymers requires the use of harsh solvents like toluene. Despite their lower stiffness (elastic modulus) of 2.2–3.3 GPa compared to silica fiber counterparts (73 GPa),[24] PS and PMMA fibers still demonstrate insufficient stretchability with elongation at break between 1.2–2.5% and 2.0–5.5%,[24] respectively, for applications involving cyclic loading and large strains, thereby limiting their potential in such contexts.[16,22] In this sense, poly(dimethylsiloxane) (PDMS) has been considered a very promising candidate. PDMS-based optical waveguides can overcome most of the drawbacks mentioned above. As a thermoset, its fabrication is possible at room temperature, and curing at higher temperatures, when needed, does not exceed 200 °C. The stretchability and flexibility provided by PDMS give the waveguides the ability to conform well to different geometrical surfaces and soft tissues, and withstand repeated strain regimes, i.e., mechanical compliance, without mechanical failure. It has been successfully implanted in vivo showing good biocompatibility.[25] Additionally, this organo-inorganic polymer combines a set of attractive properties such as high optical transparency, good thermal and chemical stability, and tunable optical and mechanical properties, that will be revisited in this text. In this context, the purpose of this review paper is to provide a summary of the fundamental properties of PDMS as well as the most recent advances in PDMS optical waveguides for the photonics and optical sensing communities. This review focuses on crosslinked PDMS rather than its liquid form. It is divided into three major sections: properties, fabrication, and applications. The first section of this review summarizes several important properties of PDMS that make it suitable for use as an optical waveguide. The second item discusses PDMS waveguide fabrication techniques, refractive index tuning methods, and post-modification treatments. The third one focuses on recent advances in practical applications. Finally, a discussion of current challenges and future outlook concludes this review.

2. PDMS Definition and Relevant Material Properties

PDMS has grown in importance in a variety of fields. The crosslinked material, with its rubber-like behavior and optical transparency, has also found a place in optical waveguiding. Among the many interesting properties of crosslinked PDMS, this section covers the chemical, optical, thermal, and mechanical properties, as well as some biological and environmental safety aspects that we believe are critical for adequate material selection and understanding its performance.

2.1. Chemical Structure and Properties

PDMS belongs to the class of polysiloxanes, also known as silicone rubbers, whose polymer backbone is formed by siloxane bonds (Si–O–Si).[26,27] For PDMS synthesis, dating back to a century ago, first silica is reduced to silicon which is then used to prepare dimethyldichlorosilane. The hydrolysis of dimethyldichlorosilane in the presence of excess water yields very short cyclic and linear chains (oligomers). The two chemical routes employed for polymerization and manufacture of PDMS are: 1) condensation of linear chains in the presence of acids or bases, and 2) ring-opening of cyclic siloxanes in the presence of ionic initiators. Details on the polymerization reactions and other polymerization routes can be found elsewhere.[26,28–30]

Non-crosslinked PDMS is usually found in liquid or paste forms. To be used as an elastomeric waveguide, PDMS undergoes a crosslinking reaction, i.e., curing, so that the polymer chains are irreversibly linked to each other by covalent bonds. The crosslinking reactions vary depending on the functional groups present in the molecular structure of the prepolymer (i.e., partially polymerized PDMS). Sylgard 184 (Dow Chemical), for instance, is a well-known commercial PDMS formulation that has been extensively studied. This product is typically supplied as a two-part transparent fluid that undergoes an addition-cure reaction. The so-called base (part A) is composed of a siloxane prepolymer possessing vinyl end groups (–CH=CH_2) and a platinum-based catalyst (Pt). The curing agent (part B) is a hydrosiloxane copolymer containing Si–H groups that react with the vinyl groups present in part A resulting in a three-dimensional polymer network.[31–33] The chemical reaction between the two components is depicted in **Figure 1** along with a schematic representation of the molecular structures and the crosslinked network.

The crosslinking reaction shown in Figure 1 happens at room temperature and can be accelerated by heat. Deviations from the ideal base-to-curing agent ratio (stoichiometry) in a formulation can lead to incomplete crosslinking, resulting in dangling polymer chains and an increased amount of non-crosslinked PDMS (sol fraction). This impacts the crosslink density, which, in turn, affects crosslink-density-dependent properties such as the elastic modulus,[33] as explained in more detail later. After curing, the extractable sol fraction has been experimentally determined to be less than 3 wt% reaching up to 30 wt% depending on the mixing ratio and curing mechanism.[34–42] Other crosslinking mechanisms include free-radical curing of vinyl-terminated PDMS with organic peroxides and condensation reactions of PDMS containing end-groups such as silanol (Si–OH) and acetoxy (–$OCOCH_3$). The curing process of acetoxy-terminated PDMS is controlled by the moisture content present in the environment and water diffusion through the material.[43] The generated by-products comprise volatile ketones, alcohols, and carboxylic acids like acetic acid.[28–30,43,44] Both peroxide and Pt-cured systems are prone to yellowing.[30,45] The addition-cure reaction has been preferred over other curing mechanisms due to the absence of by-products, negligible shrinkage, and better control of the curing kinetics and network architecture.[26,28,29,44,46] Recent efforts in preparing thermoplastic and self-healing PDMS have also introduced the transesterification reactions and other innovative crosslinking routes.[38,47–50] Geniomer (Wacker Chemie), for example, are commercial PDMS-urea copolymers that render thermoplastic processability to PDMS.[51–54] One should note that the final choice of a PDMS formulation is not solely based on the curing mechanism but also on specific application requirements

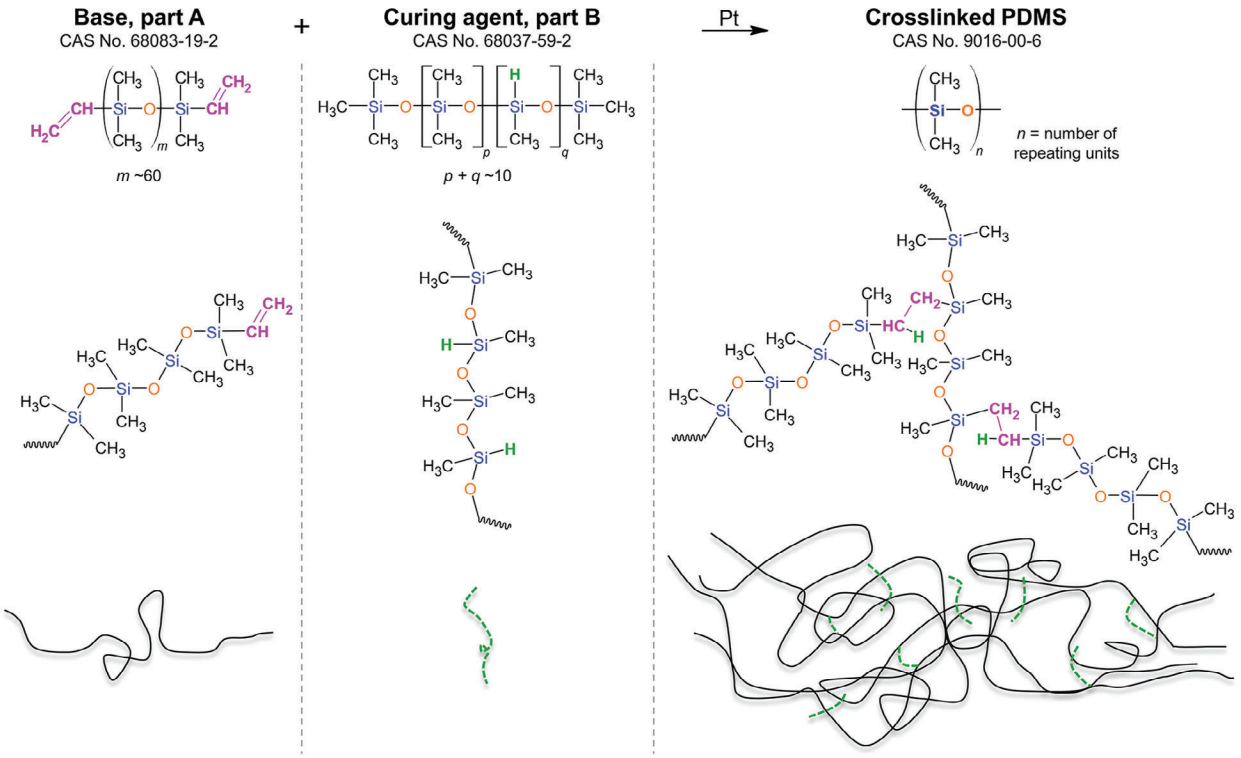

Figure 1. Chemical structure representation of (top) PDMS base prepolymer, curing agent copolymer, and the PDMS repeating unit, (middle) of the extended molecular structure of the components, and (bottom) a schematic drawing of the same components and the resulting polymer network.

such as faster curing, no yellowing, enhanced mechanical properties, etc.

The presence of certain chemical groups in the PDMS chemical structure plays an important role in waveguiding within the visible and infrared ranges as they can be a source of intrinsic absorption loss. **Figure** 2a presents the absorbance spectra of various commercial PDMS reported in the literature. Figure 2b shows the absorbance evolution with curing time of PDMS Sylgard 184 (Dow Corning, USA) prepared at a 10:1 weight ratio and cured at 21 ± 1 °C in the dark. Data were collected with a UV–vis spectrophotometer (Cary Bio-300, Variant) in quartz cuvettes (pathlength of 1 cm).

As depicted in Figure 2a, the PDMS absorbance spectra are very consistent, in the visible range, with no absorbance peaks. The vibration modes of the methyl side groups (–CH_3) and their overtones are the source of absorption in the near-infrared range, as shown in Figure 2a, and must be taken into account during light source selection.[14,56,57,60] Meanwhile, $\pi \rightarrow \pi^*$ and $n \rightarrow \pi^*$ electronic transitions characteristic of vinyl (or carbonyl groups in condensation curing reactions) are typically observed in the ultraviolet range. These electronic transitions can generate an extended tail in the blue part of the visible spectrum (Figure 2a,b), leading to considerable loss as light travels along longer distances.[45] Similarly, changing the mixing ratio between

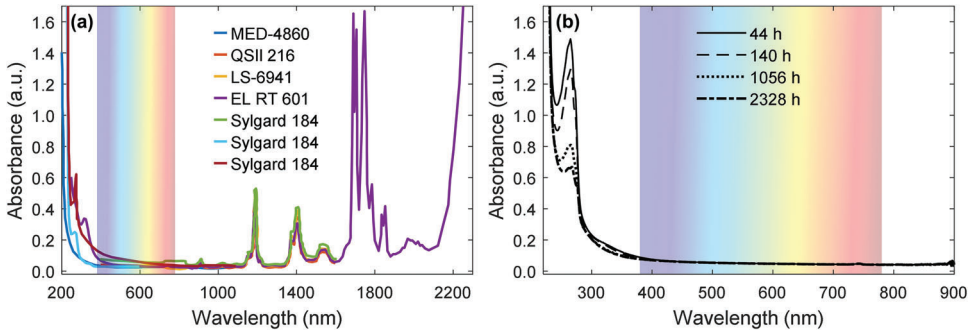

Figure 2. a) UV-NIR absorbance spectra of commercial Pt-cured PDMS: MED 4860 (NuSil),[55] QSil 216 (Quantum Silicones),[56] LS-6941 (NuSi),[56] Elastosil RT 601 (Wacker Chemie AG),[57] Sylgard 184 (Dow Corning),[56,58,59] respectively. b) UV–vis absorbance spectra evolution of PDMS 10:1 as a function of curing time at room temperature, 10 mm-thick. For reference, the visible range is highlighted in the background.

components and the catalyst concentration may result in additional attenuation as the content of reactive chemical groups is changed.[57–59] In this sense, Figure 2b shows that no significant changes in the PDMS absorbance spectra are observed in the visible range with time whereas the peak at 265 nm decreases as the curing process evolves and the concentration of vinyl groups decreases due to crosslinking.

Crosslinked PDMS is a hydrophobic polymer and insoluble in water. It presents a very low surface free energy (20.7–24 mN m^{-1}) and a static water contact angle larger than 92°, regardless of the mixing ratio.[61–65] Such surface properties are assigned to the nonpolar methyl side groups that arrange themselves around the polar Si–O backbone (Figure 1) and ensure its long-term stability in water and water-filming resistance.[26,28,63] Regarding its exposure to aqueous environments, its contact with a variety of diluted acidic and alkaline aqueous solutions has shown no significant swelling which allows PDMS waveguides to be used in these environments.[34] However, other components such as silica or salts may be part of PDMS composition greatly increasing its water uptake.[66,67] Moreover, PDMS is prone to dissolution in corrosive and concentrated mediums such as sulfuric acid, trifluoroacetic acid, hydrofluoric acid, dipropylamine, potassium hydroxide (KOH, 183 g L^{-1} at 55 °C), and tetrabutylammonium fluoride (TBAF) solutions.[34,62,68,69]

The mixing ratio between base and curing agent plays a role on PDMS chemical resistance to organic solvents. It is generally accepted that an increase in crosslink density is accompanied by a drop in the swelling ratio due to molecular mobility and free volume reduction as demonstrated by Ramli et al.[46] Notably, in another study it has been found that at a mixing ratio of 2:1, the swelling ratio in five different solvents was higher than at the manufacturer's recommended ratio of 10:1. The latter result was associated with the formation of a rigid and fragile material structure[61] that would suggest a lower crosslink density. Meanwhile, at 20:1 mixing ratio, PDMS presented the highest swelling ratio, when in contact with hexane and toluene.[61] In general, solvents with a total Hansen solubility parameter (δ) closer to the one of PDMS (between 15 and 16.9 $MPa^{1/2}$) and lower polar solubility parameter contributions, are better swelling agents either as liquids[34,61,70,71] or vapors.[72,73] The influence of raising the temperature on the swelling extent can vary depending on the solvent nature, increasing or decreasing it.[73] The swelling susceptibility of PDMS waveguides may limit their use in certain applications where dimensional stability is mandatory. Meanwhile, it can also be exploited as a sensing mechanism through changes in volume and optical properties, to detect and quantify organic solvents.[72,74–77] The incorporation of silica fillers can be used as a strategy to reduce PDMS swelling ratio.[78]

2.2. Optical Properties

PDMS has interesting optical properties so that it has been increasingly used in optical systems (adaptive lenses, tilting mirrors), sensing and photonics devices, microelectromechanical systems etc. PDMS is a transparent material with high transmittance (>90%) over a wide wavelength range beginning around 300 nm and extending up to 1100 nm in the NIR.[55,79,80] It retains its transparency even when filled with large amounts of silica fillers, which are commonly used to improve mechanical properties,[81,82] zirconium dioxide (ZrO_2),[83] or doped with germanium.[84,85] PDMS with temperature-dependent optical transparency has been fabricated by embedding paraffin and beeswax,[86,87] which may be an alternative to fine-tuning the sensitivity of PDMS waveguides to a specific temperature operating range. Additionally, PDMS has shown a glass-like autofluorescence response when excited with lasers in the visible range. The low autofluorescence signal makes it a potential candidate for use in laser-induced fluorescence sensing.[88]

Aside from the required refractive index (RI) contrast between the core and cladding for light-guiding by total internal reflection (TIR), the RI is a key property in the calculation of waveguide parameters such as numerical aperture, mode dispersion, and Fresnel losses. The dimensionless RI is the real part of the complex refractive index, $\eta^* = \eta + i\kappa$, whose imaginary component κ is the absorption index, also known as the extinction coefficient. The RI correlates with the chemical structure of polymers, more specifically with their molar polarizability and molar volume (i.e., material density). The polarizability of a molecule is the tendency of an electron cloud to form dipoles when it interacts with the electrical field of an electromagnetic wave (i.e., light). In that regard, mathematical models have been developed to estimate the RI value from the molar refraction group contribution.[89] Meanwhile, the extinction coefficient estimates the absorption loss during light propagation in a waveguide and can be obtained using a combination of ellipsometry and ray tracing methods.[90,91] **Figure 3** depicts the PDMS RI and extinction coefficient spectra in the visible and infrared ranges.

In the wavelength range of 400–2000 nm, the refractive index of PDMS is found to be between 1.45 and 1.37, as shown in Figure 3a which confirms its dispersive nature. Variations in RI of PDMS are to be expected between formulations from different brands, as well as when processing parameters such as curing agent amount or curing temperature are changed.[8,9,59,77,90–92] Section 3.2 goes into detail about how to tune the PDMS RI using the aforementioned strategies among others. In the infrared region, Figure 3b, PDMS RI ranges from 0.9 to 2, with anomalous dispersion regions around 3370 and from 6970 to 12710 nm, with minimum at 8940 nm and maximum at 12708 nm.[90] The anomalous dispersion typically occurs near vibrational and rotational resonance frequencies in the infrared and is characterized by a sharp RI variation with wavelength, as shown in Figure 3b. Because the phase velocity of light at such frequencies can be faster than the velocity of light in free space, it can result in values less than one.[93] In fact, the PDMS extinction coefficient spectra (Figure 3d) presented peaks of high intensity in the same infrared range, which have been assigned to the vibration modes of CH_3, Si–O–Si backbone, and Si–C whereas the extinction coefficient peaks in the near-infrared region (Figure 3c) have been attributed to various vibration modes of the methyl groups (CH_3).[57,90,91] Furthermore, chromatic dispersion in PDMS optical waveguides, resulting from the wavelength-dependent RI, is evident in reported modal propagation constants of −137 ps•nm^{-1}•km^{-1} at 850 nm and −47 ps•nm^{-1}•km^{-1} at 1300 nm.[45]

Figure 4 displays a comparative plot of propagation loss, primarily assessed using the cutback technique, for various PDMS formulations, including Sylgard 184 prepared under different

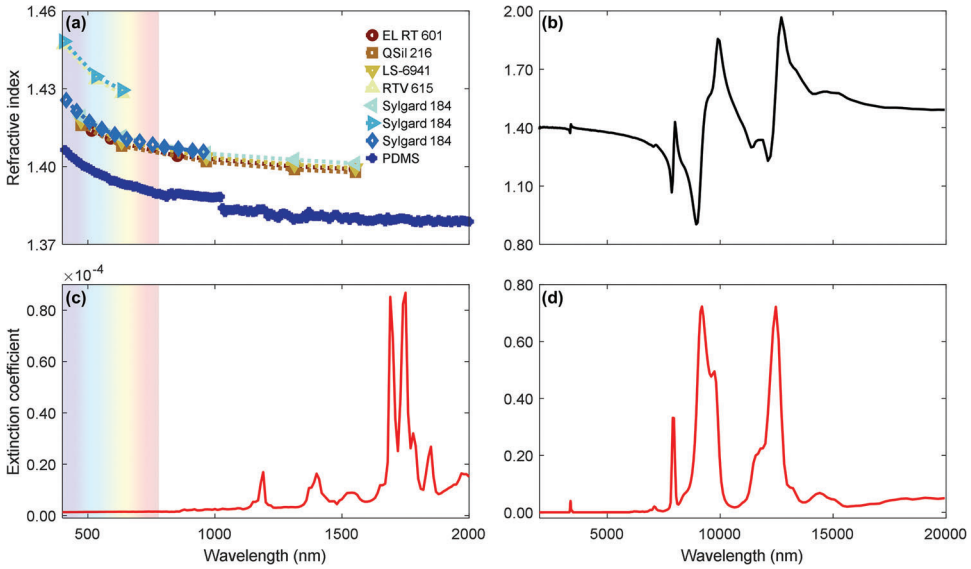

Figure 3. a) Plot of commercial PDMS refractive indices: Elastosil RT 601 (Wacker Chemie AG),[45] QSil 216 (Quantum Silicones),[56] LS-6941 (NuSil),[56] RTV 615 (GE Silicones),[77] Sylgard 184 (Dow Corning),[56,77,92] respectively, and PDMS (Dow Corning).[91] b–d) The refractive index and extinction coefficient plots of PDMS (Dow Corning) prepared at 10:1 Base-to-curing-agent ratio. Data extracted from ref. [90,91]. For reference, the visible range is highlighted in the background.

conditions, as well as UV-curable, phenyl-substituted, and thermoplastic PDMS formulations.

As shown in Figure 4, light attenuation in PDMS can vary widely in the visible range, where it's been mostly investigated, owing to different methodologies adopted for sample preparation and testing. Meanwhile, propagation losses in the NIR have yet to be measured. Although major trends are not clearly displayed in Figure 4, Sharma et al., for example, found a significant difference in light attenuation at 660 nm after curing PDMS 10:1 at 200 °C for 22 min vs 37 min at 125 °C (Figure 4, 2B). Changing the mixing ratio of Sylgard 184 away from the recommended 10:1 base-to-curing-agent ratio resulted in higher attenuation values (Figure 4, 2B vs 3B), and the standard deviation and thus, data variability, appeared to increase with the increase in the base-to-curing-agent ratio.[94] Partial or complete substitution of methyl groups in the PDMS backbone for other functional groups (Figure 4, conditions 5 and 6) have an effect not only on propagation losses but also on absorption losses.

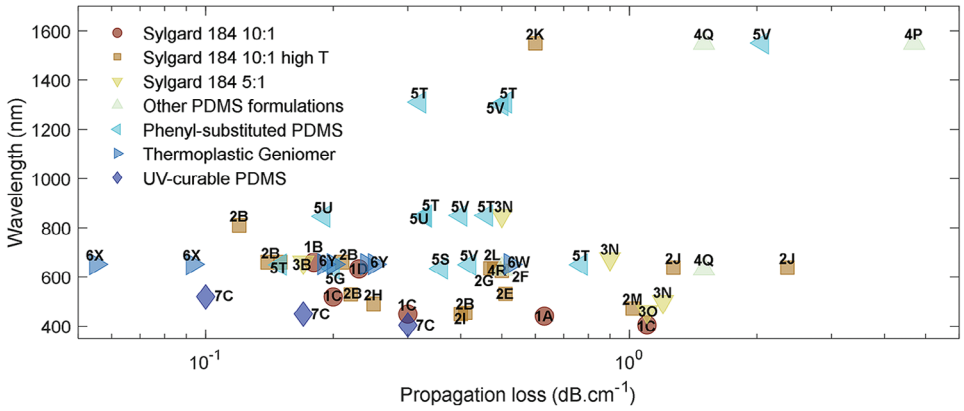

Figure 4. Plot of propagation loss for different wavelengths. Data points are identified by a combination of the category number and a corresponding letter from the reference. Category 1 PDMS Sylgard 184 prepared at 10:1 and cured at room or near-room temperatures (22–37 °C): A at 25 °C for 24 h,[6] B at 23 °C for 96 h,[94] C at 37 °C for 48 h,[95] D at 22 °C for 23 days.[96] Category 2 PDMS Sylgard 184 prepared at 10:1 and cured at high temperatures (60–280 °C): B at 75 °C for 2.5 h, 125 °C for 37 min, and 200°C for 22 min,[94] E at 80 °C for 40 min,[7] F at 75 °C for 45 min,[97] G at 80°C for 2 h,[98] H at 80°C for 2 h.[99] I at 150°C for 1 h.[100] J at 60°C for 4 h.[101] K at 70°C for 1 h,[84] L at 150°C for 2 h,[102] M at 280°C for 2 s.[20] Category 3 PDMS Sylgard 184 prepared at 5:1 and cured at high temperatures (65–125 °C): N at 80°C for 40 min,[8] B at 125 °C for 37 min,[94] O at 65 °C for 2 h.[92] Category 4 Other PDMS formulations: P Elastosil RT 601 (Wacker Chemie),[103] Q QSil 216 (Quantum Silicones),[104] R LS-6941 (NuSil).[105] Category 5 Phenyl-substituted PDMS: S OE-6550 (Dow Corning),[12] T LS-6943 (NuSil),[14] G OE-43 (Gelest),[98] U LS-6257 (NuSil),[106] V LS-6943 (NuSil).[107] Category 6 Thermoplastic Geniomer: W Geniomer 100 (Wacker),[52] X Geniomer 200 (Wacker),[53] and Y Geniomer 100, 175 and 100-HDS (Wacker).[51] Category 7 UV-curable PDMS: C KER-4690 (Shin-Etsu).[95]

For example, a decrease in absorption losses from 0.67 dB•cm^{-1} to 0.39 and 0.35 dB•cm^{-1} has been reported for phenyl and fluoro substituents at 1550 nm, respectively,[108] compared to non-substituted PDMS. On the contrary, the same substituents caused an increase from <0.01 to 0.22 and 0.05 dB cm^{-1} at 633 nm.[60,108]

With regard to thermal effects on optical properties, PDMS is known for showing a large decrease in RI as the temperature increases, with a negative thermo-optic coefficient ranging between -3.6×10^{-4} and -4.5×10^{-4} K^{-1}.[45,109] This feature has been used to devise optical fiber temperature sensors[109–111] and polarization-tunable filters[112] with outstanding performance. Furthermore, the RI of phenyl-substituted PDMS has been found to be remarkably stable after being subjected to test conditions that replicate typical printed circuit board (PCB) fabrication steps such as lamination, soldering, dry and damp heat, and thermal shock.[45] When tested using similar protocols, the insertion loss of PDMS waveguides ranged between 0.02 and 0.07 dB cm^{-1}.[45,113–115] It should be noted, however, that PDMS temperature stability is highly dependent on proper curing, as failure to do so results in a partially cured material that is more sensitive to post-processing steps involving high temperatures.

Mechanical strain can cause the PDMS dipole density to change locally, affecting the RI and other optical properties. In this regard, Park et al. evaluated the optical and mechanical properties of thin PDMS films (10–70 µm) on glass when subjected to flat-punched indentation using experimental data and a finite element simulation.[116] The authors discovered that the RI of PDMS films increased with increasing load, with a significant difference between the bulk and bottom surface values due to variations in the material's local density. The bulk RI was estimated to reach 1.476, whereas the bottom surface reached only 1.435 due to stress-strain distribution through the film. They also found that the thinner the film, the more the RI becomes sensitive to mechanical stress. In another study involving compressive forces, the effect of compression up to a relative strain of −0.5 showed that PDMS RI reached 0.5 at 1500 nm, while the transmittance at 1700 nm decreased by a factor of three.[117] On the other hand, a negligible RI change (400 to 850 nm) for strains up to 50% has been reported for PDMS films under tensile forces.[118] Such stress-induced variations in RI must be considered when designing waveguides that will be subjected to compressive forces and exploited in the development of strain sensors. Although crosslinked PDMS is considered an isotropic material, under mechanical stress, its RI can change for perpendicular and parallel-polarized light, which is known as stress- or strain-induced birefringence. Theoretically, the stress-optical coefficient (C_σ) for uniaxial tension in elastomers can be directly expressed by the ratio between birefringence and the retractive stress, $C_\sigma = \Delta\eta/\sigma$. The stress-optical coefficient is considered independent of the crosslinking density, slightly dependent on temperature,[89] and varies nonlinearly in bimodal PDMS networks as a function of the short-chain fraction.[119] In compression and tension, PDMS optical birefringence has been measured in the order of 10^{-5} to 10^{-4} in the visible and NIR ranges.[117,119–122] In tensile tests, reported C_σ values range from 0.77×10^{-4} MPa^{-1} to 2.65×10^{-4} MPa^{-1},[70,89,119,121] which can be used in the development of displacement sensors.

2.3. Thermal Properties

Knowing the transition temperatures is key for PDMS optical waveguide design and for long-term material stability. The glass transition temperature (T_g) is defined as the temperature at which a material cools from the melt going from a rubbery to a hardened glassy behavior while the amorphous molecular arrangement of the liquid state is preserved. Melting and crystallization temperatures, T_m and T_c, respectively, are related to polymers whose chains can rearrange themselves in crystalline domains. T_m is the temperature at which the crystalline domains melt upon heating, whereas T_c is the temperature at which crystals are formed upon cooling.[24] These temperatures are typically a range rather than a discrete value. They are influenced by many factors, including polymer molar mass, presence of fillers or impurities, testing methods, thermal history, crosslinking degree, and so on, as depicted in **Figure 5a**.[24,46,123–126] With regard to PDMS, the highly flexible siloxane backbone, relatively weak intermolecular interactions, and small size of the methyl groups result in very low transition temperatures (Figure 5a). Average values of neat crosslinked PDMS are found close to −120 °C for T_g while T_m and T_c are ≈−45 °C and −90 °C, respectively.[123,124,127–129] At room temperature, crosslinked PDMS is essentially amorphous with some semi-crystalline domains. Therefore, PDMS has no stable crystals to act as scattering centers during optical waveguiding.[129,130] Depending on their chemical nature, composition, and concentration, certain metal alkoxides can elevate the glass transition temperature (T_g) to higher, yet still sub-ambient, levels.[128,129] Fumed silica (FS),[123] nanosilica[124] and carbon nanofibers (CF)[131] appear to have little effect on T_m as well as other fillers that weakly interact with PDMS. Meanwhile, crosslink nature and density may shift T_m by up to 20 °C.[127]

The energy required to break apart a siloxane bond is estimated at 444 kJ mol^{-1}, whereas the carbon-carbon bond energy, typical of organic polymer backbones, is about 346 kJ mol^{-1}.[135] As a result, crosslinked PDMS presents negligible weight loss (<0.4%) below 200 °C and no significant variation in the thermogravimetric behavior up to 150 °C when prepared at varied crosslinking degrees under either inert (i.e., He, Ar, or N_2) or oxidative (e.g., O_2 and air) atmospheres, Figure 5b.[32,35,46,129,132,133,135–137] If the temperature is further increased up to 900 °C, a series of decomposition reactions take place, yielding a ceramic material in the absence of oxygen or, otherwise, char.[32,137,138] The thermal degradation products include silicon-based oligomers and cyclic species, formaldehyde, water, hydrogen, methane, ethylene, and carbon monoxide.[32,35,126,135,138] Interestingly, above 150 °C in an inert atmosphere, a lower mass loss has been observed at a 10:1 base-to-curing-agent volume ratio than at increased amounts of curing agent, Figure 5b. This thermal behavior was explained by the lower thermal stability of the curing agent compared to the base still present after curing for a few days.[32]

Based on the aforementioned transition temperatures and the thermal stability data for crosslinked PDMS, it is expected that PDMS waveguides will remain operational over a wide temperature range, i.e., −45 °C < T < 150 °C. It is noteworthy that these values are related to pristine PDMS. The presence of impurities[125,126] and fillers[134,137] may dislocate the onset of thermal degradation as well as the transition temperatures

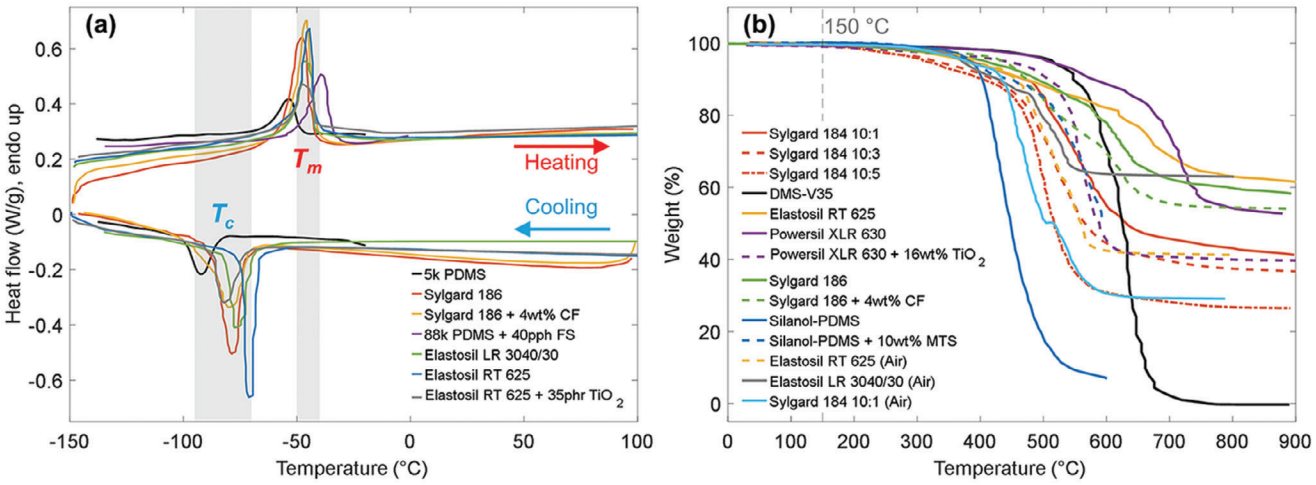

Figure 5. a) Differential scanning calorimetry thermogram of various crosslinked PDMS: 5k PDMS (5000 g•mol^{-1} end-linked PDMS, United Chemical Technologies), heating and cooling rates of 5 K•min^{-1} in N_2.[127] Sylgard 186 (Dow Corning) and Sylgard 186 + 4wt% CF (Carbon nanofibers PR-19-XT-PS, Pyrograf Products), at 10 K min^{-1} in N_2.[131] 88k PDMS (87 600 g•mol^{-1}, Dow Corning) + 40 pph FS (Fumed silica Aerosil R972, Degussa), at 10 K•min^{-1} N_2.[123] Elastosil LR 3040/30 and Elastosil RT 625 (Both from Wacker Chemie) and Elastosil RT 625 + 35 phr TiO_2 (R420, Sachtleben Chemie), at 10 K•min^{-1} in air.[132] For reference, the T_m (−50 to −40 °C) and T_c (−95 to −70 °C) ranges are highlighted in gray. b) Thermogravimetric analysis (TGA) thermograms: Sylgard 184 (Dow Corning) at Base-to-curing-agent ratios of 10:1, 10:3, and 10:5 at 10 K min^{-1} in argon.[32] DMS-V35 (Gelest Inc.), Elastosil RT 625 and Powersil XLR 630 (Both from Wacker Chemie), Powersil XLR 630 + 16 wt% TiO_2 (Hombitec RM130F, Sachtleben Chemie), at 5 K•min^{-1} in N_2.[133] Sylgard 186 and Sylgard 186 + 4wt% CF, at 10 K•min^{-1} in N_2.[131] Silanol-terminated PDMS (18 000 g•mol^{-1}, United Chemical Technologies), at 10 K•min^{-1} in N_2.[134] Elastosil RT 625 and Elastosil LR 3040/30, at 10 K min^{-1} in air.[132] Sylgard 184 at 10:1 mixing ratio, at 10 K•min^{-1} in air.[129] Reference dashed gray line at 150 °C.

to lower or higher values. Moreover, when PDMS is exposed to high temperatures for extended periods, especially above 90 °C for hundreds of hours, the mechanical properties can degrade due to thermal oxidation.[139] The low thermal conductivity (between 0.18 and 0.64 W m^{-1} K^{-1}) of PDMS combined with a high coefficient of thermal expansion (ranging from 210 to 330 µm m^{-1} K^{-1})[131,140–142] cannot be disregarded in applications that require high heat dissipation and dimensional stability. For comparison, the thermal conductivity and the coefficient of thermal expansion of fused silica (SiO_2), which is used to fabricate silica optical fibers, are close to 1.4 W m^{-1} K^{-1} and 0.4 µm m^{-1} K^{-1}, respectively.[24,143] PDMS thermal expansion can be minimized by increasing the curing temperature[141] or adding fillers such as silica nanoparticles[80] and carbon nanofibers.[131] A reduction in optical transparency may be expected in the latter case. For instance, 5% and 20 wt% of added silica fillers reduced transmittance by 10% and 70%, respectively.[80]

Recently, the thermal stability of a benzophenone-doped PDMS waveguide prepared at a mixing ratio of 20:1 has been investigated. The waveguide presented good thermomechanical stability over five transverse compression cycles (loading of 150 mm Hg) at room temperature and at 38 °C, demonstrating its feasibility for optical pressure sensing applications.[9] In another study, no significant changes in the normalized optical transmission of air-clad PDMS waveguides were detected from 30 to 45 °C.[94] Further, a linear increase in optical loss of 0.22 ± 0.01 dB m^{-1} °C^{-1} was reported for air-clad PDMS waveguides tested from room temperature (i.e., 23 °C) to 70 °C. This temperature-dependent loss was ascribed to the PDMS' thermo-optic coefficient and a mismatch in thermo-mechanical properties of the materials at the input/output connecting points.[96]

2.4. Mechanical Properties

Mechanical properties are equally important in selecting a material that is well aligned with in-service performance requirements in order to avoid premature failure due to fatigue, safety issues, or to promote appropriate cell growth.[144,145] For PDMS waveguides, this means knowing the maximum strength, stiffness, and mechanical compliance to dynamic loading regimes at various conditions, as well as other mechanical responses. **Table 1** displays selected PDMS mechanical properties, with Sylgard 184 (Dow Corning) serving as the main PDMS representative. For the most extensively researched properties, the typical, lowest, and highest values are displayed. The information in Table 1 is not exhaustive because the versatility of PDMS allows the preparation of waveguides with a wide range of mechanical properties, from brittle to hyperplastic.[64] Furthermore, by combining the appropriate fillers, curing conditions, mixing ratio, and crosslinking chemistry, these properties can be tailored for a wide range of applications.

Because of its rubber-like mechanical behavior above T_g, crosslinked PDMS is often referred to as rubber or elastomer. For temperatures below T_g, PDMS stiffens, with increased hardness and compressive strength,[142] and no longer behaves like an elastomer. An elastomer is defined as a polymer that can deform reversibly when subjected to mechanical force so as to return to its original shape and dimensions.[31] The same characteristics responsible for the very low transition temperatures, namely a flexible backbone, weak intermolecular forces, and small side groups, explain the PDMS elastic response to mechanical strain. The longer Si–O bond length and Si–O–Si bond angle of 1.64 Å and 143°, respectively, shown in **Figure 6**,

Table 1. Mechanical properties of crosslinked PDMS.

Mechanical property	Range of response	Refs.
Tensile strength at break [MPa]	Typical values: 1–5	[8,39,41,62,77, 131,146–149]
	Lowest: 0.082	[82]
	Highest: ≈10–13	[62,64,94,150]
Elongation at break [%]	Typical values: 100–200	[6,8,9,37,39,77,78,82, 94,144,148,149, 151–155]
	Lowest: 20	[64]
	Highest: 1864	[41]
Tensile modulus of elasticity [MPa]	Typical values: 1–3	[8,39,41,59,64,77,80, 94,131,144,147,149, 152,154–162]
	Lowest: 0.02	[37,41]
	Highest: ≈16	[44]
Shear modulus [MPa]	0.25–0.60	[59,147,158,163]
Compressive strength at break [MPa]	≈3–83	[144,147,164,165]
Compression at break [%]	≈55–94	[144,164,166]
Compressive modulus of elasticity [MPa]	0.17–4	[59,144,164–169]
Poisson's ratio (dimensionless)	≈0.5	[64,141,170]
Hardness (Shore A)	Typical values: 20–60	[41,46,131,140,142, 146,147,154]
	Lowest: ≈2.5	[41]
	Highest: 73	[44,151]
Tear strength [kN m^{-1}]	0.1–80	[41,151,171–173]
Impact strength [J m^{-1}]	21.2–461 (Bimodal networks)	[40]

account for the PDMS chains' remarkable flexibility, with rotation energy around a $(CH_3)_2Si–O$ bond of 3.3 kJ mol^{-1}. In comparison, the typical C–C bonds found in many polymers' backbones have a bond length of 1.54 Å with an angle of ≈110° and a rotation energy around a $H_2C–CH_2$ bond of 13.8 kJ mol^{-1}.[26,28] As a result, the compact random molecular coils can easily rotate and gradually adopt more linear conformations under tensile strain, as shown in Figure 6 (right). The full extension of the polymer chains denotes the elastic response limit (Figure 6, blue dashed line). At higher strains, molecular entanglement, complex network chain relaxation, and a limited free volume produce non-linear viscoelastic behavior that differs from the ideal linear elastic response observed in a stress-strain plot.[174] When the applied strain force is removed, the extended chains spontaneously revert to their higher entropic state. Crosslinks are essential in this process in order to avoid chain slippage, which leads to irreversible plastic deformation.[24,174] The three mechanical properties most commonly reported for PDMS are elongation at break, tensile strength at break, and modulus of elasticity, as illustrated in Figure 6 (left). Table S1 (Supporting Information) contains additional tensile test results.

The tensile strength at break is sometimes referred to as ultimate strength or the maximum tensile strength. One should note, however, that ultimate strength is the maximum stress observed in a stress-strain curve and even though both terms generally coincide in elastomers, ultimate strength is not necessarily related to the fracture point. The modulus of elasticity, also known as Young's modulus, elastic modulus or stiffness, is the slope calculated in the linear region of a stress-strain curve, Figure 6. PDMS, like many other elastomers, often does not present a clearly identifiable linear regime because the modulus of elasticity varies with strain. In such cases, alternatively, the secant modulus is used. It is taken as the slope of a secant between the origin and any point arbitrarily chosen on the stress-strain curve and reported together with the chosen stress or strain, for example at 100% (ϵ_{100}).[24,175] Equivalent properties can also be measured in compression mode. The results depend on testing temperature, sample preparation and crosslinking chemistry which will be discussed in the following paragraphs. PDMS exhibits minimal sensitivity to strain rate, demonstrating a negligible effect on its mechanical properties in both tension and compression.[155,158] Studies have shown a variation in elastic modulus of around 2% with strain rate from 0.0025 to 0.1 s^{-1}[149] and even when the strain rate increases by a factor of 100, from 0.003 to 0.333 s^{-1}, the average variation in elastic modulus remains a modest 10%.[159]

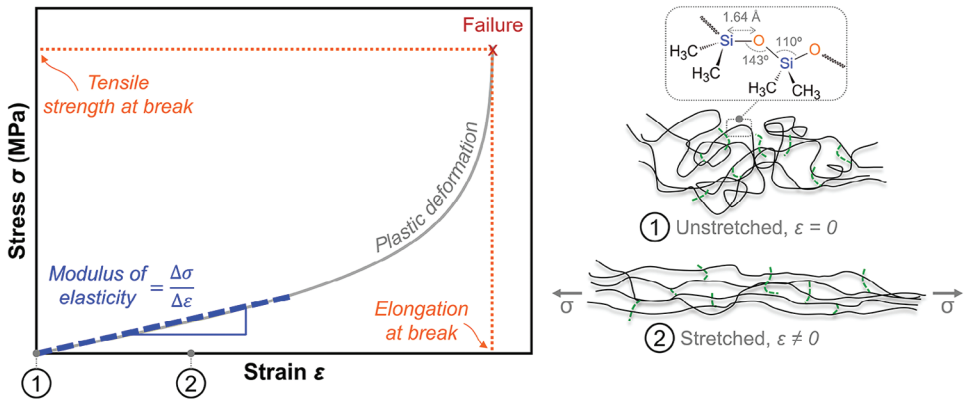

Figure 6. Representative stress-strain plot for PDMS (left) and schematic representation of crosslinked PDMS chains at an initial coiled unstressed state and at an elongated state during elastic deformation (right).

To demonstrate the effect of crosslinking chemistry on the mechanical properties, peroxide-cured PDMS has been compared to a PDMS cured by platinum-addition crosslinking mechanism, both cured under the same curing parameters.[44] The former has shown higher elongation at break, modulus of elasticity, and hardness.[44,151] Residual peroxide, however, can be activated during processes that involve heat, such as sterilization cycles (e.g., 120 °C for 30 min) or thermal aging, leading to a degradation of some mechanical properties and inferior long-term stability compared to addition-cured systems.[44,151] Additionally, other studies involving different PDMS curing systems[37] and from different manufacturers[41,149] have shown a wide range of mechanical responses. Changes in hardness[131] and in elastic modulus[160,176,177] of addition-cured PDMS have been observed with time or when the samples were subjected to thermal cycles, such as thermal aging[149] and autoclave sterilization.[62] For example, the mechanical properties of PDMS prepared at 10:1 aged over thousands of hours at room temperature tend to resemble the ones of samples freshly prepared at higher temperatures or curing times.[178] The rate of stiffness progression varies depending on the sample preparation and testing methodology used. For instance, Placet and Delobelle followed the evolution of PDMS mechanical properties for 6.8 years aged at room temperature using dynamic mechanical analysis, nano-indentation, and scanning micro-deformation.[178] Based on mathematical models developed to explain the evolution of the mechanical properties of PDMS with time, the authors estimated an increase between 40% and 50% in the elastic modulus for an infinite aging time. Hoft et al. reported an increase in elastic modulus from 0.98 MPa at day 0 to 1.2 MPa after 26 days and ≈2.2 MPa on day 470, which was associated with the progression of the crosslink over time, increasing the chain density. Stiffness increased at a faster rate for the first five days, then slowed but showed no signs of stabilization after four weeks, when it reached stress levels approximately 25% higher.[158]

The parameters involved in sample preparation, i.e., mixing ratio, curing time, and temperature, and their influence on PDMS mechanical performance have been heavily researched subjects in addition-cured systems. Changing the mixing ratio is a common strategy to modify PDMS properties that are dependent on the network structure and crosslinking degree.[33] For Sylgard 184, certain mechanical properties (e.g., elastic modulus, tensile strength at break) exhibit a nonlinear relationship with curing agent concentration. These properties typically reach a peak when the recommended 10:1 base-to-curing agent ratio is slightly exceeded before declining, as observed in **Figure 7**a,b,d.[59,64,94,144,157,159,162,179] For example, Sylgard prepared at 6:1 and cured at 150 °C for 1.5 h, exhibited a decrease in elastic modulus of ≈30% compared to PDMS prepared at 10:1 and cured under the same conditions.[157] While a moderate excess of curing agent ensures most chains are connected at both ends,[180] deviating from the stoichiometric ratio, whether excess curing agent or base, can introduce imperfections like dangling and free chains into the 3D network[33] besides decreasing the crosslinking density.[94] This leads to complex mechanical behavior and explains the observed nonlinear relationship. Furthermore, tensile strength and elongation at break are not only intrinsic material properties but are also significantly influenced by fabrication conditions and imperfections like air bubbles, impurities, and improper curing.[33] For instance, elongation at break generally decreases with higher curing agent amounts,[94,144,148,154] although one study found a minimum at an 8:1 ratio followed by an increase at higher concentrations (Figure 7c).[64] A consistent reduction in elongation at break at increasing concentrations of curing agent was only observed after post-curing for 48 h at 165°C.[64] Tear strength[172] and hardness[46] of PDMS formulations other than Sylgard 184 appear to follow the increase in curing agent concentration. However, more research on the effect of mixing ratio on these properties is necessary. Stress softening has been observed when PDMS is prepared with an excess of curing agent (5:1), with hysteresis reduced or eliminated as the amount of base increases.[148,164] PDMS samples prepared at 5:1 and 10:1 mixing ratios exhibited similar performance when subjected to 100 cycles of compressive strain while the permanent set was higher and tended to stabilize faster than at mixing ratio of 15:1.[164]

The mechanical properties of PDMS are significantly influenced by the curing conditions. Specifically, elevated curing temperatures and prolonged curing times result in increased hardness and elastic modulus, accompanied by a decrease in elongation at break in tension.[59,147,157,177] Rheological measurements have demonstrated that higher curing temperatures yield stiffer PDMS, as evidenced by a shear modulus increase from 0.65 to 1.25 MPa when the curing temperature was raised from 65 to 150 °C.[42] Notably, the elastic modulus of freshly prepared samples cured at room temperature is among the lowest, regardless of the mixing ratio.[157] In this regard, adding a single thermal post-treatment step has shown to increase the elastic modulus,[44,64,132,156] besides ensuring a more complete cure,[44] and facilitate the removal of volatile compounds.[156] Optimal post-curing conditions, such as 165 °C, can result in an exceptionally high tensile strength at break (10 MPa at 10:1 mixing ratio).[64] Conversely, excessive curing agent (2:1 and 4:1)[64] or prolonged exposure to temperatures above 90 °C for hundreds of hours or above 200 °C for a couple of hours can lead to thermal degradation and compromised mechanical properties.[139,150] In compression, the influence of curing conditions on PDMS mechanical properties is sparse. In one case, the modulus of elasticity increased slightly,[59] whereas, in another, the elastic modulus and ultimate compressive strength reduced with increasing curing temperature.[147]

Above the T_m (−40 °C), PDMS exhibits an increased stress and elastic modulus with rising testing temperature,[149,183] which is considered a typical elastomer behavior.[24,184] The entropy contribution to the mechanical response explains the increase in elastic modulus and stress with temperature in PDMS. When stretched, the majority of the changes in length are caused by chains uncoiling rather than bond stretching, which represents a decrease in entropy. The chain motion becomes more chaotic, and the system tends towards a more random state. As a result, more force (larger stress) is required to achieve the same strain.[184] Below T_m, the elastic modulus decreases with rising temperature.[124] A permanent set of up to 20%, i.e., plastic deformation after stretching, has been reported depending on the testing temperature.[183]

The thickness of PDMS thin films significantly impacts their mechanical performance, which is a crucial consideration for designing planar, ridge, and other waveguide structures.

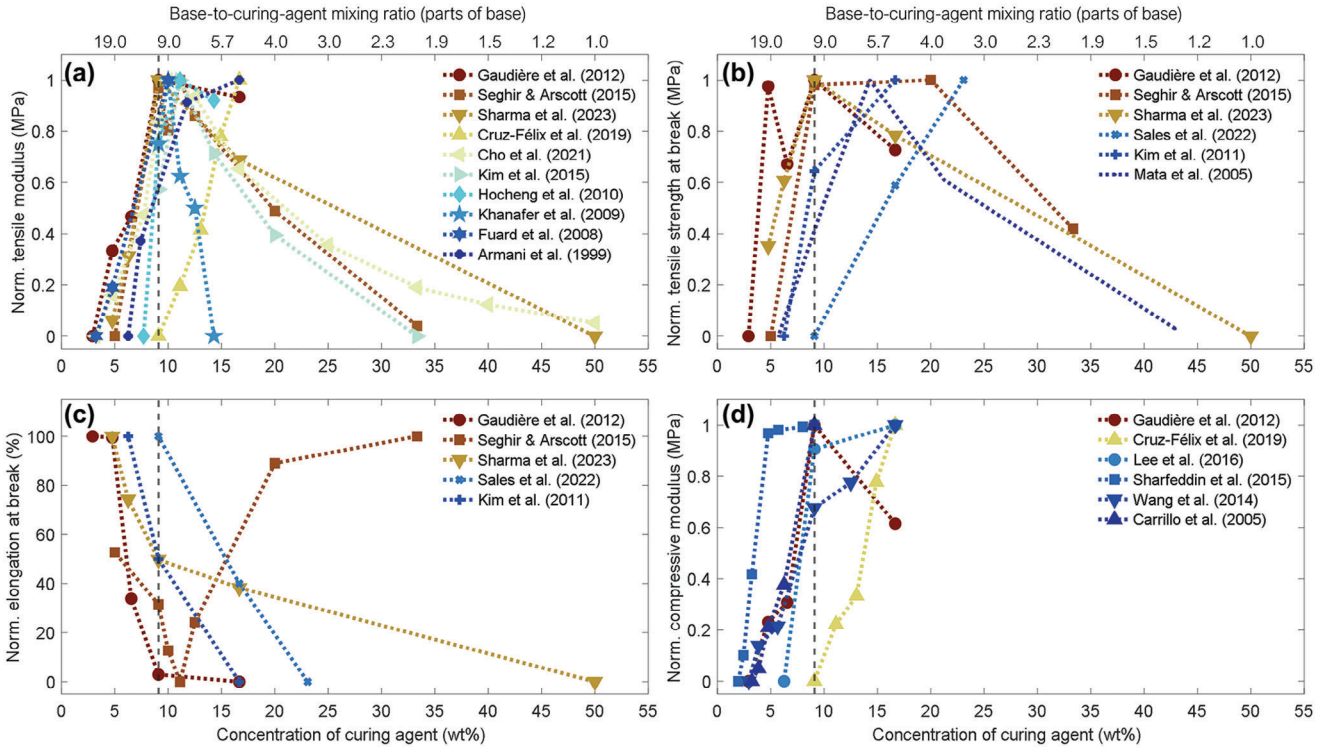

Figure 7. Plots of normalized a) tensile modulus of elasticity, b) tensile strength at break, c) elongation at break, and d) compressive modulus of elasticity as a function of weight concentration of curing agent (upper scale: base-to-curing-agent mixing ratio in parts of base per part of curing agent). Reference dashed gray line at 10:1 base-to-curing-agent ratio (9.1 wt% of curing agent). Lines are just a guide to the eye. Sylgard 184 (Dow Corning): Gaudière et al. (2012), cured at 65°C for 5 h, displacement rate of 5 mm•min^{-1},[144] Seghir & Arscott (2015), cured at 100°C for 2 h, displacement rate of 0.5 mm•s^{-1},[64] Sharma et al. (2023), cured at 125°C for 37 min, displacement rate of 100 mm•min^{-1},[94] Cruz-Félix et al. (2019), cured at 100°C for 30 min, displacement rate of 200 mm•min^{-1} and 0.08 mm•s^{-1}, for tensile and compression tests, respectively,[59] Cho et al. (2021), cured at 80°C for 2 h, displacement rate not informed,[162] Kim et al. (2015), cured at 60°C for 12 h, displacement rate of 1 mm•s^{-1},[179] Hocheng et al. (2010), cured at 85°C for 1 h, displacement rate of 4 mm•min^{-1},[157] Khanafer et al. (2009), cured at 65°C for 12 h, displacement rate of 5 mm•min^{-1},[159] Fuard et al. (2008), cured at 100°C for 3 days, displacement rate not informed,[177] Armani et al. (1999), cured at 90°C for 15 min, displacement rate not applicable,[181] Sales et al. (2022), cured at ≈25°C for 48 h, displacement rate of 500 mm•min^{-1},[154] Kim et al. (2011), curing conditions not informed, displacement rate of 1 mm•min^{-1},[148] Mata et al. (2005), cured at 100°C for 2 h, displacement rate not informed,[62] Lee et al. (2016), cured at room temperature for 48 h, displacement rate of 12 mm•min^{-1},[164] Sharfeddin et al. (2015), cured at 60 °C for 20–24 h, displacement rate not informed,[169] Wang et al. (2014), cured at 65°C for 1 h, displacement rate not applicable,[167] Carrillo et al. (2005), cured at room temperature for 2 weeks, displacement rate of 0.25 mm•s^{-1}.[182]

Notably, films with thicknesses below 200 µm exhibited a dramatic increase in elastic modulus and tensile strength at break, accompanied by a decrease in elongation at break, as thickness decreases.[152] In contrast, a separate study found that samples with thicknesses between 150 and 250 µm displayed a thickness-independent elastic modulus in monotonic tensile testing. However, after 20 tensile loading cycles, thicker samples showed a slightly higher elastic modulus, particularly at strain levels of 110 and 130% besides a permanent set of up to 13% in the first cycle.[161] Moreover, thinner films demonstrated a higher elastic modulus and pronounced strain hardening in compression,[116,185] and were more prone to mechanical ageing, exhibiting significant changes in modulus of elasticity over time.[176]

PDMS typically presents low tensile strength and an elongation at break rarely exceeding 200%, as shown in Table 1. In this sense, the incorporation of fillers, also known as compounding, has been used as a strategy to enhance PDMS mechanical strength and hardness while also reducing its stickiness for better handling.[28,131,186,187] Silica-based fillers are a commonly used approach to tailor and improve PDMS mechanical properties and can be found in commercial formulations such as Sylgard 184. The reinforcing effect has been explained by the interaction of silanol groups (Si–OH) found on silica particles' surface with the oxygen present in the PDMS backbone and silanol end-groups.[28,29,37] Increasing the silica concentration or its surface area tends to increase the tensile properties as more silanol groups become available.[187] Rajan et al.,[82] for example, prepared silica-filled PDMS nanocomposites by in situ generation of silica particles. The tensile strength at break went from 0.082 MPa for neat PDMS to values between 0.538 and 0.831 MPa, which represents an increase of at least 656%. The elongation at break increased in some cases and decreased in others, depending on the synthesis parameters.[82] Elastic moduli at least three times higher have been reported using commercial silica,[78] fumed silica, and mesoporous silica fillers.[80] The extent of improvement in tensile properties is dependent on the degree of dispersion of the silica particles inside the PDMS.

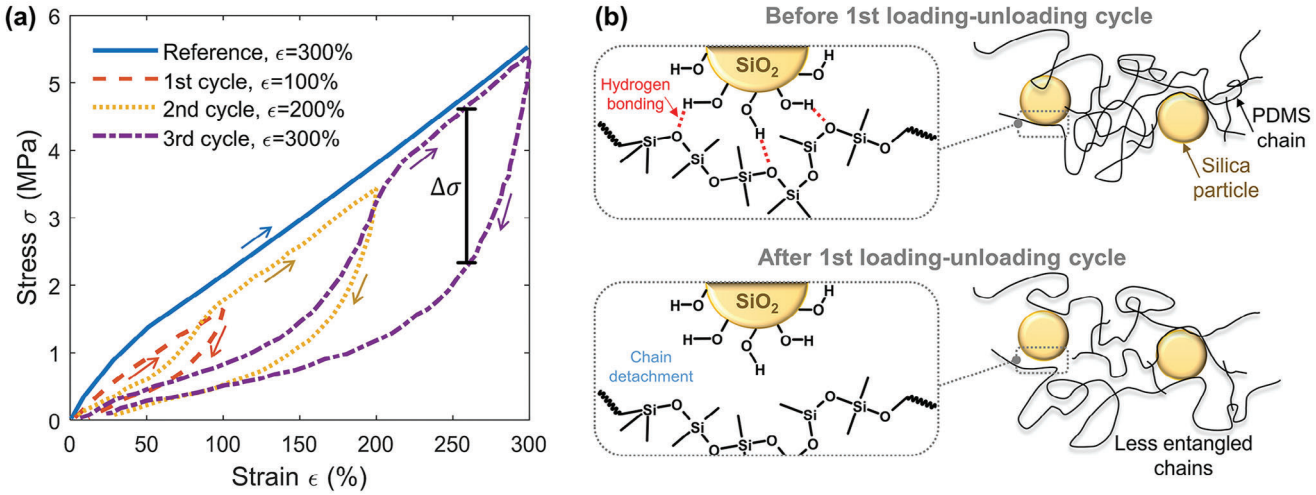

Figure 8. a) Plot of three sequential tensile loading-unloading cycles at progressive strains to demonstrate the stress softening effect. A reference loading curve up to 300% strain is included. Data extracted from ref. [190]. b) Schematic representation of the microscopic structure of the silica-filled (SiO_2) PDMS before and after the first loading-unloading cycle. The hydrogen bonding between silanol groups on the silica surface and the oxygen of the PDMS backbone is highlighted in the top left. The chain detachment from the silica particle surface at the bottom left represents the weakening of filler-PDMS interactions.

Enhancing dispersion by means of processing methods[78] or surface treatment[183] has led to smaller improvements.

Crosslinked bimodal networks with weight proportions of long and short chains of 70:30 and 50:50 have been shown to be viable alternatives for simultaneously improving elongation and tensile strength at break.[37] The larger elongation is assigned to the long chains effect on delaying the rupture nuclei spreading that leads to the material fracture. Meanwhile, short chains would counteract this by limiting elongation to some extent due to their length, resulting in higher tensile strength at break.[26,40,166] Furthermore, increasing the content of short chains to a certain extent has been shown to improve tear strength by a factor of 1.7 to 2.5 when compared to a monomodal unfilled network.[171,188] Depending on the silica loading, the addition of silica fillers to bimodal networks can have either a positive or negative reinforcement effect on tear strength. At a silica concentration of 17.2 wt%, for example, increasing the short chain content increased tear strength by up to 3.5 times compared to a monomodal-filled network. When the silica content reached 30.2 wt%, the trend reversed. The number of silica filler's —OH groups interacting chemically with the PDMS chains has been identified as the key factor governing the enhancement of tear properties.[189] Furthermore, the impact strength and tensile strength at break of silica-filled bimodal networks were found to be approximately three times greater than those of unfilled networks.[40]

However, filled PDMS may exhibit Mullins stress softening in shear and tensile strain modes, resulting in changes in the long-term mechanical performance when subjected to loading-unloading cycles in service, as well as a dependence on mechanical history.[37,131,190,191] The Mullins effect is observed by a reduction in stress with subsequent cyclic loadings for the same strain level. To reach the prior level of mechanical stress, the material must be strained at a level greater than the previous time. Once the previous strain level is passed, the stress increases as a continuation of the first loading cycle,[33,37,155,190,191] as given in **Figure 8a**. Stress softening has been linked to a reduction in chain entanglements and a weakening of filler-PDMS interactions (detachment and slippage from the filler's surface due to limited chain extensibility)[183,190–192] (Figure 8b). It is temperature-independent after the first cycle and more pronounced in silica with no surface treatment and poor dispersion.[183] This effect is weakened after successive stretching, being the first cycle of the largest hysteresis, due to reorganization and stabilization of the material's internal structure.[39,155,183] Thus, pre-stretching or applying a second tensile strain perpendicular to the original strain axis is recommended to achieve reproducibility,[37,39] or to cancel the stress softening, respectively.[190] For instance, PDMS presented a stable response over 220k cyclic uniaxial tensile strain up to 30%, retaining around 95% of the initial stress value after 200 pre-conditioning cycles.[173] The extent of static pre-stretching, i.e., 60% or 120%, before testing appears to have some effect on the elastic modulus of PDMS over time, decreasing as the pre-stretch increases from 60% to 120%, particularly in highly filled systems, which must also be considered during analysis.[176]

In terms of hysteresis, it is the difference in stress ($\Delta\sigma$) between loading and unloading in the same cycle, as depicted in Figure 8a, third cycle. This means that some of the energy used to deform the material mechanically is lost, and less energy is required to return to the initial state. The hysteresis effect is caused by changes in the material's free volume,[193] chain relaxation, internal friction, and, most importantly, stress softening.[194] In this regard, a study involving eight different commercial addition-cured silicones and their blends for five loading cycles at varying strain levels found very little hysteresis.[41] Other studies that focused solely on Sylgard 184 (10:1) found no hysteresis or stress-softening effects at strain levels below 70%.[39,155,158,161] It has been suggested that a combination of low filler content, high molar mass, and crosslinking density may limit the extent of the stress softening.[39] Although stress softening has been thought to be permanent,[190] a nanoparticle-filled PDMS

showed complete recovery at room temperature 17 h after shear loading.[191] The authors discovered in the same study that insufficient rest periods between cycles can significantly alter the shape of stress-strain hysteresis. The type of filler, crosslinking agents, and temperature are believed to affect stress-softening recovery as well.[191]

In contrast to stress softening, filled PDMS networks have exhibited strain hardening, characterized by an increase in elastic modulus and compressive strength at break, under dynamic compressive loadings,[164,195] and in thin films subjected to indentation.[185] This phenomenon has been observed regardless of the mixing ratio, with the extent of strain hardening stabilizing more rapidly as the amount of curing agent increases, likely due to chain alignment.[164] However, when exposed to physiological conditions, mimicked by immersion in phosphate-buffered saline, PDMS undergoes a significant decrease in compressive stress, from ≈25 MPa to 3 MPa, after 1 million cycles.[165] Additionally, addition-cured PDMS demonstrated a minimal stress relaxation under continuous tensile or compressive loadings, reaching a steady state within 200 seconds in one study.[155] For longer testing periods, however, Ghosh et al. reported a 23% stress relaxation under compression after 168 hours of continuous loading, although the specific compressive load was not specified.[151]

Finally, crosslinked PDMS is considered an incompressible material given that its average Poisson's ratio has been found close to 0.5[141,170] implying that deformation causes no change in volume. It is an important parameter used in mechanical behavior simulations as well as true stress-strain curve calculations. In this sense, Zhang et al. demonstrated that the volume consistency assumption typically adopted in those calculations, is only true over a small range of true axial strain (<10%).[155] The ratio between transverse and axial strain deviates from the expected linear behavior as the true axial strain increases, indicating a deviation of incompressibility at large strains for Sylgard 184 cured at 10:1 Base-to-curing-agent ratio. As a result, this assumption would benefit from further careful evaluation in the future. Nonetheless, the curing temperature appears to have little effect on the Poisson's ratios, with variations of around 0.001 when cured at temperatures ranging from 60 to 135 °C.[141] Changing the mixing ratio and/or including a post-curing step resulted in an average Poisson's ratio of 0.5 ± 0.05.[64] The bulk modulus, another parameter also related to incompressibility, however, appears to increase with higher amounts of curing agent.[148]

As demonstrated in this subsection, considerable effort has been expended in understanding and predicting PDMS mechanical properties over short and long timescales, as well as their dependence on a variety of physicochemical parameters. Even so, mechanical testing is still often required for fabricated PDMS waveguides, owing to small variations in mechanical properties that can significantly affect the optical performance, sensitivity, reproducibility, and recovery when in service.

2.5. Biological Safety and Biocompatibility

The biological safety of PDMS is unquestionably an important feature for those who envision PDMS usage in such a field. The biological safety aspects have been extensively investigated over many decades.[196–200] However, most of these results have been derived from studies using PDMS fluids, i.e., non-crosslinked PDMS of low and high molar masses, that were then extrapolated to the solid crosslinked polymer. The rationale behind this is that crosslinked PDMS shares the same chemical structure and is even safer in some cases. For instance, crosslinked PDMS is unlikely to be absorbed into the skin or from the intestinal tract due to the large molar mass and the 3D network.[197,199,200]

The Cosmetic Ingredient Review (CIR) Expert Panel and the United States Food and Drug Administration (FDA) have classified non-crosslinked PDMS as a safe material for use in cosmetics. Nowadays, PDMS is used in a wide array of everyday products, including cosmetics, food, and medical implants. PDMS is typically present in cosmetic formulations at a concentration of about 25%, but can reach 80% in some hair preparations.[197] It has also been used in chronic implantations such as urological surgical therapy, injected into the eyeball as a vitreous substitute,[199] bioscaffolds for tissue engineering,[201] and breast implants.[202,203]

PDMS biocompatibility refers to the absence of adverse effects generated when in contact with living tissues and body fluids. Taking into account the numerous review reports on the subject[196,197,199,200,204,205] as well as the information available on safety datasheets,[206,207] the following general remarks about PDMS biological safety can be made:

i. Oral and dermal absorption in clinical and animal studies have shown no PDMS absorption nor acute toxicity.[197,199,200,204]
ii. Its ingestion has no adverse effects; it is rapidly excreted unchanged in the feces. An acceptable daily intake for PDMS of 17 mg kg^{-1} body weight has been established by the European Food Safety Authority for compounds with a molar mass > 6800 g mol^{-1}.[204]
iii. Short-term dermal exposure (levels varying between 6 and 79% of PDMS fluids) demonstrated no adverse reactions, no sensitization, and only minimal skin irritation.[197,199,200]
iv. In acute and short-term inhalation studies, no adverse effects were observed. Excessive exposure may, however, irritate the nose and the throat.[197,199,200]
v. May cause temporary minimal to mild eye irritation because of its hydrophobic nature, which affects eye lubrication.[197,199,200]
vi. There is no evidence of carcinogenicity (cancer inducer), teratogenicity (defects in embryo or fetus), reproductive toxicity (infertility), mutagenicity (genetic mutation), specific-target-organ-systemic toxicity, or aspiration hazard.[197,199,200,204] No cytotoxicity has been observed for in vitro test.[173]

When used in chronic implants or injected into the body, it is widely assumed that PDMS poses no risk to the immune system. However, its biosafety and biocompatibility have recently been debated with regard to systemic responses, such as autoimmune/inflammatory syndrome induced by adjuvants (i.e., ASIA), lymphoma, breast cancer, and rheumatic diseases following PDMS breast implants.[203,205,208] The likelihood and severity of systemic reactions following implantation or injection appear to be higher in some patients and have been found to be dependent on the type of implant or injection, location, tissue,[196,202]

and surface roughness.[203] Nonetheless, the quality of evidence has been deemed low in systematic literature reviews on the subject.[196,208] Recently, the long-term implantation (4–6 weeks) biocompatibility and stability in mice brain tissue of PDMS optical waveguides has been evaluated with positive outcomes compared to silica fibers.[19,20] Still, more research on the long-term biocompatibility of PDMS (e.g. in contact with living tissue, and specifically in humans) is needed even though PDMS is already deemed safe for short-term applications. It should be noted that these results are only valid for neat PDMS and that the safety of PDMS compounds must be reexamined when other chemicals and fillers are added. Organic solvents such as ethylbenzene and 2-methyl-3-butyn-2-ol have been listed as ingredients in commercial PDMS formulations.[209,210] They have a number of negative effects that should not be overlooked during PDMS preparation, even though most of the solvent is expected to evaporate after curing, thus lowering the risks to health and the environment.

2.6. Environmental Aspects

Crosslinked PDMS is expected to end up in solid waste or incinerated (thermal recycling) at the end of its life.[211] Although PDMS is resistant to degradation by microorganisms such as common fungi, yeasts, and bacteria,[199] it undergoes depolymerization through hydrolysis when it comes into contact with soil, where the degradation rate is significantly influenced by soil moisture.[212–215] One of the primary byproducts is dimethylsilanediol (DMSD), along with other silanol-terminated and cyclic oligomers. Byproducts with sufficiently low molecular mass to become volatile, also known as volatile methylsiloxanes (VMSs), are degraded by hydroxyl radicals in the upper atmosphere, completely breaking down within 10 to 30 days.[215] The byproducts that remain in the soil further degrade into carbon dioxide, water, and inorganic silicate, which are also the products of PDMS combustion. Bioaccumulation of PDMS is thought to be unlikely because of its high molar mass and insolubility in water, having no effect on aquatic or sediment-dwelling organisms such as fish and midge larva.[199,216] Soil organisms (earthworms, for example) are equally unaffected. Moreover, no toxicity to at least 32 plant species has been observed, as well as no bactericidal or fungicidal properties.[199,200,216,217]

Despite personal care products and industrial applications being the primary source of VMSs in wastewater and sewage sludge, PDMS degradation byproducts can contribute to their generation. While VMSs appear to pose a low environmental risk,[218,219] they are a persistent and undesirable source of contamination and accumulation.[220] For instance, a study have shown that DMSD can induce phytotoxicity in wheat plants and hinder their growth.[221] VMSs have been detected in various marine environments, including the Atlantic and Mediterranean coasts,[218] a Chinese lake,[219] market seafood and freshwater fish in Spain,[222] and even the Antarctic Peninsula, a region considered remote and pristine.[223] VMSs are commonly found in biogas produced from sewage sludge anaerobic digestion. During combustion, these VMSs can form abrasive and adhesive SiO_2, damaging co-generator engines,[224] contaminating emission-control catalytic systems, and inhibiting biomethane production.[220] Furthermore, cyclic VMSs have been implicated as potential precursors for atmospheric silicon nanoparticulate pollutants through a mechanism of oxidation and gas-to-particle conversion.[225] Therefore, further research is necessary to understand the long-term environmental consequences of PDMS degradation, the fate of VMSs, and their implications for marine ecosystems[218,219,222,223] and air quality.[225]

As the circular economy gains momentum and waste reduction becomes a priority, finding ways to recover and recycle crosslinked PDMS is crucial. In this regard, the mechanical recyclability and reprocessability of PDMS have been demonstrated through its transformation into fillers[151,226] or by modifying its crosslinking chemistry.[38,47–49] Recently, chemical recycling of PDMS has garnered significant attention as an alternative to the energy-intensive steps typically involved in the production of PDMS raw materials or its thermal decomposition back into oligomers. Several PDMS depolymerization methods have been proposed to address the inherent challenges of chemically recycling crosslinked PDMS, such as low yields, harsh conditions, slow kinetics or expensive catalysts.[211,227–229] Even methods to recover the platinum catalyst used in PDMS addition curing have been explored. Feix et al., for instance, proposed acidic leaching as a means of recovering both the platinum catalyst and cleaved PDMS components for potential reuse as raw materials.[230]

Finally, another environmentally friendly aspect of PDMS is its promising influence in reducing the microplastic fiber formation of synthetic fabrics during laundering, which is considered one of the main sources of microplastics. Polyamide (nylon) fabrics coated[231] or with PDMS incorporated during melt spinning[232] exhibited a reduction in microplastic formation of around 90 and 60%, respectively, owing to a reduction in the friction coefficient responsible for the microplastic formation.

3. Fabrication of PDMS Waveguides

Many processing methods have been used to fabricate PDMS optical waveguides, allowing the preparation of waveguides with varying cross-sections and dimensions. Given the attractive properties of PDMS, considerable effort has been devoted not only to control the geometrical parameters, i.e., size and shape, but also to tune its refractive index and other surface properties for specific applications, as presented in the following topics.

3.1. Processing Techniques

Mold casting and soft lithography are two of the most commonly used optical PDMS waveguide processing techniques. However, many other processing techniques, such as direct writing, extrusion, and fiber drawing, have been used for their fabrication, as summarized in **Table 2** (see Table S2, Supporting Information, for details). These techniques offer great design, dimension, and cross-sectional geometry flexibility for PDMS waveguides. A preference for one technique over another may be dictated by the availability of materials and resources, as well as the desired final sample dimensions and feature size.

As shown in Table 2, PDMS waveguide fabrication is typically limited to thermosetting polymer processing techniques compatible with low- and medium-viscosity PDMS precursors (i.e., base

Table 2. PDMS waveguide fabrication techniques and design parameters.

Fabrication technique		Waveguide designs	Core dimensions (μm)	Length (cm)	Cross-section	Refs.
Core	Cladding					
Mold casting	Mold casting, dip coating, or air-cladding	Buried, rib, tapered, and step-index	500–3000	1–20	Circular, square, or rectangular	[6–10,12,13,233]
Soft lithography	Spin-coating, blade casting, or mold casting	Buried, rib, and step-index	3–250	0.4–8	Square, rectangular, or trapezoid	[14,92,97–101, 103,106,113, 114,153]
Direct writing	Spin-coating, soft lithography, mold casting or air-cladding	Buried, ridge-like, Mach-Zehnder, and graded index	0.08–5000	3.5–4	Gaussian, square, or rectangular	[84,102,104, 234–237]
Fiber drawing	Air-cladding, dip coating	Core only, step-index. Constant, or tapered diameter	10– 2000	0.07–50	Circular	[20,76,105, 238,239]
Lost-wax casting	Air-cladding	Core only	150–250	0.2–2	Circular	[240]
Liquid extrusion	Mold casting, coextrusion	Buried, and step-index	100–550	3–50	Heart-shaped top and flat bottom, or circular	[95,107,241]
Blade coating	Blade coating, dip coating	Planar, buried, and step-index	70–1800	0.15	Rectangular	[12,14]
Spin coating	Not applicable	Core only, and planar	600	5	Rectangular	[242]
Melt extrusion	Air-cladding, dip coating	Core only, and step-index	450–980	15–100	Circular	[51–53]

and curing agent) and serial production, in which the waveguides are handled one at a time. Crosslinking is required to produce a final product that retains its shape by restricting the movement of the polymer chains relative to one another. The disadvantage is that reshaping becomes difficult once cured. The first step in the fabrication of PDMS waveguides involving two-component curing systems is to mix the base and curing agent at predetermined weight or volume ratios. The employed mixing method may affect the waveguide's optical attenuation, homogeneity, and reproducibility. For instance, Novak et al. found that the ultrasonic bath produced the most homogeneous samples in terms of variance of the attenuation constant despite having the highest optical attenuation compared to a laboratory shaker or manual stirring.[243] Once deposited into a mold or onto a substrate, the curing process will proceed until a crosslinked elastomer is obtained. Although heating is not mandatory, it can be used to considerably speed up curing from 4 h at 25 °C down to 10 min at 150 °C,[244] or to tune mechanical (see Section 2.4) and optical properties (see Section 3.2). A variety of recommended curing times and temperatures are typically provided by the manufacturers and most recently, Bardelli et al. studied the crosslinking kinetics under isothermal and dynamic conditions of Sylgard 184.[245] This study provided valuable insights on the processing parameters of PDMS including a kinetic model that can be used as a resource to optimize PDMS curing conditions. Elevating the curing temperature to 120 °C has been shown to induce a shrinkage of 3%, whereas negligible shrinkage was observed at 21 °C. This temperature-dependent shrinkage must be considered in applications where dimensional tolerance is critical.[246]

The fabrication of PDMS waveguides with circular cross-sections can be achieved through mold casting, lost-wax casting, liquid extrusion, and fiber drawing. Such circular waveguides can promote better optical coupling with conventional laser sources and optical fibers.[247] It is also critical to consider losses due to optical scattering caused by surface roughness, impurities, and air bubbles when fabricating waveguides. In particular, the onset of an exponential increase in scattering-induced optical losses is expected to occur when the average sidewall roughness is larger than the wavelength (λ) divided by 20.[45] The roughness of the mold walls determines the surface roughness of the waveguide's features since PDMS is capable of replicating mold features down to the nanometric range.[11,45] To reduce losses induced by air bubbles, various techniques such as filtering (e.g. nylon filter),[96] centrifugation,[94,144,248] pressure casting,[249] and vacuum processing (e.g., in a desiccator, oven or vacuum chamber)[9,147] are recommended. Interestingly, researchers have also exploited the presence of air bubbles to improve the light coupling between stacked PDMS waveguides for intrusive passive optical tapping.[250]

3.1.1. Mold Casting

Mold casting's attractiveness lies in its simplicity and low cost. The method consists of designing and preparing a negative mold, casting the PDMS mixture into the mold, and leaving it to cure until extraction. Typical core dimensions are in the order of hundreds of micrometers up to a few millimeters and lengths of dozens of centimeters, ideal for multi-mode waveguiding. Metallic and plastic molds have been carefully designed for the fabrication of square or rectangular waveguides.[9,13,14,101] The removal of excess PDMS and leveling can be accomplished by using a rod or blade, where pressure, speed, and angle of application have to be properly controlled to avoid the formation of interlayer (crosstalk) or deformed cross-section (poor coupling) that contribute to increased optical loss.[45] Alternatively, silicone,[6–8]

poly(tetrafluoroethylene) (PTFE),[12,94,96,248] polyethylene,[251] and glass[233] tubes represent readily available and cost-effective mold options for PDMS waveguide fabrication. Waveguides prepared using these tubes exhibit a circular cross-section, with diameters defined by the inner diameter of the tube and lengths that can be precisely controlled by cutting the tubing. Extraction of the PDMS waveguides from the tubes can be achieved through various methods, including pressurized air injection,[6] water injection,[8,251,252] or careful longitudinal cutting of the plastic tubes.[12,96] In the case of glass tubes, extraction has been successfully performed by hammering the tube while immersed in water, facilitating removal of the PDMS waveguide.[233]

PDMS cladding of circular cores has been accomplished by dip-coating the core into a cladding mixture, followed by thermal curing.[8,12,94] The cladding thickness can be controlled by immersion time or by vertically spinning the dip-coated waveguide before curing.[8] Another method involves pulling the solid core through a syringe with a needle filled with liquid PDMS, in order to form the cladding, and curing it at 50 °C for 5 min. The final cladding thickness, in this case, was controlled by the needle gauge.[5] It is also possible to use tubing with a larger diameter than the core. For instance, core-cladding waveguides were fabricated by inserting a 254-µm diameter PDMS core into a larger tube with an internal diameter of 380 µm, which was subsequently filled with molten poly(lactide-co-glycolide) to form the cladding layer.[253]

The mold material must be carefully chosen, as chemical affinity and high adhesion may prevent waveguide extraction while also affecting the refractive index near the mold/PDMS boundary. Martincek et al. investigated the refractive index (RI) changes in PDMS slabs (10:1 ratio, 5 mm thick, cured at 22 °C) when molded with various materials (brass, Teflon, glass, polystyrene (PS), and PDMS). The most significant RI changes were observed near the boundary, particularly at the PDMS/PDMS interface, with a maximum change of 0.001 within the first 2 mm at a wavelength of 633 nm, suggesting that the PDMS boundaries exhibit cladding-like behavior. In contrast, the PS mold showed the lowest RI repeatability, while the glass mold yielded the highest RI repeatability and the lowest variation in RI (on the order of 10^{-4}), limited to a small region near the boundary (≈200 µm).[254]

3.1.2. Soft Lithography

Soft lithography, also referred to as replica molding and microtransfer molding, is a popular mold-casting technique used in the manufacture of microfluidic devices.[255,256] Unlike traditional mold casting, photolithography is used to prepare the mold, allowing for the production of PDMS waveguide cores as small as a few microns, as given in Table 2, and compatible with single-mode waveguiding. Soft lithography has also been used to create waveguide arrays with 4 to 12 channels,[14,98,99,113,114,153] rib waveguide with Bragg gratings,[257] and monolithic waveguides integrated with microfluidic structures.[99,100] Singer et al. used this technique to create PDMS waveguide bundles compatible with an integrated circuit's array spacing for use in optogenetics.[103] However, this method is not suitable for the preparation of circular cross-section waveguides and requires specialized installations, complex facilities (cleanrooms), and specific materials for mold fabrication in addition to numerous processing steps.

The procedure starts by dispensing a photoresist, such as SU-8, a photocurable epoxy resin, on a silicon wafer and prebaking it. It is then exposed to UV light through a photomask, generating high-resolution patterns according to the required waveguide design. The higher the mask resolution the more expensive it is. The exposed regions crosslink, whereas the unexposed ones are removed after post-baking and using appropriate developers.[255,256] This procedure results in a patterned master mold. The mold can be designed so that the voids filled with PDMS produce the cores, as illustrated in **Figure 9**a, while the cladding layers are fabricated via spin-coating, blade casting, or by simply pouring a PDMS cladding mixture into the mold.[14,103,114] Alternatively, Figure 9b shows how to create a hollow structure that is later filled with PDMS via capillary. Typically, one of the cladding layers is a flat PDMS slab, while the other contains hollow waveguide channels. Both parts are typically bonded together using plasma to form the hollow structure that will be filled with the PDMS core mixture.[92,153,258,259] Plasma treatment can add a significant cost and requires specialized equipment and installations besides a limited window for part assembling before hydrophobic recovery. Because of that, other bonding alternatives have been devised, such as deposition of reactive coatings,[260] corona discharge, partial PDMS curing prior assembling, changing mixing ratios, using uncured PDMS mixture or the curing agent as a glue.[261] Further details on plasma treatment and some of the bonding alternatives are given in Section 3.3. To help spread the still liquid PDMS mixture and achieve uniform layers, spacers, and a doctor blade are frequently used.

Missinne et al. embossed the waveguide core rather than filling the master mold with PDMS. To accomplish this, the mold was pressed against a liquid silicone mixture that had previously been poured onto a cured undercladding layer, forcing the liquid to fill the core-designated spaces.[106] After the core had been cured, the mold was removed. This method avoids the problems that can arise when attempting to control the blade angle and speed for proper liquid leveling. However, this embossing replica technique may result in a residual thin layer connecting the multiple cores, resulting in crosstalk and losses. Aside from the traditional photolithography used to create the mold, Pérez-Calixto et al. used direct laser ablation to carve centimeter-long microtrenches in an acrylic sheet.[101] With significantly fewer and simpler steps, the authors demonstrated the fabrication of 2.5-cm long rib and buried PDMS waveguides with micrometric cross-section and features comparable to those obtained by soft lithography. Propagation loss was measured at 1.27 and 2.36 dB•cm^{-1} (638 nm), for buried an rib waveguides, respectively.[101] Additionally, reactive ion etching, a plasma etching technique that uses reactive gases for material removal, has been used to fabricate PDMS waveguide lamellas measuring 40 × 600 µm integrated to a Si-chip for flow sensing (see details in Section 4.1.2).[262]

Although not required, coating the mold with demolding spray,[14] gold, poly(vinyl alcohol),[106] or detergent solution[100] has been reported in some cases to facilitate PDMS removal from the mold. A fluorinated hydrocarbon coating was deposited on an SU-8 mold via plasma deposition, serving a dual purpose:

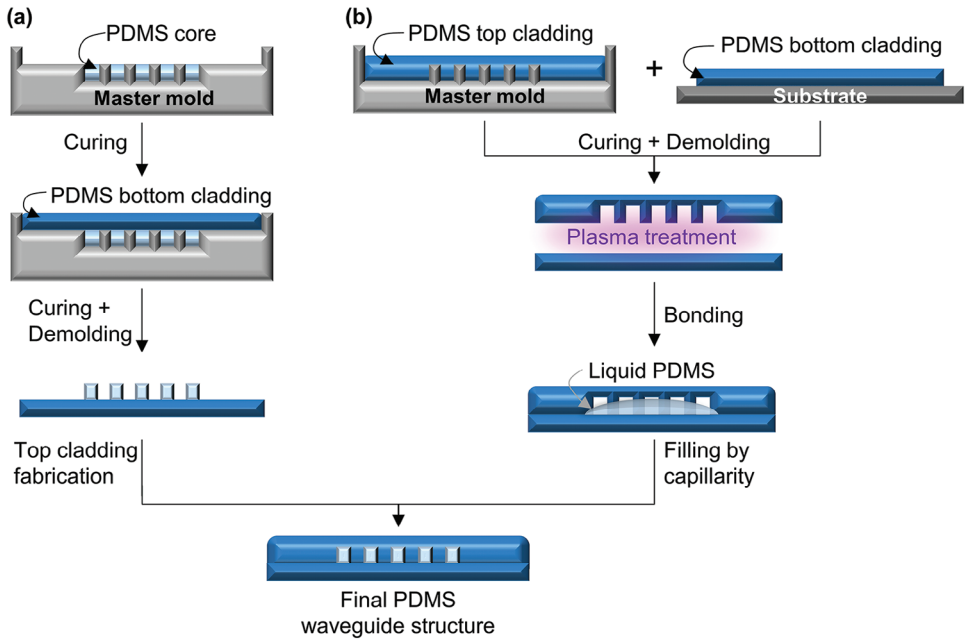

Figure 9. Cross-sectional view schematic representation of the fabrication steps of an all-PDMS core-cladding buried waveguide arrays prepared by soft lithography. Cores filled by a) casting or b) capillarity.

preventing PDMS adhesion and reducing surface roughness on the mold walls.[98,99] However, residues from these demolding products can be a source of contamination and variation in waveguide performance. Moreover, carrier layers made of FR4 and Kapton laminates have been added during cladding fabrication to aid in waveguide handling and to serve as an interface for use in PCBs.[113,114]

3.1.3. Direct Writing

Direct writing refers to various techniques that share the same operating principle of contactless writing waveguides, whether using a femtosecond laser in the UV–vis range, a proton beam, or another source of irradiation. A translational stage is used during patterning to move the irradiation source or the sample. The patterning host material comprises cured, flat PDMS slabs and films, which are prepared using various techniques such as spin-coating, mold casting, and soft lithography. Direct writing is considered a powerful and low-cost tool due to the absence of complex intermediate steps compared to soft lithography. It enables rapid prototyping, scalability to large substrates, and precise lateral alignment of waveguides crossed by fluidic channels.[236,263] The technique appears to be compatible with industrial scale-up using roll-to-roll. However, a proper setup must be carefully considered to eliminate substrate vibrations that may affect the writing consistency.

Direct femtosecond (fs) laser writing consists of focusing fs-laser pulses on a PDMS sample, inducing a series of photochemical reactions, and, hence, changing locally the refractive index.[84] To maximize the RI index difference of inscribed structures upon laser writing, a variety of photosensitizers have been added to PDMS as further discussed in Section 3.2.[84,85,129,264] Investigations on the chemical reactions caused by an F_2-laser (157 nm) revealed the formation of silica-like optical waveguides on PDMS following swelling (chain scission), gas-phase photodissociation, and surface modification steps.[104,265] The reactions were mostly restricted to the PDMS surface due to the strong absorption of UV irradiation in this region. The process was conducted in nitrogen (N_2) to prevent the absorption of short wavelengths by ambient oxygen. Despite this, Okoshi et al. demonstrated that residual oxygen in both the N_2 atmosphere and inside the film played an important role in the photochemical reactions that resulted in a photooxidized silica-like waveguide as the final product.[104] In another study, where the F_2-laser was compared to an ArF laser (193 nm), only swelling was observed without conversion to silica-like products. These results were attributed to the inefficiency of the ArF laser in producing reactive oxygen atoms from the photodissociation of O_2.[265] Furthermore, –OH were detected on the surface of PDMS, and methane (CH_4) and carbon dioxide (CO_2) were generated as by-products of the photodissociation of Si–C and C–H bonds.[265,266] Ridge-like waveguides have been fabricated using a 157-nm laser,[104] whereas inscribed graded-index buried waveguides have been written with a 515-nm laser[84] as shown in **Figure 10**. In both cases, the waveguides presented a cross-section that resembles a Gaussian beam profile, with propagation loss at 1550 nm below 1.5 and of 0.6 dB•cm^{-1}, respectively. PDMS samples presented an improvement in the average tensile strength, elastic modulus, and elongation at break of 74%, 44%, and 18%, respectively, after waveguide direct writing, even though the variations were within the standard deviation. The addition of photosensitizers had a detrimental effect on the mechanical properties.[129]

The number and duration of pulses, writing speed, number of passes, and delivered energy are processing parameters to control. High exposure times can lead to microcraking of the

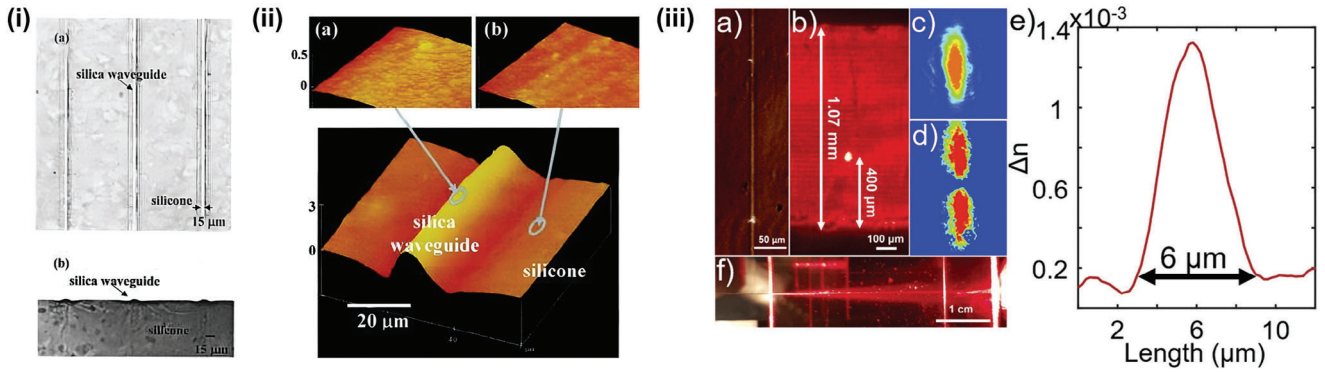

Figure 10. i) Microscope images of optical waveguides 15 μm wide written on a PDMS slab: a) top view, and b) end view. ii) Atomic force microscopy (AFM) image of a 3 × 3 μm^2 area of the PDMS surface showing the fabricated silica waveguide topological profile. Surface roughness of the a) waveguide and the b) nonirradiated area is shown in the enlarged images. Vertical scales are in micrometers. i, ii) Reproduced with permission.[104] Copyright 2005, The Optical Society. iii) Waveguide written inside a PDMS slab: a) top view under the microscope, b) side view and location inside the PDMS slab, c,d) two different modes supported by the waveguide, e) the refractive index profile, and f) light propagation into a 4 cm fabricated waveguide butt coupled using an SMF-28 fiber. Reproduced under the terms of the OSA Open Access Publishing Agreement.[84] Copyright 2020, The authors, published by The Optical Society.

patterned waveguide.[104] The delivered energy must be lower than the ablation threshold, which is used for micromachining. Otherwise, photolysis and/or pyrolysis occur, leading to PDMS degradation and the formation of powdery silica-like products and graphitic carbon.[267] In this sense, Zakariyah et al. used laser ablation to micromachine trenches in a polysiloxane core deposited on a silicone cladding.[268] The structure was then cleaned to remove debris generated by the process, and finally another polymer layer was poured into the trenches, forming a waveguide array.

Nonetheless, in a photolithographic-like procedure, fs-laser writing has been used to create waveguides using photocurable polysiloxanes other than PDMS.[263,269] In addition, phenylacetylene monomers[270] and silanol-terminated dimethyl diphenyl polysiloxanes with acryloxyl silanes[271] were polymerized inside a PDMS matrix to produce waveguides with high RI contrast. Instead of a fs-laser, Valouch et al. fabricated optical PDMS waveguides using a low-pressure mercury lamp (185 and 254 nm) assisted by a conventional mask, as given in **Figure 11a**.[237] The direct writing process produced an asymmetrical ridge-like waveguide with a slightly asymmetrical mode profile (Figure 11c), and propagation loss at 635 nm of 0.47 dB•cm^{-1}. The authors discovered that multiple modes could be excited in waveguides with widths of 10 or 15 μm. Waveguiding was achieved at 635 and 808 nm wavelengths and remained stable for 3 months while stored in ambient air.

The use of proton beam irradiation is another method for direct writing. In this case, a beam of finely focused high-energy protons (750 keV) has been used to pattern straight and Mach-Zehnder waveguides close to 20 μm deep in PDMS.[102,234,236] The proton beam modifies the refractive index along the ion path due to chemical reactions and compaction (**Figure 12i**), that take place in PDMS caused by nuclear collision events.[236,272,273] These changes are usually localized at the end of the range of the protons, forming an RI profile that resembles the shape of a Proton Bragg curve (Figure 12ii). The RI differences between surface and deeper regions are between 0.03 and 0.08 at 400 nm. The order of magnitude of the RI change has been found to be stable over time, even though fluctuations of up to 0.03 were observed without an evident trend.[235] The penetration depth of the proton beam is precisely controlled by its energy, which, combined with minimal lateral spreading, enables the fabrication of buried waveguides with well-defined boundaries as depicted in Figure 12iii, and makes proton beam direct writing an attractive technique for this application.[236,274]

The surface topography of the irradiated area changes, as does its wettability, due to chemical and structural changes. Depending on the processing parameters, such as the spacing

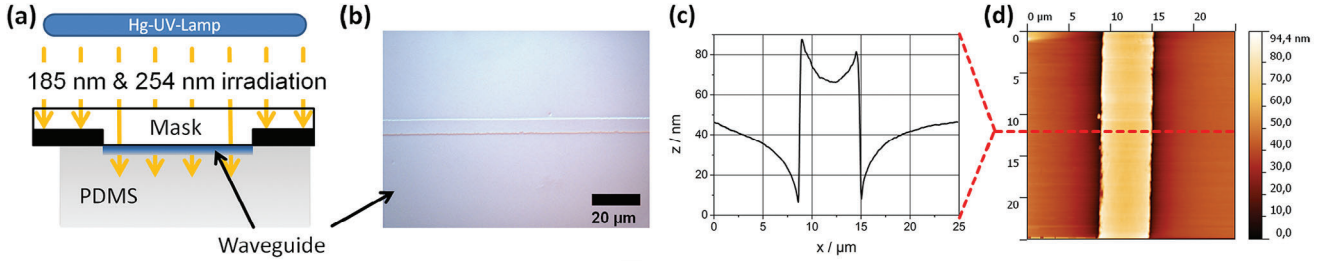

Figure 11. a) Schematic representation of the waveguide fabrication process using a direct UV irradiation and a mask. b) Microscope image of the fabricated waveguide. AFM (c) cross-section profile and (d) top view of a 25 × 25 μm^2 area of the PDMS slab. Adapted with permission.[237] Copyright 2012, The Optical Society.

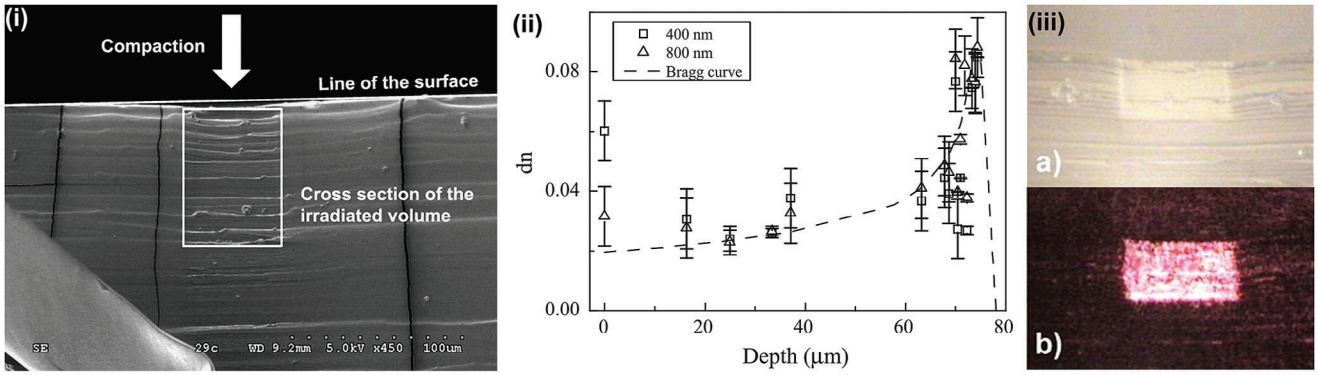

Figure 12. i) Scanning electron microscopy cross-section image of the PDMS slab irradiated with proton beam at a fluence of 1200 nC mm^{-2}. The scale bar is 100 μm. Reproduced with permission.[275] Copyright 2009, Elsevier ii) Profile plot of refractive index change as a function of proton beam penetration depth at 400 and 800 nm. A representative Bragg curve (dashed line) is included as a guide to the eye. Reproduced with permission.[235] Copyright 2011, Elsevier. iii) Cross-section view of a waveguide written inside a PDMS slab: a) bright field image with reflected white light, b) 633 nm light emitted from it. Adapted with permission.[235] Copyright 2011, Elsevier.

between inscribed structures and fluence (i.e., the beam energy divided by the illuminating area), the compaction can reach values up to 3.5 μm, which corresponds to approximately 6% of the proton penetration depth.[273] Chain scission, crosslinking, recombination, and the depletion of small molar mass fragments all contribute to the formation of silica-like waveguides.[276] By varying the delivered energy while keeping the same fluence, it has been found that different chemical reactions occur because of the energy dependency of ion-molecule interactions. The mechanisms taking place in PDMS at low and high-energy protons are described in detail elsewhere.[272,276] Besides fluence and delivered energy, the scanning speed is another important parameter in proton beam writing, as the release of gases produced during irradiation may affect the process efficiency.

3.1.4. Fiber Drawing

Fiber drawing has been devised to overcome the challenges posed by the fabrication of circular PDMS waveguides with small diameters (20–100 μm) and high aspect ratios (>100) since the low stiffness lead to the collapse and poor handling when prepared by mold casting.[238] Typically, PDMS is partially cured prior to the drawing process to achieve an optimal viscosity for processing and to ensure that the PDMS network has reached the critical point of chain entanglement, thereby facilitating successful drawing.[19,105,238] Rheology and calorimetric measurements can be used to track crosslinking evolution and determine the best processing parameters.[245] Three approaches that have been used in PDMS fiber drawing are illustrated in **Figure 13**.

The most basic fiber drawing method involves applying partly cured PDMS (8 h after mixing the components) to the end faces of conventional fibers (Figure 13a). Then, gradual elongation is applied until the PDMS fiber reaches the desired length between the two fibers. Afterward, the PDMS fiber is cured at higher temperatures to stabilize its geometry. This procedure yields tapered symmetrical waveguides that are coaxial with the conventional fiber if properly aligned during drawing.[76,239] Martincek et al. developed a similar technique in which an optical fiber is drawn with a plastic rod, as illustrated in Figure 13b.[105] Important processing variables are viscosity, drawing speed, and the amount of PDMS pulled with the rod. Using this method, the authors were able to prepare fibers with diameters ranging from 10 to 2000 μm and lengths ranging from a few millimeters up to 50 cm, besides the fabrication of unconventional optical waveguide structures, such as looped and twisted fibers and X-fiber couplers. Surprisingly, the diameter along the fiber presented good uniformity. For instance, a 37-mm-long fiber presented diameters varying between 44.2 and 46.4 μm. Similarly, 7 cm long PDMS waveguides were fabricated with an average diameter of 126 ± 5 μm.[19] Cao et al. used a glass rod to pull the fiber through a tubular heater set at 280 °C for quick crosslinking of the PDMS core in ≈2 s instead of partially curing the PDMS mixture. Following that, the waveguides were oxygen-plasma

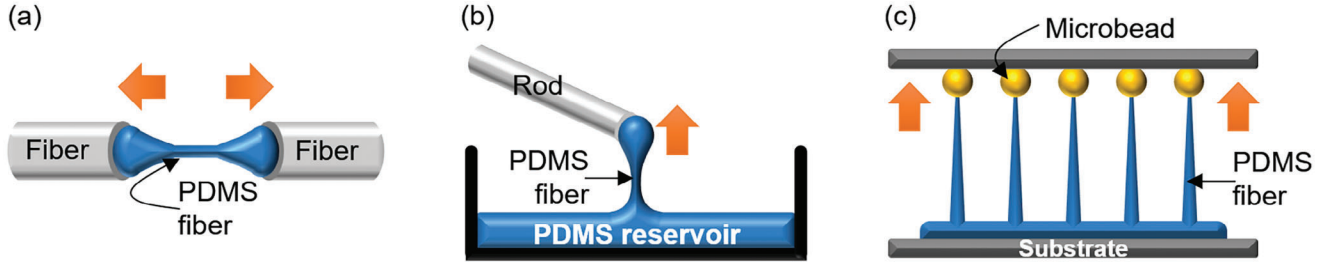

Figure 13. Schematic representation of tapered PDMS fibers produced by a) pulling apart two conventional fibers connected with PDMS, b) pulling PDMS using a rod, and c) PDMS micropillars drawn with microbeads attached to a movable upper substrate.

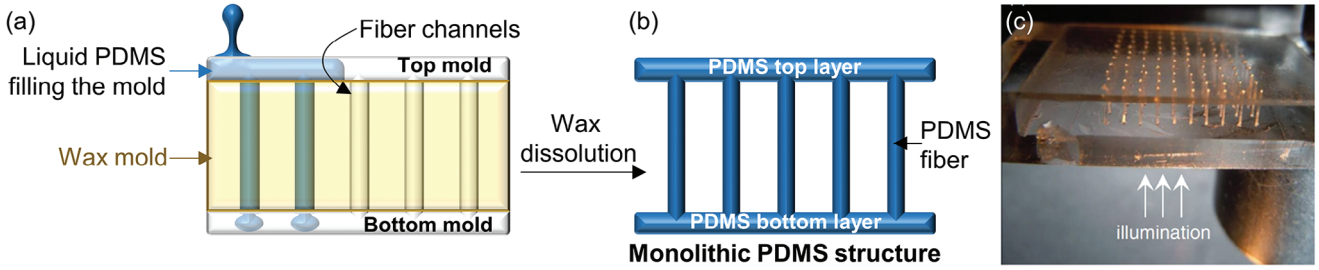

Figure 14. Schematic representation of a monolithic PDMS waveguide structure prepared via lost-wax casting. a) Mold-filling with liquid PDMS, b) monolithic PDMS structure obtained after mold dissolution, and c) picture of a PDMS waveguide array produced using this technique. Adapted with permission.[240] Copyright 2011, IOP Publishing.

treated and coated with a poly(vinyl alcohol)/poly(acrylic acid) interpenetrating network to form a hydrogel cladding.[20]

A more elaborated approach has been used by Paek & Kim to fabricate arrays of upright waveguides with aspect ratio higher than 40.[238] The authors used microbeads (Figure 13c) as drawing probes. These microbeads remained integrated into the waveguides to be used as self-aligned reflectors, finding application in airflow sensors (Section 4.1.2). PMMA and Ag-coated hollow glass microbeads with 50 and 58 µm of diameter, respectively, were used as drawing probes. The PDMS bed from which the micropillars were drawn was prepared by spin coating and prebaked in order to accelerate its partial cure. The microspheres were assembled with the aid of an SU-8 grid prepared via photolithography and attached to a glass substrate by double-sided tape. After that, the microspheres were partially immersed in the prebaked PDMS and lifted with a micromanipulator, drawing the fibers. After curing, the PDMS fibers containing the microbeads were gently detached from the double-sided tape. Several combinations of height and tapered fiber diameters were achieved. Waveguides with 2.4 mm of length and an average diameter of 21 µm had the highest aspect ratio of 112 achieved using this technique.[238]

3.1.5. Lost-Wax Casting

The lost-wax casting technique has enabled the manufacture of cores with circular cross-sections, even though this method is not limited to this geometry. Lost-wax casting was originally used to cast metal parts and involves several steps.[24] A simplified lost-wax inspired process has been used by Lee and Kim to prepare arrays of 10 × 10 waveguides directly anchored to PDMS slabs with very high aspect ratios (the highest aspect ratio of 167:1).[240] For that, a water-soluble wax mold was first prepared using metal wires fixed to a polycarbonate substrate. Once the mold was ready, PDMS was poured into it, as depicted in **Figure** 14a. After PDMS cured, the wax mold was removed by dissolving it in water, Figure 14b.

Microwaveguides ranging from 150 to 250 µm in diameter and length between 2 and 20 mm were produced at a success rate of around 96%. Advantages of this technique include the fabrication of very complex monolithic geometries and easy demolding. A disadvantage is that, once used, the mold is completely lost, which increases the processing time and cost.

3.1.6. Liquid Extrusion

Liquid extrusion here is defined as a method of forcing a liquid through a die. In some ways, it is similar to additive manufacturing, in which a nozzle or translation stage moves to create the waveguide without, however, creating complex 3D structures. Nakakubo et al. used liquid extrusion to write PDMS waveguides on glass and PDMS substrates.[241] The authors used a syringe filled with a so-called super-PDMS solution mounted on a translation stage to accomplish this. They were able to write 3-cm-long waveguides with a width of 200 µm and a thickness of a few microns by controlling processing parameters such as discharge pressure, feed flow rate, needle inner diameter, and distance between the needle and the substrate. Adequate solvent and PDMS concentration are also important solution parameters to consider as they affect viscosity and surface tension. The fabricated waveguide cross-section, on the other hand, had a heart-shaped top and flat bottom due to solvent evaporation. The ensuing cured structure was then placed inside a mold to create a PDMS top cladding via casting.[241] Alternatively, wet-spinning has been used to fabricate long PDMS fibers with uniform diameter of ≈0.55 mm and lengths of up to 1 m.[277] It consists of extruding liquid PDMS from a syringe directly into a hot oil coagulation bath (170–230 °C).[277,278] Solidification occurs rapidly, within seconds, allowing for the fibers to be drawn out from the bath. However, a subsequent oil removal step, utilizing soap water or isopropyl alcohol, is necessary.[277,278] Notably, the process may result in flattened fibers depending on the processing parameters.[278]

The Mosquito method has been used to prepare graded-index circular polysiloxane-based waveguides.[247,279,280] The name derives from the fact that the core is dispensed inside an uncured cladding pool with the aid of a needle. The needle moves longitudinally inside the cladding to create the waveguide. The monomer diffusion profile and final core diameter can be controlled through scanning speed, dispensing pressure, and needle inner diameter to fabricate uniform or tapered parallel waveguides compatible with on-board interconnections. Cladding and core are cured with UV light and baked at 100 °C.[247,279,280] Inspired by this technique, Prajzler et al. recently prepared circular waveguide cores by injecting a PDMS copolymer, LS-6943 (NuSil), with the aid of a needle into partially cured Sylgard 184 slabs and curing them at high temperatures afterward.[107]

To ensure the continuous production of circular cross-section waveguides, Feng et al. employed a poly(ethylene oxide) (PEO) and poly(propylene oxide) (PPO) triblock copolymer with acrylate end groups (Pluronic-DA) as cladding. This copolymer presents a sol-gel transition below 10 °C at 33.3 wt% and is UV-curable. It served not only as cladding but as a supporting shell during liquid PDMS extrusion. The extrusion was carried out at 18 °C using a commercial printer with an extrusion head containing a coaxial nozzle. Either Sylgard 184 or a UV-curable PDMS were employed as core materials. The core diameter could be varied between 100 and 550 µm by adjusting the printing pressure of either the core or cladding.[95] Further advancements in PDMS additive manufacturing have been witnessed over the last two decades in terms of innovative liquid processing approaches[281] and molecular engineering to confer thermoplasticity to PDMS.[50,282] Thus, it is expected that in the near future, such approaches will be exploited in the fabrication of regular and complex waveguide architectures.

3.1.7. Blade Coating

Blade coating, also known as doctor blading, knife coating, or tape casting, is a popular and simple fabrication technique used to prepare thin and flat films with well-controlled and uniform thickness. It involves placing the coating material next to a blade-like piece and either running it over the substrate or moving the substrate underneath it.[283] Thickness control is achieved by using spacers that limit the distance between the blade and the substrate and by adjusting parameters such as spreading speed and the concentration and viscosity of the coating material. Little material waste (estimated at approximately 5%) and industrial scale-up compatibility are some of the advantages of this technique.[283] Prajzler et al. employed this technique to produce planar core-cladding PDMS waveguides on glass with a total thickness of 70 µm.[14] Blading is also present during mold casting, photolithography, and soft lithography for leveling and spreading.[103,284]

3.1.8. Spin Coating

Spin coating has been used in the fabrication of thin PDMS planar waveguides,[242] the substrate for direct writing[104,234,237] besides being an integral part of photo[285] and soft lithographic[92,97,153,249] processes. It is a simple and low-cost technique used to prepare flat, uniform thin films of high finishing quality, ranging from a few nanometers (10 nm) to micrometers. In a typical process, a polymer solution is dispensed onto the center of a flat substrate, e.g., glass or silicon wafer, and spun at high speed.[283,286] The centrifugal forces spread the polymer and also remove the excess material. Rotation is maintained until the polymer solution completely covers the substrate or the desired thickness is achieved.[286] As PDMS hardening time at room temperature takes hours, enough time is given for the polymer to settle and form a more uniform film. Otherwise, its cure has been sped up by baking the material, for example, at 150 °C for 2 h[102] or at 100 °C for 5 min.[287] Ramuz et al. used this technique to fabricate planar rectangular PDMS waveguide with gratings for light in and out-coupling. The 600 µm spun PDMS waveguide, was partially cured at 100°C for 1 h for subsequent embossing gratings using a stamp, and peeled off from the Si wafer.[242] The dispensing method, i.e., static or dynamic (with the substrate spinning), and the dispensed volume influence the substrate coverage. Micropipettes are usually employed to dispense a known, reproducible volume. For the preparation of molds used in soft lithography, most commonly, a SU-8 layer is spun on a Si wafer prior to its exposure to UV light. On the spin coating of PDMS, diluted and undiluted PDMS mixtures (base + curing agent) have been used. A disadvantage of this technique is the high material waste, which may be critical when the amount of available material is scarce or expensive.

The final film thickness is determined by the polymer solution and solvent properties, specifically concentration, viscosity, surface tension, and, if applicable, solvent evaporation rate.[287] Thicker films are obtained from highly viscous or concentrated solutions as well as solvents with a higher evaporation rate and surface tension because the solution has less time to be flung off.[283] Mata et al. observed that increasing the amount of curing agent decreased the film thickness because of the lower viscosity of the resulting mixtures.[62] The spinning parameters influence the final thickness as well. The higher the spinning speed and the longer the spinning time, the thinner the film. If acceleration is too low, solution spreading may be compromised, rendering a discontinuous film.[62,286] For instance, thicknesses between 18 and 90 µm have been achieved by spin coating 450 µL of Sylgard 184 prepared at a 10:1 mixing ratio. The spinning time was fixed at 30 s, and the speed was varied from 4000 to 1000 rpm in order to increase the thickness of the PDMS films on glass.[102]

3.1.9. Melt Extrusion

Industrially compatible melt processing techniques are expected to become more viable options for the mass production of continuous PDMS waveguides as thermoplastic PDMS synthesis advances.[38,47–50] Wacker Chemie's Elastosil R series and Geniomer PDMS-urea copolymers are commercial formulations already available in the market that are compatible with extrusion, compression, and injection molding.[51–54] Melt extrusion, for example, has been used to prepare 1-m long thermoplastic silicone waveguides of varied diameters (0.5, 0.75, and 0.8 mm), with an optical loss between 0.16 and 0.25 $dB \cdot cm^{-1}$ at 652 nm.[51,288] The method consists of melting the polymer with a combination of heat and friction using an extruder. The molten material in then forced through a die or spinneret, after which it solidifies in contact with cool air acquiring the final form. Draw-down speed, extrusion temperature zones, and die diameter are processing parameters to control.[52]

3.1.10. Other Potential Processing Techniques

Although UV-curable PDMS is commercially available[95] its use in the direct fabrication of PDMS-core waveguides by photolithography has yet to be demonstrated. Photolithography is

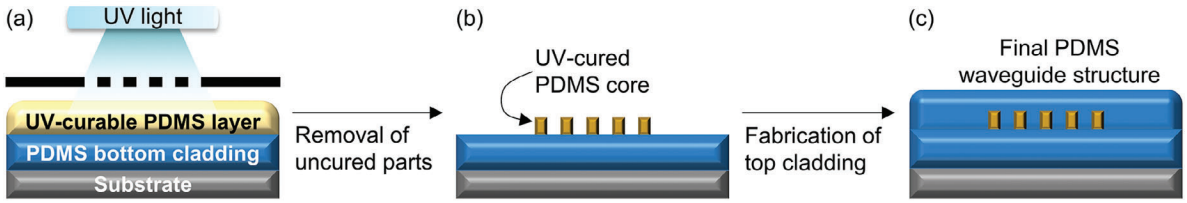

Figure 15. A cross-sectional view schematic representation of a photolithographically prepared all-PDMS core-cladding buried waveguide array.

based on the projection of a reduced pattern onto a film made of a material sensitive to UV light and as such, it is limited to planar configurations. Photolithography is a straightforward method compared to soft lithography and has been used to fabricate waveguide arrays up to 24.5 cm long made of photocurable polysiloxane on a polyimide substrate.[285] The requirement of using a photocurable PDMS may explain why soft lithography is preferred over this technique. A schematic representation of the procedure is illustrated in **Figure 15** and begins with spin-coating and curing a PDMS bottom cladding on a flat substrate. A photocurable PDMS core mixture is then spun on top of the cladding. Using a photomask, this core layer is exposed to UV light to selectively cure specific PDMS regions, as shown in Figure 15a. Afterward, the uncured part is washed away with acetone before the top cladding is spun on top of the structure and cured (Figure 15b).

The floating-on-water technique appears to be a simple and straightforward technique for preparing free-standing micrometric planar waveguides without the size constraints imposed by spin- and blade coatings, as well as the additional steps for removal from the substrate.[289] The technique consists of pouring the PDMS mixture into a container filled with water and exploiting the PDMS' hydrophobicity to allow it to spread over the water surface and create a thin film that can be recovered after curing. Thickness can be controlled by the amount of PDMS dispensed, initial PDMS mixture temperature, and water temperature.[289] However, because of capillary action, the thickness is not uniform near the edge, with standard deviations between 0.6 and 1.4 µm for membranes measuring between 3 to 5 µm thick.[289] Other potential techniques for the fabrication of PDMS waveguides include a combination of etched templates prepared by inkjet printing and replica molding,[290] roll-to-plate nanoimprinting,[291] and near-field and melt electrospinning to produce submicrometric waveguides with the aid of an electric field.[292–294]

3.2. PDMS Refractive Index Control

When it comes to the fabrication of core-cladding all-PDMS waveguides, one of the main requirements to be met is the preparation of a core with a refractive index larger than the cladding. This refractive index (RI) mismatch is critical for successful light guidance via total internal reflection (TIR). The most common strategies used to control the RI value of PDMS samples can be summarized as follows:

1) Varying the mixing ratio
2) Varying the curing conditions
3) Using solvent
4) Adding silicone oil
5) Using different PDMS formulations
6) Incorporation of photosensitive organic compounds
7) Incorporation of metal-based compounds (oxides, metallic nanoparticles, organometallic, and organometalloid compounds), and
8) Preparing PDMS copolymers.

Figure 16 depicts the changes in RI values reported in the literature for each of these strategies. Table S3 (Supporting Information) gives more details in this regard. Some of these strategies will have an impact on transparency at certain wavelengths and on the mechanical properties, as discussed in Section 2.4. Thus, the selection of the most appropriate approach for tuning the RI must take into account the desired final optical and mechanical properties. Furthermore, the RI standard deviation, when reported, has been found to be near ±0.0004, reaching ±0.01 in some cases due to method inaccuracy, sample inhomogeneity, and/or experimental errors.[9,56,77,295] Hence, reproducibility and agreement on the magnitude of RI change employing some of the aforementioned strategies are debatable, in particular when the RI modulation is quite small.

3.2.1. Varying the Mixing Ratio

Between 400 and 2000 nm wavelength range, PDMS RI may vary according to the mixing ratio (Figure 16, strategy 1).[8,9,59,91,92] The maximum achieved RI contrast across the literature using this strategy is debatable, going from a negligible effect[57] to a difference approaching 0.015 (Figure 16, 1D).[92] There is no general agreement on how increasing the amount of curing agent affects RI contrast, with some studies reporting a minimum[91] or maximum[162] RI value at a mixing ratio of 10:1 (Figure 16, 1C and 1E, respectively) and others showing a consistent increase with higher curing agent concentrations.[59,92] In addition, Prajzler et al. found that altering the mixing ratio resulted in an RI peak at 5:1 more pronounced at shorter wavelengths (Figure 16, 1A).[56] A further increase or decrease in the curing agent amount led to lower RI values, with the same trend observed regardless of the curing conditions investigated. Such mixing ratio effect seems negligible at longer wavelengths (2000–20000 nm) and, notably, has little to no effect on the measured extinction coefficients in the visible to infrared range.[90,91]

3.2.2. Varying the Curing Conditions

Varying the curing conditions may have a similar effect for controlling the PDMS RI (Figure 16, strategy 2).[59,100,296] By combining higher temperatures with shorter curing times, a RI variation

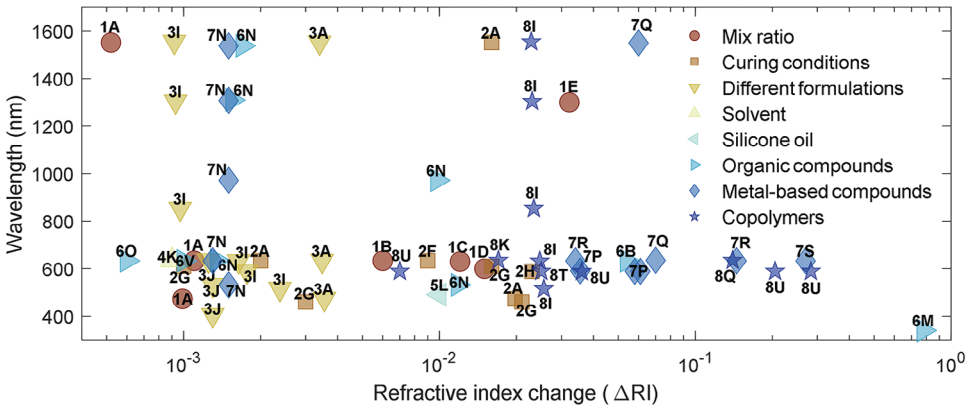

Figure 16. Plot of refractive index change achieved by strategy for different wavelengths. Data points are identified by a combination of the strategy number and a corresponding letter from the reference. Strategy 1 Mix ratio: A,[56] B,[9] C,[91] D,[92] E.[162] Strategy 2 Curing conditions: A,[56] F,[296] G,[100] H.[59] Strategy 3 Different formulations: A,[56] I,[57] J.[77] Strategy 4 Solvent: K.[98] Strategy 5 Silicone oil: L.[99] Strategy 6 Organic compounds: B,[9] M,[297] N,[129] O,[96] V.[264] Strategy 7 Metal-based compounds: N,[129] P,[298] Q,[295] R,[299] S.[83] Strategy 8 Copolymers: K,[98] I,[57] Q,[295] T,[114] U.[300]

close to 0.023 (at 589 nm wavelength) was reported, Figure 16, 2H).[59] Another study on the PDMS curing parameters showed an RI change of just 0.0008 which was deemed not statistically significant because it was within experimental error (Figure 16, 2A).[56] To the best of our knowledge, the precise effect of individual curing condition parameters and their possible interactions has not yet been systematically evaluated via a design of experiments (DoE). Yet, based on published data, the temperature stands out as the main curing parameter responsible for producing the RI changes.[100,296] Furthermore, by parallelly optimizing the mixing ratio and curing conditions, a refractive index (RI) variation of up to 0.037 can be achieved, e.g., PDMS prepared at 10:1 ratio and cured for 30 min at 100 °C, compared to another prepared at a 10:2 ratio and cured for 10 min at 240 °C.[59]

3.2.3. Using Different PDMS Formulations

Owing to the diversity of crosslinking chemistries and formulations, another straightforward method to prepare PDMS waveguides with the desired RI contrast is to use different PDMS formulations (e.g., Elastosil RT 601, GE RTV 655, and QSil 216), with RI differences reaching between ≈0.001 and 0.0035 (Figure 16, 3A, 3I, and 3J).[56,57,77] We note that PDMS waveguides designed for applications requiring mechanical performance must have core and cladding with matching mechanical properties, which may limit the options available. However, the practical implementation of this approach may be impeded by the difficulty in knowing the exact chemistries of commercial PDMS formulations, as well as their continuous reproducibility and availability over time.

3.2.4. Using Solvent or Silicone Oils

The incorporation of other materials into PDMS has been proposed by many to impart RI control. For instance, Kee et al. achieved an RI contrast of 0.001 by adding 10 wt% of hexane during PDMS mixing and then evaporating the solvent (Figure 16, 4K).[98] However, the study found that increasing hexane concentration to 20 wt% led to severe warping after evaporation with no additional changes in the RI. The evaporation of the solvent is thought to create voids in the material, lowering the RI. Alternatively, adding 10 wt% of silicone oil resulted in RI changes of 0.01 (Figure 16, 5L).[99] Besides the changes in RI, silicone oil also affects the mechanical properties and may exudate from the crosslinked network with time.[301,302]

3.2.5. Incorporating Photosensitive Organic Compounds

High RI changes have also been demonstrated with the use of photosensitive organic compounds such as the ketones shown in **Figure 17**. Changes in transparency in the UV–vis range are to be expected, in particular when compounds containing unsaturated (double or triple) bonds are employed. Benzophenone is an example of such a compound that, at a concentration of 2.5 wt%, increased PDMS RI by 0.054 at 633 nm wavelength (Figure 16, 6B).[9] In another study involving benzophenone and its derivatives, UV laser writing was used to promote the chemical attachment of these molecules to the crosslinked PDMS backbone. An RI modulation of approximately 0.0010 was achieved at concentrations between 1 and 4 wt% (Figure 16, 6V).[264] Similarly, the fabrication of waveguides via fs-laser writing in PDMS has resulted in an RI maximum enhancement of 0.015 through photochemical reactions of benzophenone and other ketones, with good RI stability over 100 days of aging (Figure 16, 6N). For comparison, fs-laser writing in a neat PDMS induced RI changes in the order of 0.001.[85,129]

Other interesting candidates include photochromic dyes such as arylazopyrazoles (AAPs) and spiropyrans (SPs). These dyes can alter the RI when incorporated into PDMS and also enable an additional temporary photoregulated RI tuning effect. APP is an organic photochromic dye that undergoes reversible photoisomerization upon irradiation with UV light, changing between *trans* and *cis* conformations whereas SPs isomerize to the merocyanine form, as given in **Figure 18**. When incorporated into PDMS, the RI changed not only as the AAP concentration

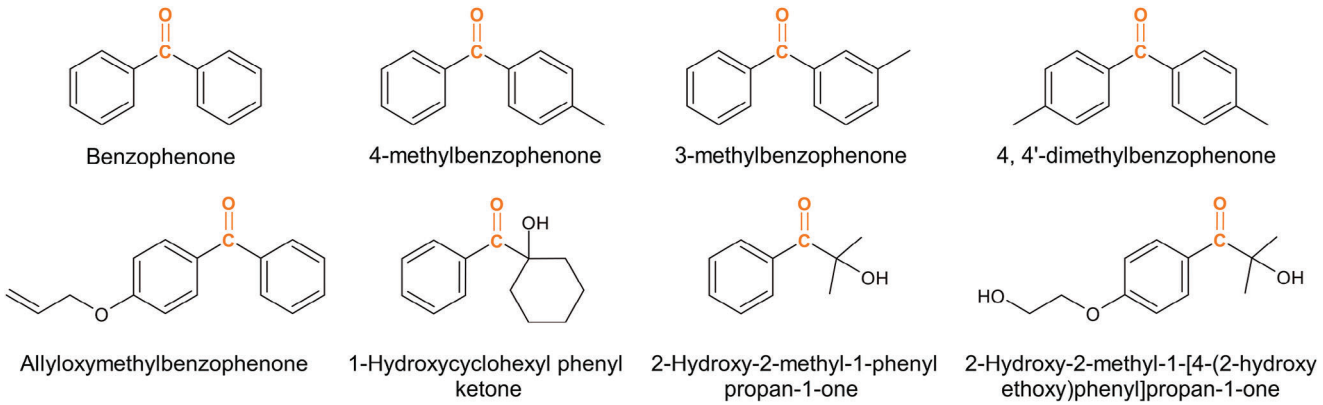

Figure 17. Chemical structure representation of common ketones (functional group highlighted in orange) used to increase PDMS refractive index.

increased but also as the APP reversible isomerization occurred. The prepared material presented remarkable RI tunability, increasing the RI up to 0.78 for the highest AAP content before irradiation and an RI decrease of up to 0.67 when irradiated with UV light (Figure 16, 6M).[297,303] Recently, our research group reported a 0.0006 increase in RI at 633 nm upon exposure of a PDMS film doped with 0.05 wt% of SP to UV-A irradiation (Figure 16, 6O).[96]

While this approach provide valuable functionalities such as photosensitivity for further processing (e.g., fiber grating engraving[264,304] and direct laser writing)[85,129] and the capacity for temporary photoregulated RI adjustment it must be carefully considered. Incorporating organic molecules bearing chromophores can alter the absorption spectrum at certain wavelengths, particularly towards the blue end of the visible spectrum and in the IR range. This can lead to higher optical attenuation, in addition to unwanted crystallization.[9,96] SPs, for example, exhibit absorption bands up to 350 nm and may demonstrate negative photochromism depending on the SP molecular structure and its susceptibility to chemical interaction with PDMS.[96]

3.2.6. Incorporating Metal-Based Compounds

On the use of metal-based compounds, PDMS RI has been increased to a large value of 0.27 via the addition of up to 20.8 v% of diamine-modified zirconium dioxide (ZrO_2)[83] (Figure 16, 7S) and by 0.20 with 0.36 wt% of titanium dioxide (TiO_2)[305] nanoparticles, respectively. In the former, PDMS films with thickness between 270 and 300 nm retained more than 92% of transparency in the 400–700 nm wavelength range, even at such high nanoparticle loading.[83] The incorporation method and surface modification play a crucial role in the preparation of PDMS with high RI, as incompatibilities may result in aggregation, poor final properties, and a negligible effect on RI.[295] Beyond the direct addition of metal oxides, in situ formation and sol-gel syntheses have also demonstrated promising results. For instance,

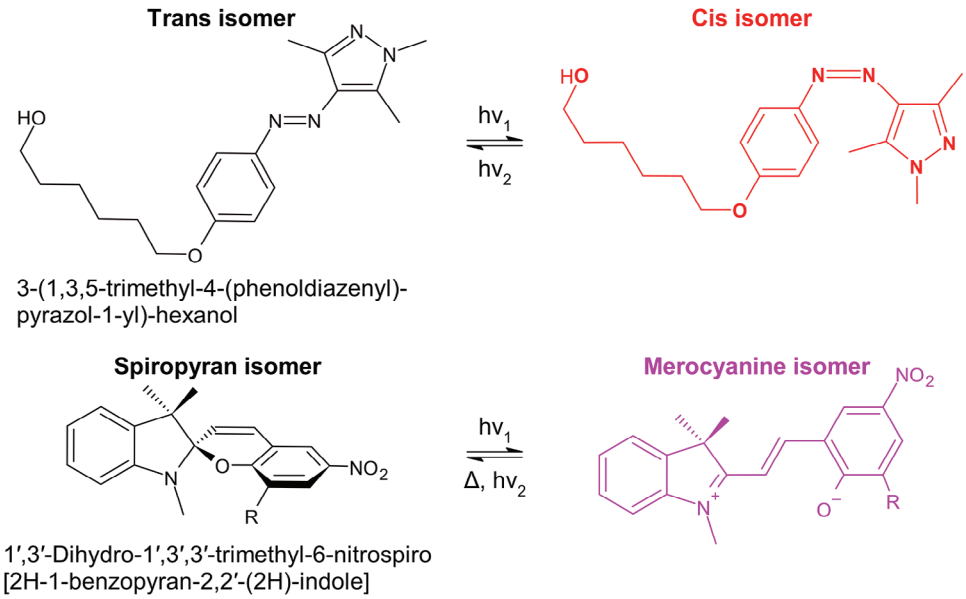

Figure 18. Chemical structure representations (top) of the arylazopyrazole (AAP) trans to *cis* conversion, and (bottom) of the spiropyran to merocyanine conversion upon UV irradiation.

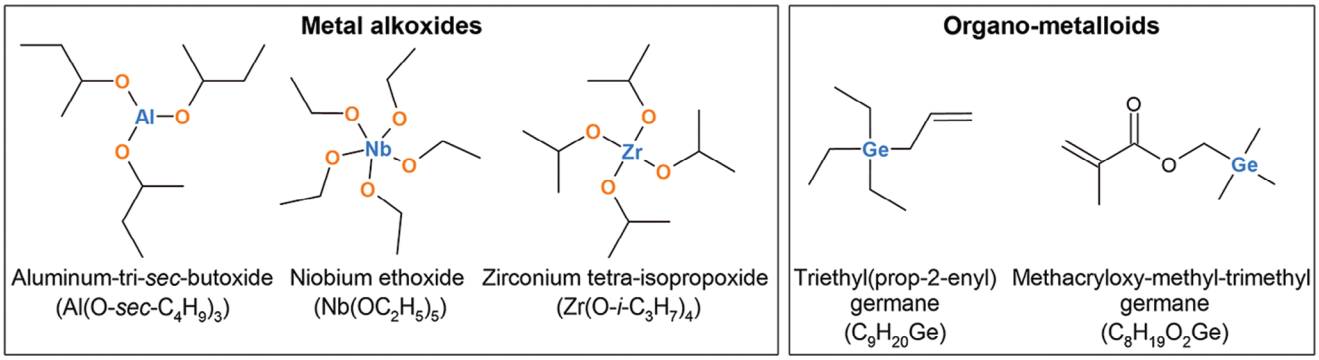

Figure 19. Chemical structure representation of some metal alkoxides and organo-metalloids used to increase PDMS refractive index. Metal and metalloid atoms are highlighted in blue.

metal alkoxides and organo-metalloid compounds such as the ones shown in **Figure 19** have been combined with PDMS, resulting in metal(loid) atoms covalently bonded to the PDMS network.[84,85,295,298,299,306]

The increase in PDMS RI using this strategy has varied between ≈0.04 and ≈0.14[295,298,299] (Figure 16, 7P–R) depending on the synthesis procedure and organometallic characteristics such as polarizability, molar volume, and susceptibility to form chemical bonds with PDMS.[298] Meanwhile, a decrease in PDMS RI by up to 0.0013 has been reported with the addition of zirconate and organogermanium compounds, used as direct fs-laser writing photosensitizers (Figure 16, 7N).[129] With the latter approach, RI changes between 0.002 and 0.004 have been observed after direct writing in PDMS samples containing 2–4 wt% of TiO_2, zirconium isopropoxide, or organogermanium compounds.[84,85] When triethyl(prop-2-enyl)germane (ATEG) was combined with benzophenone a RI change as high as 0.016 was achieved after direct writing.[85,129] For the tested photosensitizer concentrations, the transmittance of 1-mm thick films decreased by up to 10%.[85,129] Despite the desired effect on RI, the addition of such compounds may degrade PDMS elastomeric properties and even prevent the fabrication of optical waveguides free of defects or increase optical attenuation.[129,299]

Regarding metallic nanoparticles, in situ preparation of palladium, iron, nickel, silver, and gold nanoparticles in PDMS has been demonstrated[295,307,308] and RI modulation of PDMS containing silver nanoparticles has been estimated for different particle sizes, concentrations, and temperatures by numerical analysis.[112,309] However, empirical RI measurements are missing in most cases, and in the presence of gold nanoparticles, it has been found that PDMS did not present statistically significant differences in RI at 635 and 1550 nm wavelengths.[295]

3.2.7. Preparing PDMS Copolymers

The preparation of PDMS copolymers by the addition of side groups, different from the methyl groups already present in PDMS chemical structure, can be used to modulate the RI as well.[56,60,295,300] The degree of RI change is dependent on the chemical nature of the side group and the degree of substitution. PDMS copolymers have been prepared by attaching naphthyl-, anthracyl-, and *n*-perfluorooctyl-ethylene groups to poly(dimethyl-co-methylhydrogen)siloxane, P(DMS-*co*-MHS), via hydrosilylation. The copolymers whose chemical structures are given in **Figure 20** showed an RI change as high as 0.28 when modified with aromatic side groups, whereas the addition of *n*-perfluorooctyl side groups caused a RI drop of 0.04 compared to the P(DMS-*co*-MHS) with 2.4 %mol MHS, Fig. 16 8U.[300] The lower RI presented by perfluorinated PDMS makes it particularly suitable to be used as a cladding material.[17] The combination of this strategy with the incorporation of metal alkoxide has yielded an RI increase of 0.14 (635 nm) at 10 mol% Ti (Figure 16, 8Q).[295] This RI difference is of the same magnitude as of the incorporation of metal oxide nanoparticles. Because the change is at the molecular structure level, this method, while more laborious, may provide a more homogeneous RI distribution and greater long-term RI stability.

3.3. PDMS Post-Processing

Any processing step that occurs after PDMS crosslinks into a solid elastomer is considered post-processing. Various post-processing techniques have been employed to modify the optical, mechanical, and surface properties of PDMS, such as the direct writing technique described in Section 3.1.3. In Section 3.3, thermal post-curing, solvent-assisted post-processing, and several surface modification methods are presented and discussed.

3.3.1. Thermal Post-Curing

One of the simplest post-processing methods is to post-cure PDMS at high temperatures, e.g., 165 °C for 48 h or 200 °C for 4 h. It has been used as a tool to reduce the volatile content in PDMS, for example, low molar mass silicones and solvents in accordance with safety regulations[44,156] and to delay the hydrophobic recovery after plasma treatment.[310] The extent of volatile compound evaporation depends on the sample's surface-to-volume ratio, post-curing temperature,[156] duration,[310] and potentially on the mixing ratio owing to unreacted low molar mass silicones. Post-curing has also been used to guarantee a proper cure,[44] to modify the mechanical properties[64] (as discussed in section 2.4), and to enhance stability over time of PDMS's mechanical and electrical properties (e.g. electrical breakdown strength).[132] Prolonged

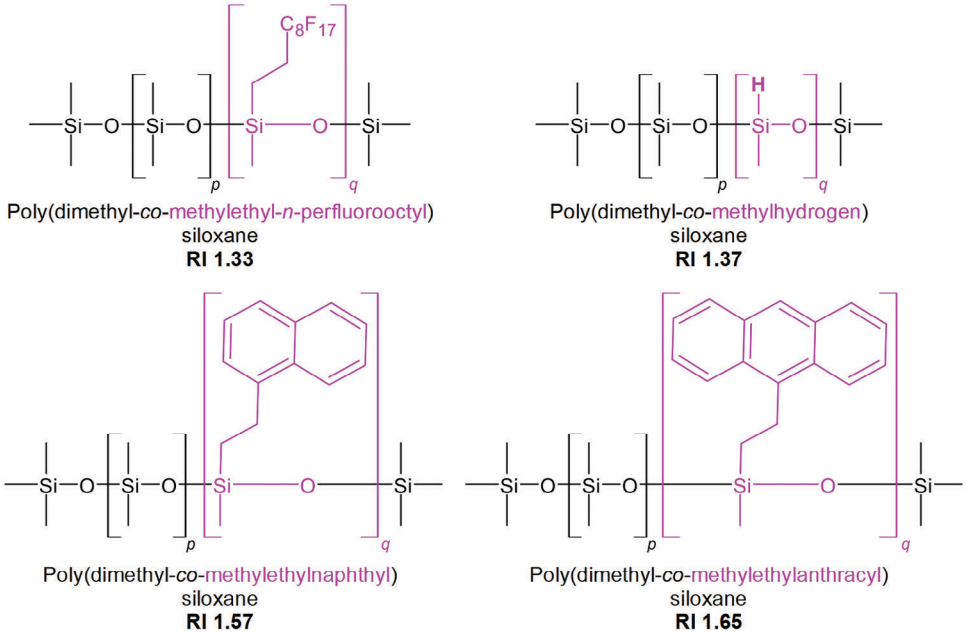

Figure 20. Chemical structure representation of PDMS copolymers and their respective refractive index as reported in ref. [300]. Indices *p* and *q* refer to a varied number of repeat units in the copolymer structure. Repeat units different from PDMS ($SiOC_2H_6$) are highlighted in magenta.

exposure to high temperatures (>90 °C), however, may lead to thermal oxidation and degradation of mechanical properties.[139]

3.3.2. Solvent-Assisted Post-Processing

Solvent extraction is undoubtedly another straightforward post-processing technique for removing low-molar-mass silicones from PDMS.[34–41,311] It was used to extract cyclic and linear dimethylsiloxane oligomers to promote plasma bonding[41] or to slow down the hydrophobic surface recovery.[34,312–314] In this sense, Park et al. investigated the bonding susceptibility of several commercial PDMS using oxygen plasma-induced surface modification. They found that oxygen plasma bonding occurred only when PDMS presented a Shore A hardness above 15.[41] They reasoned that the lower hardness could indicate a greater amount of silicone oligomers migrating to the surface, hindering the bonding reaction. After solvent extraction using toluene, the hardness increased to 15, at which point plasma bonding was possible.[41]

Alternatively, Ryabchun et al. used chloroform solutions of benzophenone derivatives to post-dope PDMS films for subsequent grating engraving with a 355-nm laser diode. The authors were able to add up to 4 wt% of benzophenone using the solvent swelling technique.[264] Meanwhile, Almutairi et al. used a benzophenone solution to prepare the PDMS surface for polymer grafting.[314] Toxicity and flammability represent notable disadvantages of using organic solvents.

3.3.3. Oxidative Surface Treatments

Post-modifications of PDMS surface properties have been extensively researched, most notably in the field of microfluidic applications.[315–317] Table S4 (Supporting Information) summarizes some of these approaches, including water contact angle values and remarks. A comprehensive recent review on PDMS surface wettability modification can be found in Neves et al.[318] Oxidation of PDMS surface via plasma, corona discharge, and UV/ozone treatments constitute the most common post-modification processes. Plasma treatment consists in using an ionized gas to interact with the PDMS surface. It has been used to bond and assemble PDMS parts, such as in waveguide fabrication by soft lithography (see Section 3.1.2),[92,153] to improve epoxy adhesion to PDMS,[311] to turn PDMS surface hydrophilic or to create reactive sites for grafting or coating.[62,311,318–320] Although PDMS can easily attach to itself due to van del Wals intermolecular interactions, irreversible intramolecular bonding occurs via the reaction between silanol groups. Under certain conditions, enough reactive sites are generated on PDMS surface by its exposure to air (or oxygen) plasma.[311,321,322] When exposed to oxygen plasma, several chemical reactions take place along with the formation of silanol groups. For instance, some Si—OH groups form new Si–O–Si bonds that are responsible for the irreversible bonding between plasma-treated PDMS parts.[311,323] Furthermore, a small amount of methyl groups are oxidized to alcohol (C—OH), ketone (C═O), carboxylic (O—C═O), and ether (C—O—C) groups besides the formation and release of volatile species such as carbon dioxide (CO_2).[311] When treated with ammonia plasma, a weak layer of amino-functional groups is formed with no resistance to polar solvents. The extent of surface modification and hence, changes in wettability are controlled by the process gas used, plasma power, and treatment time.[311]

Besides plasma, other oxidative treatments capable of generating a graded, thin, and stiff silica-like layer (SiOx) with elevated oxygen and reduced carbon content on the PDMS surface include UV irradiation,[267,324–326] corona discharge,[327] and ion

beam irradiation[276] which are discussed in further detail below.

- UV irradiation: Aside from creating waveguide structures in PDMS, UV irradiation has been found to also modify the PDMS surface. Graubner et al., for instance, irradiated PDMS samples using a Nb:YAG laser at 266 nm and reported the generation of hydroxyl groups on the irradiated surface.[267] In another study, PDMS was irradiated with a Xe_2*-excimer lamp at 172 nm in vacuum.[287] In this case, PDMS film thickness decreased by ≈30%, accompanied by an increase of 0.041 in RI, attributed to material removal, changes in composition, and densification of the surface.[287] Steady ozone generation and a series of other photochemical reactions take place when UV irradiation at 185 and 254 nm is carried out in the presence of oxygen. The process is then called UV/ozone treatment.[324,325,328] On the one hand, the required treatment time with UV irradiation is typically longer than plasma, which allows a slower formation of the silica-like layer and a deeper penetration up to 14 µm into a PDMS sample.[325] On the other hand, it represents extra processing time and cost. Moreover, in a particular study, the measured bonding strength of UV/ozone-treated bonded PDMS parts was one fourth of that of O_2-plasma-treated ones.[260] Thus, the treatment conditions must be finely adjusted to prevent premature bond failure.
- Corona discharge: It consists of electrical discharges, typically produced by a Tesla coil, that initiate chemical reactions on PDMS, leading to an oxidized layer of up to 100 nm in thickness.[327] For treatment times between 1 and 3 h, the hydrophobic recovery rate has been found to increase with crosslinking density but slower than air plasma treatment. It also presented an Arrhenius-type dependence on temperature.[327] Furthermore, corona-bonded PDMS parts performed similarly to O_2-plasma-bonded ones.[261]
- Ion beam irradiation: Chemical and surface wettability changes have been induced by a 2 MeV helium ion (He^+) beam in ultra-vacuum. The PDMS surface with an initial contact angle of ≈107° became considerably more hydrophilic as the irradiation dose increased, reaching a contact angle plateau at around 60°. The generation of an oxidized and uniform layer of around 9 µm, free of cracks and compact enough was believed to hinder the typical hydrophobic surface recovery observed after plasma, UV/ozone, and corona treatments, as the infrared spectra of the modified surface remained stable for over 5 months.[276]

The thickness of the silica-like layer varies between 5 and 200 nm according to the processing conditions and analytical method used to measure this layer.[323,325,326,328,329] The changes in the surface composition also influence the mechanical properties. The elastic modulus of an O_2-plasma-modified layer was estimated at 37 MPa, which is 10 times higher than the measured modulus of the bulk,[329] and was susceptible to cracking upon mechanical deformation. An increase in modulus and a change in other mechanical properties have similarly been observed in UV/ozone-treated samples.[325] Cracking has been reported for prolonged UV/ozone or plasma treatment times caused by shrinkage and cumulative thermo-mechanical stress between the dissimilar PDMS bulk and its surface.[312,323,324,329]

It is well known that, for most oxidative treatments, PDMS-oxidized surfaces can easily recover their hydrophobicity, and the surface properties once obtained partially degrade within a few minutes to a few dozen days after treatment.[310,311,326,327] It is generally accepted that this recovery is explained by the diffusion and migration of highly mobile low-molar-mass oligomers to the PDMS surface with time to lower the surface free energy, which corroborates with the quicker recovery of thinner samples because of the shorter diffusion path.[310,311,313,325] It has been observed that for O_2-plasma-treated samples, the recovery driving force is proportional to the modification extent, meaning that the more silanol groups formed, the faster the recovery to the original hydrophobicity.[311,327] The process can be further accelerated by microcracks formed due to internal stresses or mechanical deformation during handling,[319,327] through which the oligomers can rapidly diffuse. To extend the durability of the oxidized hydrophilic layer, the treated PDMS must be put in contact with water or polar organic solvents.[62,319] If kept in a gaseous atmosphere, regardless of its composition, a hydrophobic recovery will occur.[323] Other devised strategies to achieve long-term stability of the oxidized surface include the extraction of low-molar-mass silicones by post-curing,[310] solvent extraction[312–314] or cold storage at −80 °C that was demonstrated to extend hydrophilicity for at least 100 days.[330]

3.3.4. Other Surface Post-Modification Methods

Polymer coating is a long-lasting approach to tuning the surface chemistry of PDMS with other functional groups and could be further explored as PDMS waveguide coatings for spectroscopy and biosensing, as pointed out in the IPSR-I.[331] In this sense, a variety of polymers have been grafted onto the surface of PDMS using numerous strategies. Polymers have been anchored to the reactive groups via silanization following a plasma treatment,[248,311,316,319,320] or UV irradiation.[314] In situ polymerization has been undergone using cerium IV catalyst,[332] UV photogenerated radicals,[333] and chemical vapor deposition (CVD) polymerization.[260,334] CVD-polymerization was carried out following sublimation, pyrolysis, and condensation steps on the PDMS surface kept at 15 °C. Chen et al. used this process to coat the PDMS surface with two different reactive polymers for bonding different parts. This process provided excellent adhesion not only between PDMS parts but also between PDMS and a wide range of materials, including glass, PTFE, and metals, in most cases with bonding strength superior to O_2-plasma-bonded PDMS parts cured at 120 °C.[260] More recently, poly(vinyl alcohol) (PVA),[335,336] and polydopamine[337] have been used to coat the PDMS surface using static and dynamic solution deposition, with reported stability between 7 and 30 days. Metal nanoparticle coating has been accomplished by immobilizing gold nanoparticles onto the PDMS surface or in situ reduction of chloroauric acid ($HAuCl_4$) using chitosan or a PDMS residual curing agent.[315]

By allowing a precursor solution containing the metal alkoxide to diffuse into the PDMS it is also possible to prepare a sol-gel metal oxide layer. After diffusion, the metal alkoxides are hydrolyzed with water, rendering an inorganic oxide layer similar to the approach used to tune the PDMS refractive index.[315,338]

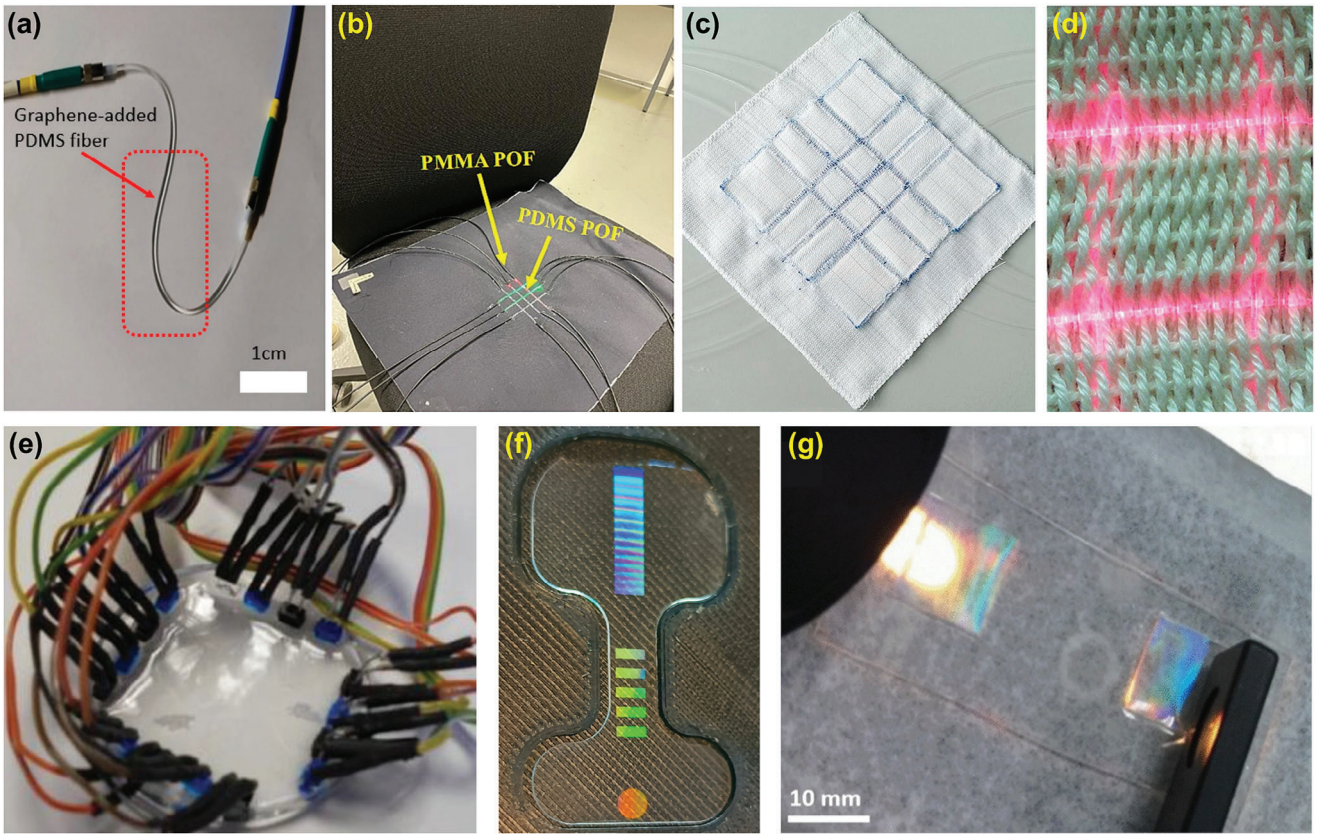

Figure 21. PDMS optical waveguide photos: a) Single fiber, doped with graphene. Reproduced with permission under the terms of CC-BY 4.0 license (https://creativecommons.org/licenses/by/4.0/).[6] Copyright 2019, The Authors, published by MDPI. b) PDMS patch 3 × 3 fiber array, sewn to a fabric and placed on a chair for real-time sensing. Reproduced with permission under the terms of CC-BY 4.0 license.[94] Copyright 2023, The Authors, published by Elsevier. c) PDMS patch 3 × 3 fiber array sewn between fabric sheets. Reproduced with permission.[52] Copyright 2017, Elsevier. d) 2 × 2 fiber array weaved into cotton woven textile. Reproduced with permission under the terms of CC-BY 3.0 license (https://creativecommons.org/licenses/by/3.0/).[53] Copyright 2008, The Authors, published by MDPI. e) Planar waveguide with integrated LEDs and photodiodes. Reproduced with permission under the terms of CC-BY 3.0 license.[342] Copyright 2013, The Authors, published by MDPI. f) Dog-bone shaped planar waveguide under white light showing the diffraction gratings. Reproduced with permission under the terms of CC-BY 4.0 license.[341] Copyright 2022, The Authors, published by MDPI. g) Planar waveguide with light-coupling via nanogratings at the ends. Reproduced with permission under the terms of CC-BY 4.0 license.[349] Copyright 2012, The Authors, published by Springer Nature.

This method, however, may change the dimensions and geometry of the PDMS substrate, which must be accounted for in the waveguide design.[317] Furthermore, layer-by-layer (LBL) assembly has been achieved by immersing PDMS in a series of polyelectrolyte solutions of opposite charge.[315,316] Brown et al., for example, used positively charged polyethylenimine and negatively charged polystyrene sulfate solutions to coat PDMS with six alternating layers.[145] Other LBL polyelectrolyte pairs include chitosan and DNA, and PVA and glycerol.[315–317] As the process is based on physisorption, the durability of the deposited layers is dependent on the medium characteristics with which they will come into contact, such as temperature, pH, and solution composition.[317] Taking advantage of the dynamic (temporary) adsorption of some nonionic surfactants that can strongly adsorb onto the PDMS surface, Tween-20, polyoxyethylene dodecanol, *n*-dodecyl-D-maltoside, and polyethylene oxide block copolymers have also been used to temporarily coat PDMS's surface.[315,317]

Recently, surface modification approaches have been employed to impart pH, glucose, and matrix metalloproteinase (MMP) sensitivity to PDMS waveguides for would healing monitoring.[248] It consisted of a plasma treatment to activate the PDMS surface, followed by a silanization reaction with (3-aminopropyl)triethoxysilane (APTES). The resulting amino-functionalized surface served as a substrate for the covalent attachment of fluorescein isothiocyanate (FITC) and core-shell glucose oxidase functionalized silica nanoparticles for pH and glucose sensing, respectively. To impart sensitivity to MMP, the PDMS waveguides were coated with poly(diallyldimethylammonium chloride) after plasma treatment and functionalized with FITC-conjugated chitosan gelatin-based nanoparticles.[248] This demonstrates PDMS's great versatile for surface modification. The benefits of other post-modification methods in the design and preparation of innovative waveguides remain to be investigated. Further advancements in post-modification techniques may enable the development of PDMS waveguides with dynamic features, novel cladding materials, and customized sensitivity, ultimately leading to improved performance and expanded functionality.

4. PDMS Waveguide Applications

PDMS optical waveguides have been employed in a variety of applications leveraging the material's promising properties. These applications can be grouped into five main categories which will be reviewed in the following subsections: sensing applications, optogenetics and other biomedical applications, optical interconnects, optofluidic devices, and solar energy harvesting.

4.1. Sensing Applications

Within this subsection, the diverse applications of PDMS waveguides are systematically examined in sensing technologies, categorized according to their respective measurands: mechanical strain (or stress), flow, chemicals, and miscellaneous (temperature, and UV light).

4.1.1. Strain Sensors

The idea of using PDMS optical waveguides as stress, strain, touch, or displacement sensors can be traced back to patents dating to the 1980s[339,340] thanks to PDMS mechanical, optical, and skin-like properties. As such, a plethora of mechanical strain sensor designs composed of fiber arrays, single fibers, fibers knitted into or sewn to textiles, or planar waveguides can be found in the literature as depicted in **Figure 21** and summarized in **Table 3**. Such waveguide-based strain sensors are relevant for healthcare monitoring of breathing rate,[6,7,288] pressure wounds,[52,94,252] electronic skin,[341,342] soft robotics,[94,343] wearables,[7,51–53,233,344] among others.

The working principle of most stress/strain sensors is based on microbending loss due to frustrated total internal reflection. It implies that geometrical and refractive index changes in the waveguide induced by mechanical stress or strain, result in a proportional variation in the propagating optical signal that can be detected and transduced into a magnitude of deformation (or stress). Typically, the monitored variable is the transmitted optical power intensity, and only requires a photodetector located in the output end of the waveguide. Alternatively, the detection method can be based on wavelength shifts, and requires an optical spectrometer.[239,345] Other monitoring strain modalities involving PDMS but out of the scope of this review include diffraction wavelength and diffracted angle shifts, as well as reflected color variation achieved by means of diffraction gratings in bulk PDMS,[84,264,304,346,347] and photonic multilayer cladding.[348]

Recent advancements have seen the incorporation of dyes,[7,252] benzophenone,[9] luminescent upconversion nanoparticles (UCNPs)[251] and graphene[6] into PDMS waveguides, aiming to enhance sensitivity to mechanical deformation and impart additional functionalities such as temperature monitoring[251] (Table 3). In this regard, Liang et al. have identified copper-doped zinc sulfide (ZnS:Cu) mechanoluminescent particles as a promising material for combining with PDMS to fabricate self-powered optical waveguides. The authors prepared an optical waveguide comprised of a methylphenyl siloxane core, PDMS cladding, and a 3-cm-long sensing area doped with ZnS:Cu particles. The ZnS:Cu phosphors converted the mechanical strain into a mechanoluminescent light signal, which dispensed the need for a light source.[352] In an alternative approach to improve PDMS waveguide performance, a gold reflective layer was wrapped around the waveguide core, inducing microcracks under strain that modulated the transmitted light intensity and exhibited a dependence on distinct deformation modes.[343,350] Furthermore, a PDMS waveguide cantilever has been proposed for use as a disposable microoptoelectromechanical system (MOEMS) due to its low cost, ease of processing, and monolithic integration compared to silicon nitride waveguides. The devised waveguide cantilever presented a resonant frequency of 83 ± 1 Hz, and numerical mechanical and optical sensitivities of 48 μm mg^{-1} and 14 dB mg^{-1}, respectively despite the low quality factor of 5.1 ± 0.4.[353]

Shape recognition and spatial resolution have also been part of recent efforts in devising e-skins, touch screens, and biomedical pressure mapping devices based on PDMS waveguides.[53,242,342,351,354,355] Koeppe et al. (2009), for example, combined a PDMS waveguide with a position sensitive device constituted of organic photodiodes, which was able to detect the pressure site based on the light scattered out of the waveguide with a precision better than 1 mm after calibration.[355] From the standpoint of data and signal processing, neural networks[351] and tomography backprojection[342] have been employed to this end. Moreover, Mak et al. developed an autoregression-based learning framework for 3D shape decoding. The authors first used multiphysics finite element analysis (FEA) to optimize the position of LEDs and photodiodes in the PDMS waveguide. Computational FEA was then applied to enriching the sparsely collected data for model training, showing good reliability over 1000 motion cycles.[354]

4.1.2. Flow Sensors

Flow sensing finds application in industrial processes, water plant treatments, environmental monitoring, and medical instruments. The working principle of waveguide-based flow sensing also relies on microbending optical losses, but in this case, induced by fluidic drag forces on the waveguide surface. To exploit this phenomenon, high aspect-ratio PDMS waveguides have been prepared as micropillars for airflow detection, as depicted in **Figure 22a–c**. The devised sensor demonstrated limits of detection between 0.55 and 1.82 mm•s^{-1} depending on the waveguides' aspect ratio for steady airflow regimes, and resonance frequencies near 100 Hz.[238] Concurrently, tapered PDMS waveguides have been devised for liquid flow monitoring based on the wavelength shift tracing method. It presented a linear trend up to 600 μL•min^{-1} with a flow rate sensitivity of 2.3 pm•(μL min^{-1})$^{-1}$ and resolution of 1.1 μL•min^{-1} with water.[356]

Inspired by nature, some researchers developed optoelectronic flow sensors based on PDMS waveguides that mimic fish neuromasts (lateral fish hair cells used as a hydrodynamic sensory system),[10,262,357–359] shown in Figure 22d. Klein and Bleckmann,[357] for example, built an artificial lateral line canal (ALLC) with PDMS Elastosil RT 60 (Wacker Chemie) as neuromasts with diameters ranging from 0.4 to 1 mm, a few millimeters long. By combining optical light guiding with MEMS

Table 3. PDMS-based waveguide sensors by proposed applications, core-clad compositions, performance parameters, and remarks.

Proposed application	Composition		Design	Performance parameters	Remarks	Refs.
	Core	Clad				
Biomedical pressure sensing, soft robotics	Sylgard 184 10:1	Air or THV 221AZ (Dyneon)	3 × 3 fiber array, sewn to a fabric	Transverse compressive strength sensitivity of: • Air-clad: 0.065%/kPa • THV-clad: 0.010%/kPa	THV-clad waveguide exhibited localized debonding of the cladding after compression cycles. Both waveguides presented reversible and reproducible changes in optical signal intensity over 10 compressive cycles at loads of 0.1, 1, and 5 N.	[94]
Biomedical pressure sensing	Sylgard 184 20:1 + 0.1 wt% BPh	Air or Sylgard 184 20:1	Single rectangular waveguide	Transverse compressive strain sensitivity, x and y directions, respectively: • Air-clad: 0.10 and 0.06 dB/%ϵ • PDMS-clad: 0.06 and 0.03 dB/%ϵ	Higher sensitivity in the x direction due to its reduced thickness. Thermal stability under a fixed 150-mmHg load at 38 °C, stretchable up to 150% elongation. Sensitivity decreased in core-clad samples	[9]
Wearables and smart textiles, joint motion detection	Sylgard 184 10:1 + 5×10^{-4} wt% graphene	Air	Single fiber	Not informed	Maximum elongation of 150%. Length stability over 500 cycles. Good repeatability and sensitivity in detecting a range of human body motion. Used for monitoring breathing, wrist, elbow, knee and hand movements. Similar response in water or air.	[6]
Smart bandage for wound dressing	Sylgard 184 10:1 + 2.5×10^{-4}% Rhodamine B	Air	Fiber embedded in gauze fabric and hydrocolloid wound dressing	Transverse compressive stress sensitivity: ≈1.6 a.u./kPa Transverse compressive strength dynamic range: 0.1–0.3 kPa Low detection limit: 0.1 kPa	Strain and pH dual sensing. Two different signal demultiplexing techniques were tested and compared, based on changes in optical power intensity or wavelength shift	[252]
Wearables and smart textiles, human motion detection	Sylgard 184 10:1 + (2.5×10^{-4} to 1×10^{-3}) wt%/v Rhodamine B	Air	Single fiber	Tensile strain dynamic range: 0–100% Tensile strain sensitivity: 0.86–3.62 dB/ϵ	Measurements taken as the dual wavelength differential loss. Several diameters and dye concentrations tested. Used for monitoring deep breathing, speaking, and finger motion	[7]
Wearables, human motion detection	Sylgard 184 10:1 + Upconvertion nanoparticles	Air	Single fiber	Not informed	Used for monitoring deep knee, and finger motion. Stability over 5k cycles at 60% strain. Temperature and strain dual sensing with sensitivity crosstalk of 6% between 20–80°C.	[251]
Wearables, structural health monitoring	Sylgard 184 10:1	Air	Single fiber	Tensile strain dynamic range: 0–40% Tensile strain sensitivity: 3.5 a.u. of optical loss/ϵ	Turning point and decreased sensitivity above 25% tensile strain. Tensile strain and brine concentration dual sensing	[233]
Microfluidic soft sensing	1 part of PDMS + 9 parts of EcoFlex Gel (Smooth-On)	Gold (Au) layer + (PDMS: EcoFlex gel) mixture	Single semi-circle waveguide	Transverse compressive strength dynamic range: 0–200 kPa Tensile strain dynamic range: 0–90%	Black coating to prevent ambient light interference. Detection of multiple deformation modes: pressure, stretching and bending. Optical signal was independent of loading rate and consistent over 30 stretching cycles	[350]
Soft robotics	Sylgard 184 20:1	100 nm Ti + 300 nm Au layer + PDMS	Single semi-circle waveguide	Transverse compressive strength sensitivity: 3.5×10^{-5} μW/kPa Tensile strain sensitivity: 2.5×10^{-4} μW/mm	Elongation at break of the sensor varied with tensile strain rate. Good signal repeatability for over 30 cycles of compression or elongation, even though some drift was observed with cycling. Hysteresis loop ascribed to a low sensitivity in the low force range and the relaxation time of PDMS	[343]

(*Continued*)

Table 3. (Continued)

Proposed application	Composition		Design	Performance parameters	Remarks	Refs.
	Core	Clad				
Wearables and smart textiles	Geniomer 200 (Wacker Chemie)	THV (Dyneon)	2 × 2 fiber array weaved into cotton woven textile	Transverse compressive force dynamic range: 0–30 N Lateral resolution:10 mm	Waveguides with smaller diameter were more sensitive to load but reached saturation faster. The top fibers at the intersections were more sensitive due to direct contact with the strain source. Cross-sensitivity not significant. Optical signal drift <4.6% over 25 compression cycles	[53]
Wearables and smart textiles, computing systems	Geniomer 100, 100-HDS, and 175	Air	Single fiber sewn to a woven textile (FRTT1022), in a "half-oval" design	Transverse compressive force dynamic range: 0.05–40 N	PDMS content of 70–90% depending on Geniomer formulation. Geniomer 175 worked better at lower forces, and Geniomer 100-HDS at larger ones	[51]
Smart textiles, pressure ulcer monitoring	Geniomer 100 (Wacker Chemie)	Air	1 × 1 fiber array, inserted into laser-welded breathable polyester channel	Transverse compressive force dynamic range: 0–6 N Sensitivity: 3.8%/N Recovery time: 3s	Withstood 250 cycles of compressive loading-unloading	[52]
Smart textiles. Friction, and pressure monitoring socks	Geniomer 100	Air	3 knitted inlay structures: single jersey, 1 × 1 rib, and 1 × 1 interlock, and a knitted sock	Curves were fitted by a second order polynomial and evaluated qualitatively	Single jersey presented larger sensitivity in compression and friction tests. Sensitivity was higher in friction. This structure was chosen to knit a sock with 3 optical fibers at different positions along the sock	[344]
Electronic skin, touch screen, soft robotics	Sylgard 184 10:1	Air	Planar waveguide	Transverse compressive strength dynamic range: 0–160 kPa Peak sensitivity: 1.93 kPa^{-1}	Strain location reconstruction with technique similar to tomography backprojection. Limited spatial resolution due to the small number of emitters and detectors used, 8 of each, but enough to show multiple simultaneous loadings	[342]
Electronic skin	Sylgard 184 10:1	Air	Planar waveguide. Light coupling via nanogratings	Transverse compressive force dynamic range: 0–1 N Tensile strain sensitivity: 0.1 dB/%	Tested under compressive force with a PE foam on top to minimize the direct contact of the testing tip. Hysteresis of ≈20% after 5 compression cycles. Minimum bending radius of 1.7 mm	[341]
Tactile sensing, wearables, pressure sensing	PDMS 10:1	Air	Planar waveguide. Light coupling via nanogratings	Tensile strain dynamic range: 0–12.5% Transverse compressive force dynamic range: 0–0.023 N	The waveguide presented good stability over 3k stretching cycles	[349]
Pressure sensing, touch screen	Sylgard 184 10:1	Fluoro silane coating	Planar waveguide. Light coupling via nanogratings	Transverse compressive strength dynamic range: 0–35 kPa Peak sensitivity: 0.2 kPa^{-1} Response time: 300 ms	Non-linear response, and small hysteresis. Higher sensitivity in the 0–5 kPa range. Good stability over 900 loading-unloading cycles. Pressure sensitivity declined with organic LED and photodiodes	[242]
Distributive pressure and shear sensing, shape decoding	Sylgard 184 10:1	Air	Crisscrossing waveguide array of 4 × 4	Transverse compressive force dynamic range: 0.05–0.2 N	Neural network for data processing, four different pressure shapes and loading magnitudes were identified with accuracy of >97%	[351]

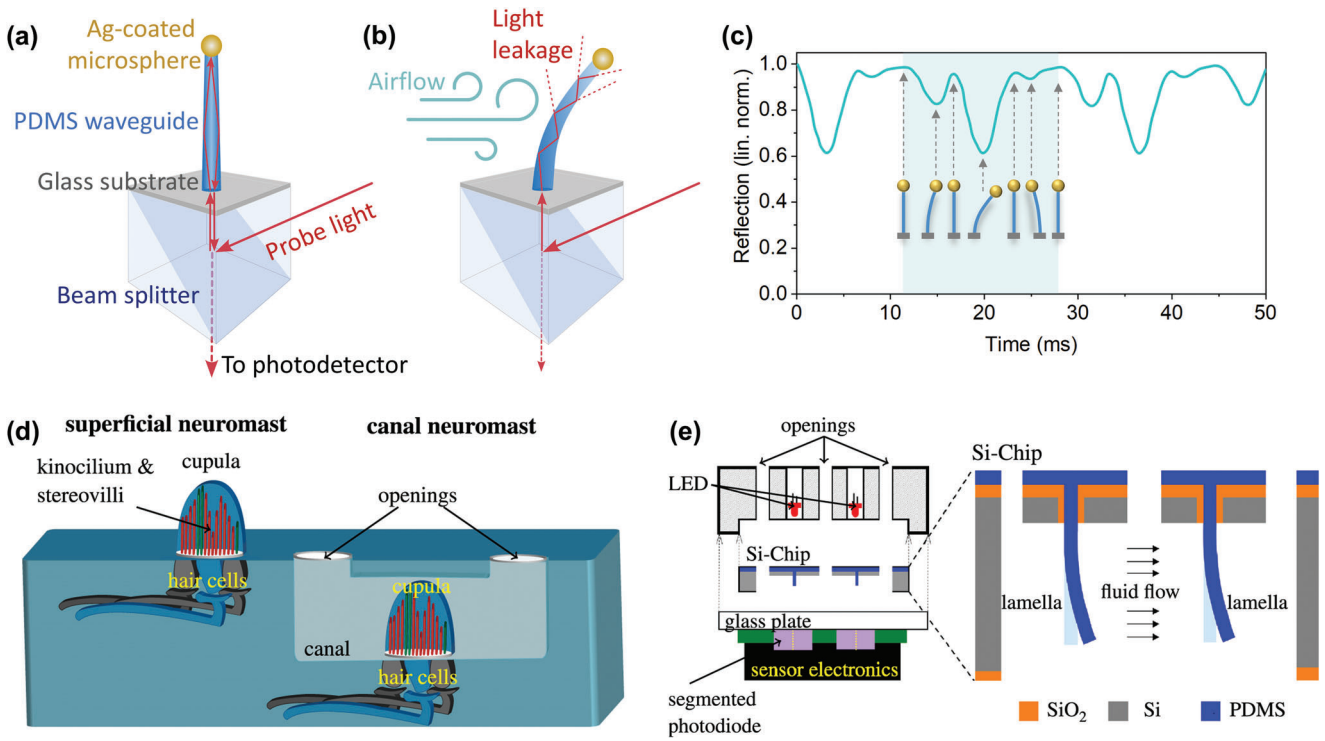

Figure 22. Schematic representation of the airflow sensor working principle based on PDMS waveguides (micropillars): a) the initial upright PDMS waveguide reflects back the probe light, whereas in b) the light intensity that reaches the photodetector decreases under airflow due to bending losses. c) Reflection change plot in response to sound waves at 60 Hz. Based on data extracted from ref. [238]. d) Schematic representation of a fish lateral line superficial and canal neuromasts. A gelatinous cupula covers the hair cells from which kinocilium and stereovilli (or stereocilia) grow. The hair cells are connected to support cells and sensory nerves. e) Schematic representation of a neuromast bioinspired flow sensor based on PDMS waveguides (in blue). d,e) Reproduced with permission.[262] Copyright 2015, IOP Publishing.

technology, measurements were based on the degree of deflection of the waveguides, which produced a variation in the amount of light reaching the phototransistor located near one of the ends. The sensor was capable of detecting finger movements 2-cm apart alongside the ALLC, water motion, and vortices. Furthermore, the bulk flow velocity, size and position of the object that caused the perturbation could be determined from the collected hydrodynamic data. A similar approach was used to build an airflow sensor, as shown in Figure 22e, exhibiting a dynamic range of 2–42 m s^{-1}. It could withstand velocities up to 47 m s^{-1} and remained undisturbed by sound waves or electrical noise.[262] Intending to improve bending sensitivity and allow its operation with opaque and corrosive fluids, a sealing layer has been added to other proposed flow sensors.[358,359] Such a flow sensor has also been proposed for use as a disposable low-cost spirometer.[10]

4.1.3. Chemical Sensors

Chemical sensors are indispensable in a myriad of applications that involve the detection and quantification of chemical species. In this context, PDMS waveguides have been proposed for volatile organic compound (VOC) detection,[76] liquid identification,[360] pH monitoring,[248,252] and glucose,[248] matrix metalloproteinase (MMP),[248] and salt quantification.[233] For instance, PDMS tapered waveguides were able to detect acetone vapor at concentrations up to 17000 ppm with a sensitivity of ≈4.2 × 10^{-4} nm ppm^{-1} and a resolution of 4.8 ppm.[76] Furthermore, an innovative PDMS pillar-type waveguide sensor containing gold nanoparticles (Au), **Figure** 23a, has been proposed for the identification of various liquids and implementation in a robotic finger. The working principle was based on guided and radiated optical modes dependent on the optical properties of the liquid under analysis. The sensor response was measured as a variation in transmitted optical intensity, Figure 23b, by collecting the light in the region above the pillars that worked as a T optical junction.[360]

In recent years, there has been a growing interest in the development of smart wearable bandages for wound monitoring, with the ultimate goal of enhancing wound care management and consequently patient outcomes. By doing so, these advanced wound dressings aim to reduce the healthcare burden and associated costs, especially in the context of chronic and pressure wounds. Monitoring their progression can be achieved by assessing key parameters, e.g., pH, glucose, and localized pressure. Leal-Junior et al., for example, doped a PDMS waveguide with a pH-sensitive dye, rhodamine B. The waveguide was embedded in gauze fabric and hydrocolloid wound dressing for use as a pH and pressure dual-sensing smart bandage (Figure 23c). It presented a sensitivity of 0.67 nm pH^{-1} unit (Figure 23d) with response and recovery times of 17.2 and 31.5 s•pH^{-1}, respectively.[252] Besides pH, Giovannini et al. developed

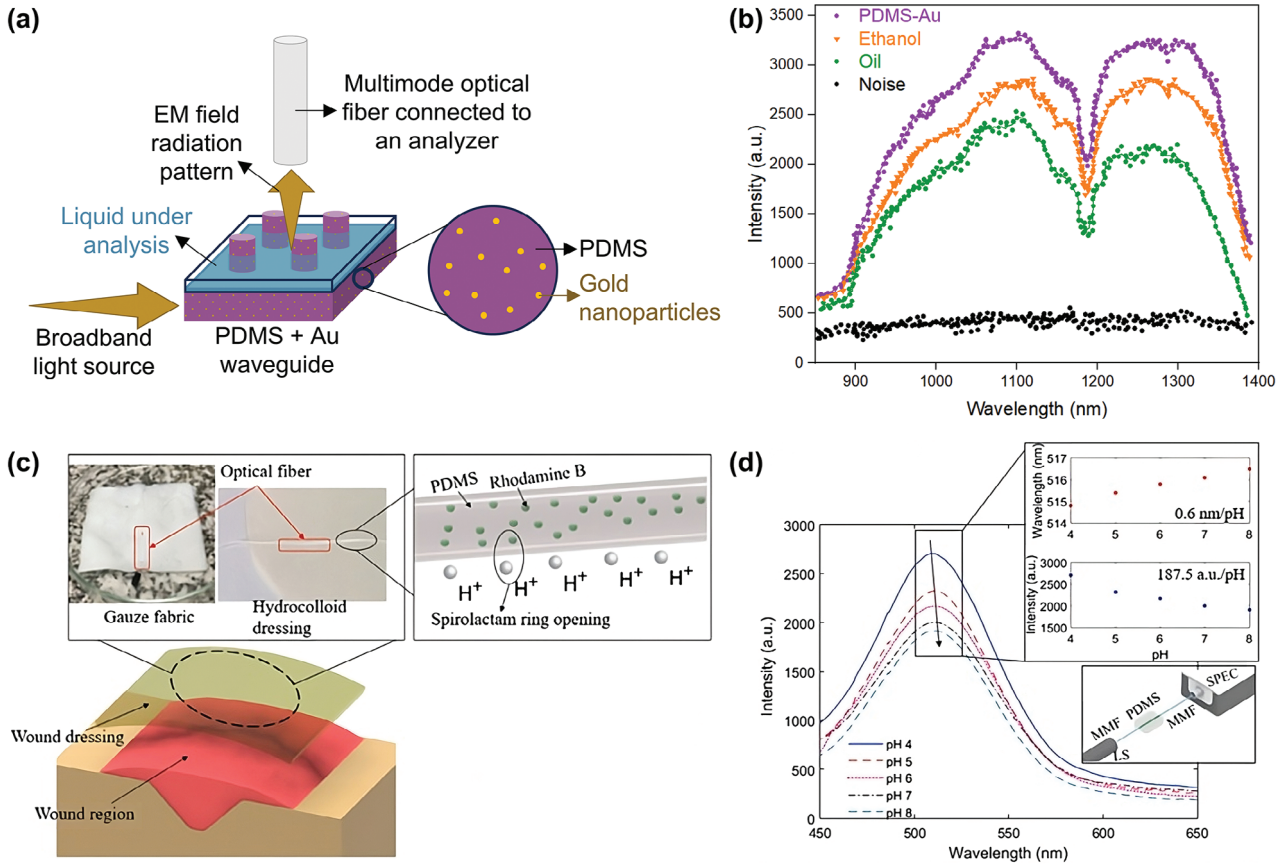

Figure 23. a) Schematic representation of the pillar-type sensor fabricated with PDMS-Au nanoparticles. b) Transmitted optical spectra as a function of analyzed liquid. Data extracted from ref. [360]. c) Schematic representation of the smart bandage with the rhodamine-doped PDMS waveguide embedded in the wound dressing. d) Transmitted optical spectra of the smart bandage as a function of pH. Insets highlight the wavelength shift and the optical intensity variation evolution with pH, and the experimental setup used in the measurements. c,d) Reproduced with permission.[252] Copyright 2021, Chinese Laser Press.

a wearable multi-sensor comprising three surface-functionalized PDMS waveguides for simultaneous pH, glucose, and MMP assessment. The waveguides were integrated into a commercial cotton pad and validated using complex solutions, including a simulated wound exudate. Following calibration, the wearable device demonstrated accurate quantification of the targeted parameters within relevant ranges for wound healing assessment, as detailed in Table S5 (Supporting Information).[248]

4.1.4. Miscellaneous Sensors

Thermally sensitive UCNPs have been embedded into PDMS for the fabrication of luminescent waveguide temperature sensors, as given in **Figure** 24a.[8,251] Upon excitation with a near-infrared laser (980 nm), the UCNPs exhibited dual-wavelength emission at 525 nm and 545 nm, whose intensity ratio was used for signal detection. The sensor exhibited a linear and rapid responsivity from 25 to 70 °C, with a detection limit of ±0.3 °C, and sensitivity of 1.8%•°C^{-1}. No hysteresis was observed over heating-cooling processes, with a stable performance under tensile strain up to 80% and under bending. The latter sensor was tested on a volunteer for monitoring the temperatures of the skin and mouth, as well as monitoring nasal breathing with good repeatability, as shown in Figure 24b,c.[8] In another study, the authors used the UCNP-doped PDMS waveguides for temperature and strain dual-sensing.[251] Demultiplexing the optical signal was accomplished considering that the emission at 525 nm is independent of temperature.

Recently, a novel approach to UV sensing has been demonstrated, wherein polydimethylsiloxane (PDMS) optical waveguides are doped with the UV-sensitive dye spiropyran (Figure 18), offering a flexible alternative to conventional stiff UV photodetectors. Because of the spiropyran-to-merocyanine isomerization triggered by the UV-A light, the formation of the merocyanine-colored species caused a sharp decrease in the optical signal of a He-Ne laser (633 nm). The developed optical sensor exhibited a reversible and consistent response over many irradiation cycles and under bending, with a sensitivity of 115% cm^2 J^{-1}, a dynamic range of 0–0.4 J cm^{-2}, and decay and recovery time constants of 42 and 107 s, respectively. The sensing parameters could be tailored by white light, waveguide length, and temperature.[96]

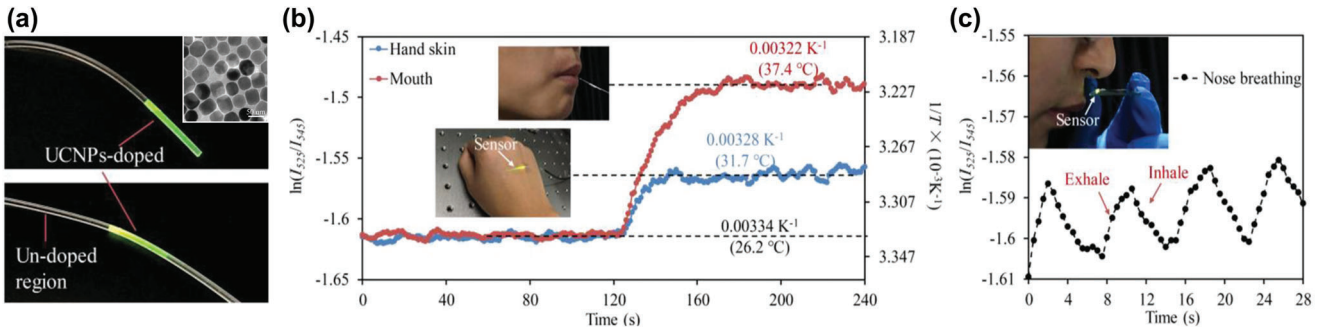

Figure 24. a) Visible green emission under near-infrared excitation of the UCNPs-doped regions in the PDMS waveguide. Inset shows a transmission electron microscopy image of the UCNPs. b) Sensor response when in contact with the hand or mouth of a volunteer. c) Sensor response to nose breathing. a–c) Adapted with permission.[8] Copyright 2019, John Wiley and Sons.

4.2. Optogenetics and Other Biomedical Applications

Optogenetics is an emerging healthcare technique based on light neuromodulation to potentially treat a range of neural conditions such as epilepsy and Alzheimer's disease. It consists of introducing opsins, light-reactive proteins, into neurons and activating them via optical neural implants as exemplified in Figure 25a.[361] The minimal light intensity required for opsin activation is estimated at ≈10 mW mm^{-2}. This value might be higher, depending on the distance from the light source, positioning, etc. Light

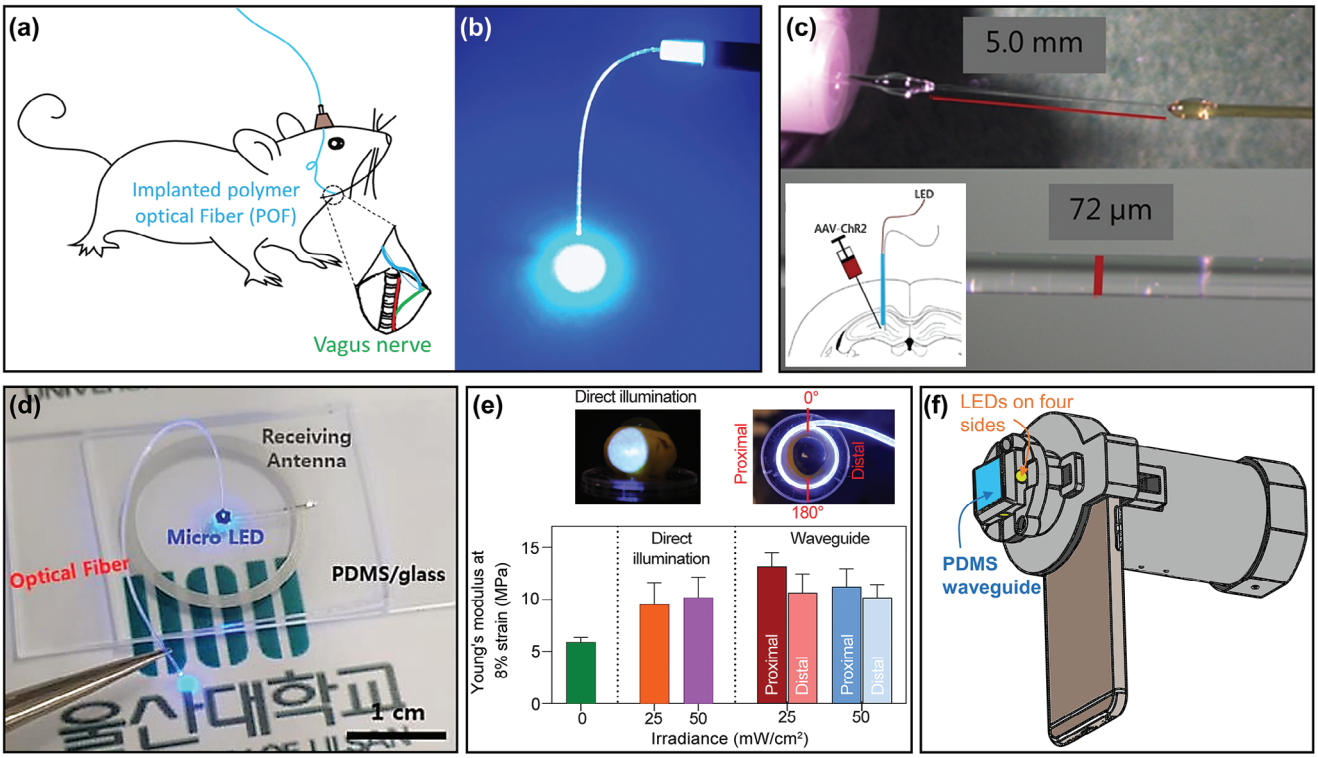

Figure 25. a) Schematic illustration of the PDMS waveguide for vagus nerve stimulation in mice. b) Picture of the waveguide coupled to a blue light source. a,b) Adapted with permission under the terms of CC-BY 4.0 license.[20] Copyright 2023, The Authors, published by Springer Nature. c) Top: Picture of a PDMS waveguide used for optogenetic stimulation attached between a Plexon stub (left) and a commercial optical fiber (right). Bottom: a close-up lateral view indicating the PDMS fiber diameter and inset showing a schematic representation of the optogenetic experimental setup, including a viral injection of AAV-ChR2 and the PDMS waveguide (blue) connected to an LED. Adapted with permission under the terms of CC-BY 4.0 license.[19] Copyright 2023, The Authors, published by Springer Nature. d) Picture of a wireless optogenetic device with PDMS waveguide coupled to a blue micro LED and a receiving antenna on a PDMS/glass substrate. Adapted with permission under the terms of CC-BY 4.0 license.[253] Copyright 2023, The Authors, published by MDPI. e) Top: pictures of the sclera under direct light and with a PDMS waveguide wrapped around it for crosslinking. Bottom: a plot of Young's modulus at 8% strain of the sclera under different treatment conditions. Adapted with permission under the terms of CC-BY-NC-ND 4.0 license.[13] Copyright 2017, The Authors, published by ARVO. f) Schematic representation of the smartphone-based compression-induced scope prototype built with a PDMS waveguide and LEDs as probe for breast cancer screening, based on ref. [365].

delivery by direct implantation of LEDs or silica fibers at the stimulation sites is associated with discomfort and undesired mechanical and thermal damage to the tissues.[249,253,362] Thus, PDMS' biocompatibility, ability to deliver light to deep tissues without exacerbated heating, and mechanical properties close to those of biological tissues make it an ideal candidate for this field of application, as attested by recent efforts.[12,19,20,95,103,253,363,364]

Rudmann et al., for instance, prepared core-clad PDMS waveguides with cores measuring between 130 and 200 µm of side length, and 3–8 mm long for optical stimulation of optogenetically modified cochlea of a Mongolian gerbil. The waveguides were inserted in the inner ear for in vivo hearing activation with promising results despite the high optical losses obtained (4.8 dB cm^{-1} at 472 nm).[249] Zhao et al. prepared a hybrid flexible intracortical penetrating optical PDMS waveguide electrode measuring 300 µm of diameter and with lengths between 5 and 20 mm, capable of delivering light intensity between 11.3 and 70.4 mW•mm^{-2} for optogenetics.[364] Additionally, 4.5 cm long PDMS core with poly(vinyl alcohol)/poly(acrylic acid) interpenetrating polymer network (PVA/PAA IPN) cladding waveguides have been prepared with a diameter of 250 µm. They were proved effective when implanted into the primary motor cortex of freely moving mice for vagus nerve optogenetic stimulation (**Figure 25**a,b). By delivering adequate light power to the targeted area, the mice experienced motor impairment, decreased heart rate, and prolonged anxiolytic-like behavior. The PDMS waveguides presented excellent long-term biocompatibility and stability after 4 weeks of implantation.[20] In another study, PDMS waveguides (Figure 25c) presented a reduced inflammatory response compared to silica fibers following a 6-week implantation in the brains of rats. The delivered light intensity increased in the first week and roughly stabilized afterward.[19] Nonetheless, this study also pointed out some disadvantages of the use of PDMS waveguides. Because of the sticky surface, there is a higher chance of small dust particles adhering to the surface, which can increase optical losses and cause contamination of the operation site. A guide pin is usually required during implantation because of its flexibility, and the light leakage along the waveguide can potentially activate opsins in undesired locations or cause wanted behavior if noticed by the animal.[19] To tackle some of these drawbacks, poly(lactide-co-glycolide), a stiff but biodegradable polymer, was employed as a temporary shell. The shell was expected to degrade within the postoperative period of 3–10 days, resulting in a PDMS core only by the time of the optogenetic stimulation.[253]

Apart from optogenetics, PDMS waveguides have been used for scleral cross-linking.[13] Scleral crosslinking is another potential medical intervention that has been proposed to prevent severe myopia progression by stiffening the equatorial band of the sclera. Light at the blue end of the spectrum is combined with a photosensitizer (riboflavin) to induce intermolecular collagen crosslinking. It is considered less invasive and ensures better light distribution than lasers and other light-delivery devices introduced in the eye cavity. To demonstrate its feasibility, 10 cm long flat and tapered rectangular PDMS waveguides were wrapped around fresh adult porcine eyes. It was found that tapered waveguides delivered light more uniformly than flat ones along the treated area and delivered similar power efficacy as direct laser illumination,[13] as shown in Figure 25e. A PDMS waveguide illuminated with LEDs has also been employed to capture compression-induced images as part of a smartphone-based compression-induced scope (SCIS-T) (Figure 25f). By compressing the soft waveguide against the target, the light scatters into an iPhone CMOS image sensor, from which an image is created for further analysis. This device may become an important tool in the identification of inflammatory breast cancer up to 3 mm deep in tissue based on color, texture, and temperature changes.[365] Other biomedical applications in which PDMS waveguides have yet to be exploited include phototherapy to treat infections and cancer,[366–368] in vivo deep tissue imaging,[369,370] photochemical tissue bonding,[371] and real-time monitoring of biomarkers.[372,373]

4.3. Optical Interconnects

The use of electro-optical printed circuit boards (PCBs) has garnered significant attention over the past two decades, principally driven by the need to enhance bandwidth density in high-performance computing systems. This need has been further exacerbated by the exponential growth in data volumes resulting from the widespread adoption of artificial intelligence, which is currently hindered by the limitations of electrical interconnects.[374,375] Optical waveguides in general present smaller propagation delay and higher bit rate compared to electrical wires.[374] Because of the relatively low optical losses in the datacom region of 600–1600 nm, multimode PDMS waveguides have been proposed for use in variable optical attenuators (VOAs)[108] and for the fabrication of cost-effective low-loss and high bandwidth optical interconnects.[108,115,376–379] In addition, PDMS waveguides are immune to electromagnetic interference, and set themselves apart from waveguides made from stiffer materials by allowing unmatched versatility in design and assembly.[377] These unique properties were demonstrated with the fabrication of single-mode rib Y-branch splitters[98] and other unconventional designs.[105]

A bit error rate lower than 10^{-12} has been reported for digital data transmission at 10 Gbit•s^{-1} using PDMS waveguide arrays.[113] In another study, PDMS waveguide arrays developed for chip-to-chip high-speed optical backplane transmission (**Figure 26**a,b) presented error-free transmission up to 15 Gbit s^{-1} with negligible crosstalk.[378] Moreover, PDMS waveguide arrays with integrated sources and detectors, Figure 26c,d, exhibited optical losses below 0.7 dB under bending and 30% tensile strain, without visible degradation of the optical link after 80,000 stretching cycles at 10% elongation.[153] When tested for integration into PCBs and their multiple fabrication steps, PDMS waveguides performed well, presenting very low optical attenuation at 850 nm and consistent adhesion strength to the laminates that typically compose a PCB.[114,115]

More recently, Dominguez et al. prepared an intrusive passive optical tapping device (Figure 26e), for use in data networks as well. The authors stacked multiple PDMS planar waveguides to form a device with a tailorable number of optical sniffers by adding or removing such layers. Although thicker waveguides reduced insertion losses (Figure 26f, D1 vs D2), they resulted in a less balanced light coupling to the outputs in the proposed configuration. Interestingly, PDMS waveguides containing trapped

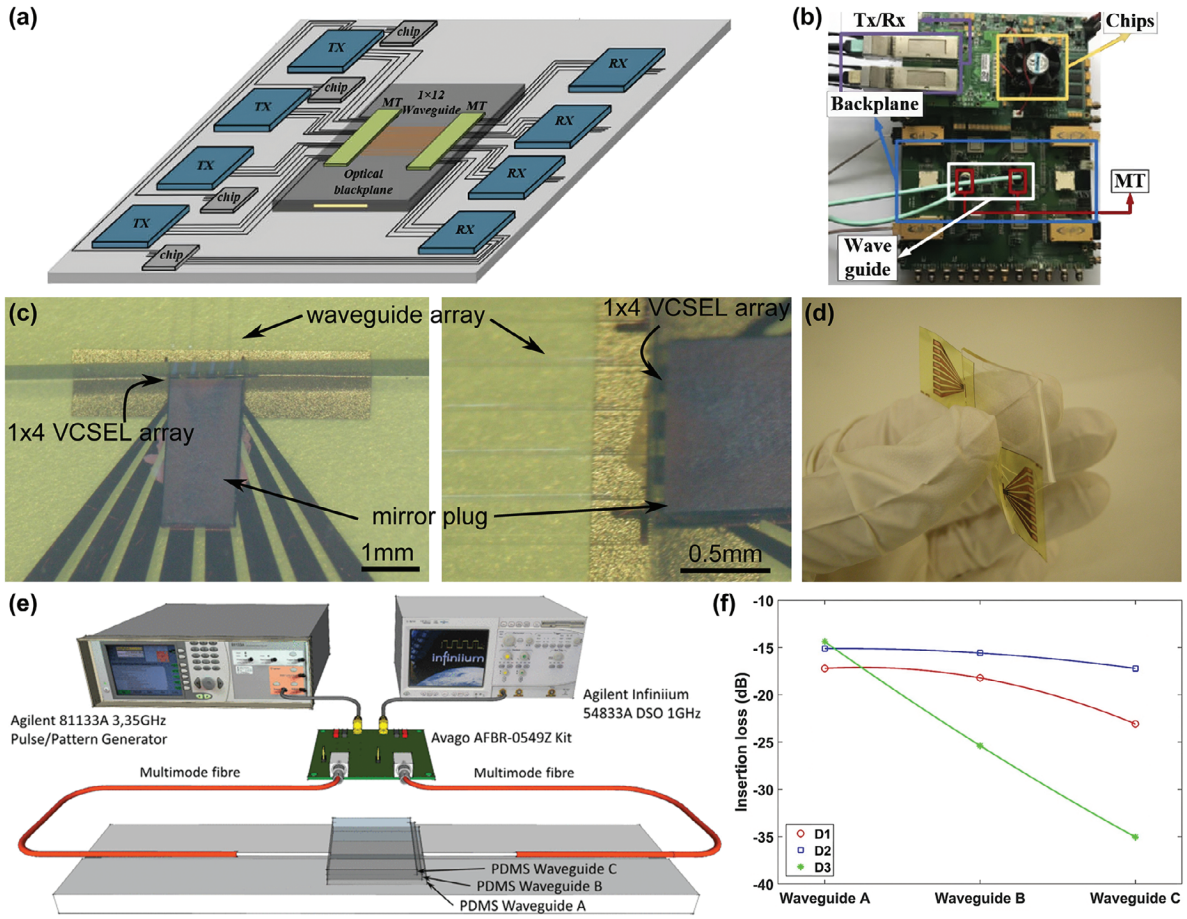

Figure 26. a) Schematic representation of a chip-to-chip high-speed optical waveguide backplane, and b) a photograph of the optical communication backplane system. a,b) Reproduced under the terms of the OSA Open Access Publishing Agreement.[378] Copyright 2020, The authors, published by The Optical Society. c) Photograph of a PDMS waveguide array coupled to an embedded 1 × 4 vertical-cavity surface-emitting laser (VCSEL) array, and (d) a photograph of the full stretchable optical link. c,d) Reproduced with permission.[153] Copyright 2014, The Optica Society. e) Optical setup for performance evaluation of the optical tapping device. f) Plot of insertion loss for three waveguide configurations; D1: thicker waveguides (0.8 mm) with trapped bubbles, D2: thinner waveguides (0.5 mm) with trapped bubbles, and D3: thinner waveguides without bubbles. e,f) Adapted with permission under the terms of CC-BY 4.0 license.[250] Copyright 2021, The Authors, published by IEEE.

air bubbles facilitated coupling between stacked waveguides because of the higher scattering, and were preferred instead of the bubble-free ones even though incurring in higher insertion loss.[250] A planar PDMS waveguide has also been employed to couple probe light into a gallium phosphide planar photonic crystal (PPC) nanocavity array as part of a compact high-resolution spectrometer.[380]

Despite the promising results, some challenges remain to be addressed for the effective commercialization of PDMS waveguide interconnects such as optimized optical losses below 0.1 dB cm^{-1} at all wavelengths over the next decades.[2,375] PDMS waveguides also require more waveguide division multiplexing channels to match electrical interconnect bandwidth density, as well as more space between waveguides to prevent crosstalk because of the large mode field diameter.[374] Such drawbacks could be minimized by the development of graded-index PDMS waveguides instead of the typical step-index architecture. Furthermore, they are more susceptible to dust contamination because of their sticky nature, and to temperature fluctuations during operation. Finally, their wider adoption is dependent on the development of design flows, standardization, packaging methods, and tools not just for better temperature management but also for its integration into already existing photonic and electronic technologies.[2,375]

4.4. Optofluidic Devices

The integration of PDMS optical waveguides is also advantageous in microfluidics and lab-on-a-chip applications for the development of seamlessly connected components with limited use of dissimilar materials. Integrated optofluidic devices enable cost and size reductions and enhanced performance due to better contact and alignment of the optical elements.[258,259,284] Lien et al., for example, prepared fluidic-photonic integrated circuits with PDMS waveguide arrays for highly sensitive cytometric detection (suspended particles and cells).[258] Flow cytometry is an important analytical tool for counting white blood cells, detecting

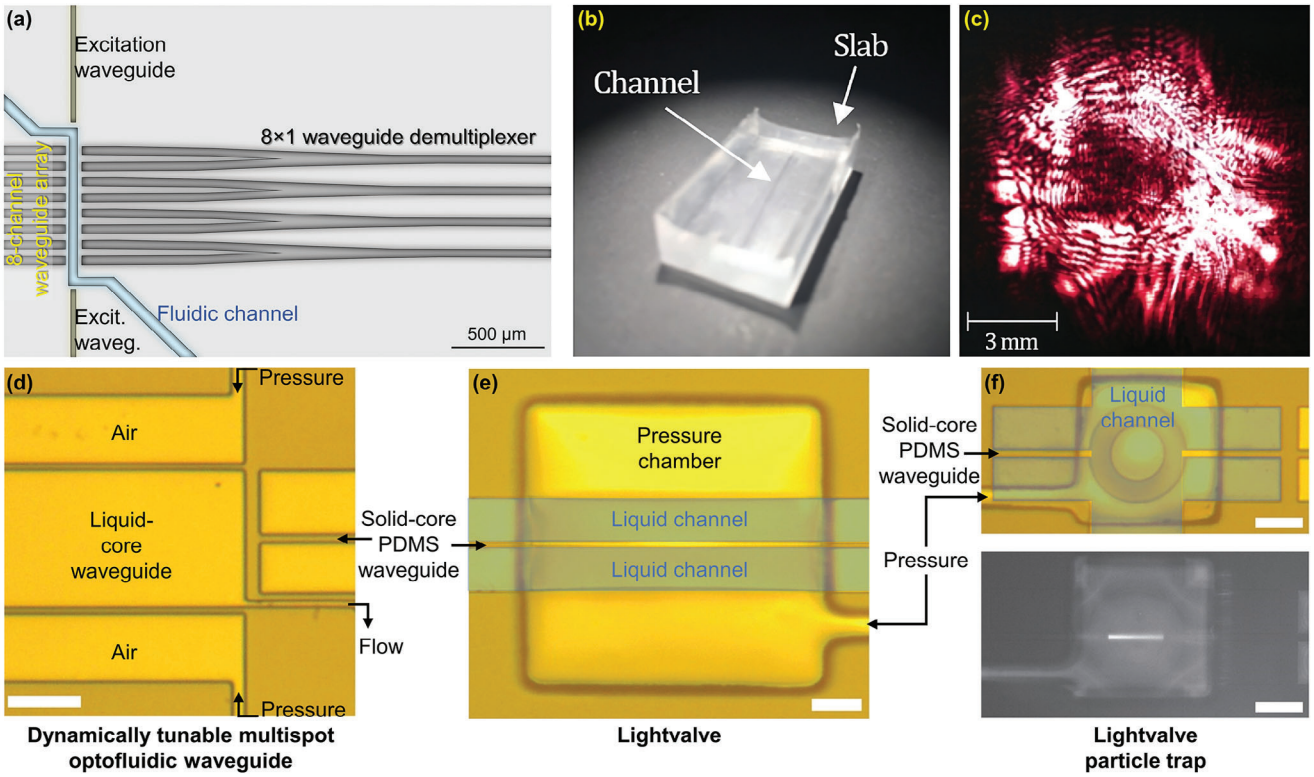

Figure 27. a) Schematic representation of an optofluidic device showing the 8 × 1 PDMS waveguide array presented in ref. [258]. b) Photograph of a PDMS gradient-index optofluidic device whose channel passes at the center of the waveguide, and c) the output light profile captured by a camera. b,c) Reproduced with permission.[296] Copyright 2017, The Optica Society. d) Micrographs of the dynamically tunable multi-mode interference (MMI) waveguide, e) lightvalve, and f) lightvalve particle trap (top), all in the empty state. f, bottom) Image of the lightvalve particle trap filled with a fluorescent solution and excited with a 488 nm laser coupled to the solid-core PDMS waveguide on the left (not shown). d–f) Adapted with permission under the terms of CC-BY 4.0 license.[383] Copyright 2016, The Authors, published by Springer Nature.

cancer, and sorting stem cells, to name a few. The device comprised an array of 8 parallel waveguides integrated monolithically with the microfluidic channels (**Figure 27a**), so that a single cell was detected 8 times. The design allowed for the use of an array of 8 detectors or to combine the waveguide's output into a single detector and demultiplex the signals in the time-domain. Both configurations yielded signal detection sensitivity nearly 1000 times higher due to improved signal-to-noise-ratio even for very small cell sizes (1-μm), compared with single-channel devices.[258] Another sophisticated microfluidic photonic integrated circuit for cell sorting was prepared by Cho et al. with low and high refractive index polysiloxanes.[259] Similar efforts have been devoted to the use of liquid PDMS pre-polymers as optical waveguides.[381,382]

Besides cell counting, Odeh et al. prepared a PDMS gradient-index optofluidic device (Figure 27b,c), where the fluid under analysis was transported in the center of the waveguide, while the graded-index profile ensured light guidance by TIR.[296] This configuration was believed to enhance the interaction between fluid and guided light and, hence, its performance in evanescent sensing applications.[296] Moreover, Parks and Schmidt demonstrated the fabrication of optical waveguides capable of simultaneously acting as fluidic microvalves (Figure 27e–f).[383] One of the lightvalve designs was used to trap bioparticles for fluorescence detection analysis and withstood 100,000 switching cycles without degradation. The same authors also devised a multimode interference (MMI) waveguide composed of solid-PDMS-core and liquid-core waveguides (Figure 27d). The optofluidic platform was able to create length- and wavelength-dependent spot patterns upon the propagation of multimodes. By changing the core liquids or applying pneumatic or hydraulic pressures, the waveguide modes could be easily engineered for multiplexed detection of biological samples.[383] Despite the mentioned advances, PDMS waveguide coating and other surface modifications mentioned in Section 3.3.4. are yet to be exploited, for example, in microfluidic biosensing.

4.5. Solar Energy Harvesting

PDMS waveguides are playing an important role in solar energy harvesting systems as luminescent solar concentrators (LSCs). An LSC is an optical waveguide doped with luminophores that, upon solar radiation, re-emit light at longer wavelengths, as depicted in **Figure 28a**. This light is then guided by TIR along the waveguide structure until it reaches the solar cells at the edges of the waveguide for conversion into electricity. For instance, Chou et al. reported an external photon efficiency (η_{ext}) of 29.3% with an LSC made of PDMS doped with disodium fluorescein (DSF) combined with a backside reflective layer.[384] By

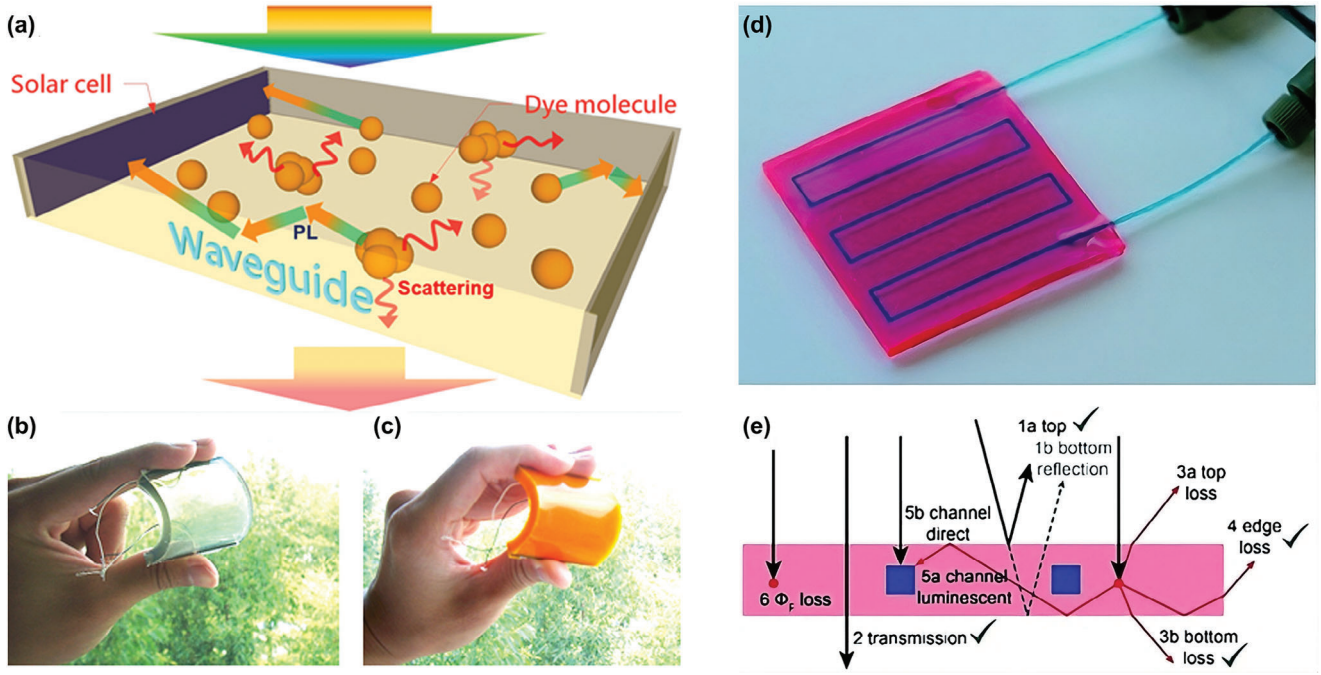

Figure 28. a) Schematic representation of a LSC made of PDMS doped with luminescent dyes as part of a flexible waveguiding photovoltaic module, and photographs of these modules doped with b) C440, and c) DSF. a–c) Reproduced with permission.[384] Copyright 2015, Elsevier. d) Photograph of an LSC-PM based on PDMS doped with Lumogen F red 305. e) Schematic representation of the possible fate of the photons reaching the LSC-PM: 1a) top reflection, 1b) bottom reflection, 2) transmission, 3a) top emission, 3b) bottom emission, 4) edge emission, 5a) luminescent photons, 5b) direct irradiation, and 6) non-radiative losses. d,e) Reproduced with permission under the terms of CC-BY-NC 3.0 license.[388] Copyright 2017, The Authors, published by RSC.

stacking a PDMS waveguide doped with coumarin 440 (C440) onto a DSF-doped PDMS waveguide, the η_{ext} further increased to 33.2% while improving the device efficiency (η_{dev}, LSC-PV system) from 4.6% to 5.2%. Both PDMS waveguides doped with C440 and DSF are shown in Figure 28b,c, respectively. In addition, Sadeghi et al. were able to achieve an η_{ext} as high as 37% and a η_{dev} of 0.9% in solar cells whose LSC consisted of fluorescent copper-doped indium phosphide (InP) quantum dots embedded into PDMS waveguides.[385] Furthermore, wearable LSCs have been fabricated with coumarin 6 embedded into an amphiphilic polymer conetwork composed of PDMS and an acrylate phase. When integrated with fiber dye-sensitized solar cells (FDSSC), the two-side configuration reached a η_{dev} of 7.85%, which represents an improvement of up to 84% compared to the bare FDSSC.[386]

PDMS-based LSCs have also been used to harvest solar energy for efficient and sustainable photochemical reactions. Inspired by the photoreaction mechanisms found in vegetable leaves, microfluidic channels designed into a LSC slab fabricated with doped PDMS served as the flow photoreactors, named LSC-PhotoMicroreactors (LSC-PMs), Figure 28d.[387,388] The luminophore, Lumogen F red 305, and the reaction photocatalyst, methylene blue, were carefully selected based on their spectral features in the visible range. The working principle is based on the absorption of incident sunlight by the luminophore and its re-emission at a longer wavelength range that matches the absorption spectrum of the photocatalyst. The emitted photons are guided within the waveguide, reaching the channels filled with the reaction medium, Figure 28e. The photocatalyst then triggers the photoreactions inside the microreactor channels. When LSC-PMs were tested using outdoor sunlight, reaction conversion increased from 57% to 96% on average, with reduced susceptibility to fluctuations in cloud coverage, highlighting the promising application of this approach in the sustainable production of pharmaceuticals and organic compounds.[387]

5. Current Limitations and Future Prospects

PDMS is a well-established polysiloxane whose properties have been exhaustively studied over the years. It is a very versatile polymer that combines optical transparency, great flexibility and stretchability, a wide working temperature range, biocompatibility, and environmental safety. Most of the research on PDMS optical waveguides, however, has been limited to addition-cured two-component systems, owing to the convenient availability of cost-effective commercial formulations. This has helped democratize and grow the research on PDMS waveguides and their applications in the last decade. Still, the interesting properties of PDMS have fueled the development of copolymers, different crosslinking routes, and post-modifications that have yet to be exploited in waveguide technology. For instance, with the advances in thermoplastic and self-healing PDMS, we should expect not only the fabrication of continuous waveguides via industrially compatible melt-processing techniques but also with unique new properties. Additionally, UV-Curable PDMS represents a viable option for the fast production of waveguides to be further explored

in photolithography, and even in the fabrication of long fibers via fiber drawing, additive manufacturing, and other processing techniques that allow for a UV light source integration to the fabrication setup. Moreover, PDMS waveguide post-modification such as coating and surface functionalization, remains to be explored in optofluidic devices as a means to improve selective interaction of analytes and device sensitivity.

The development of novel PDMS formulations through filler compounding, doping, and copolymerization necessitates a comprehensive investigation to optimize the balance and trade-offs among various properties. For instance, poly(dimethyl-*co*-methylethylnaphthyl)siloxane presents an RI higher than PDMS, proving the required mismatch for TIR in step-index waveguides. Bulky aromatic groups, however, are known for increasing stiffness and are more susceptible to weathering because of the benzene rings. The vibrational spectrum in the infrared region also changes, which may cause unwanted attenuation at certain wavelengths. Meanwhile, fluorinated PDMS copolymers have shown smaller RI and absorption loss values compared to PDMS at the near-infrared range. Their use, however, seems limited and less popular, particularly in datacom, where this wavelength range is more useful. Fillers and dopants provide an additional avenue for tailoring specific properties or incorporating supplementary functionalities, such as self-powered waveguides via luminescent particles and reversible modulation of optical properties using photochromic dyes. Nevertheless, it is crucial to consider that these materials are susceptible to aggregation, which can compromise transparency, introduce additional scattering centers, and increase the stiffness of PDMS. Achieving adequate filler dispersion and distribution may necessitate additional processing steps, e.g., ultrasonication and surface modification, which can be costly. Furthermore, changes in biocompatibility and thermal stability are anticipated.

Biocompatibility is an important subject concerning wearable and implantable devices. While PDMS has been extensively used in medical applications and is considered safe for the overall population, long-term side effects in population subsets are an ongoing topic that has to be carefully examined. Furthermore, PDMS is considered inert and does not pose a risk to the environment. Still, aiming towards environmental responsibility and circular economy, it is good practice to mitigate pollution through the development of long-lasting waveguides, thermoplastic recyclable PDMS, and fabrication processes that are energetically efficient, solventless, and zero waste. Continued research and the implementation of efficient chemical recycling strategies through PDMS depolymerization and filler transformation are crucial to providing viable end-of-life alternatives.

PDMS waveguide fabrication techniques are plentiful and provide great versatility for waveguide design, even though they are mostly limited to methods compatible with thermoset processing. Among the many, sometimes creative, solutions to prepare PDMS waveguides, direct writing offers the possibility of preparing micrometric silica-like waveguides in fewer processing steps and with great design flexibility. Fiber drawing is interesting from the point of view of dispensing the use of a mold, with fixed dimensions, and for allowing the preparation of circular waveguides with high aspect ratio. Fiber drawing with thermally assisted fast curing seems to be an alternative for the fabrication of non-tapered PDMS core fibers, contrary to what is typically achieved by this method. Additive manufacturing using UV-curable PDMS may provide the means for automatic integration of optical interconnects thus eliminating laborious manual alignment and fixation in integrated microchips. Processing methods that impart changes in PDMS's original composition, however, such as the formation of a silica-like core or the use of photosensitizers, are expected to impart changes in mechanical performance and need to be better investigated. The same goes for the doping strategies employed to tune the refractive index and post-modification treatments. In this sense, organic photosensitive compounds, particularly those that undergo reversible photoisomerization, can provide additional RI modulation with light and are worth exploiting. Their long-term photostability has to be considered, as they are prone to photooxidation.

PDMS waveguides have shown remarkable promise particularly in optical strain sensing applications, with various designs and adaptable operating ranges proposed in recent years. While these waveguides offer considerable versatility, a key aspect that warrants further investigation is the seamless integration of location awareness and spatial resolution capabilities without resorting to intricate fabrication processes. To fully harness the potential of PDMS waveguides, advancements in algorithm development may be crucial to achieve high-resolution strain mapping. Additionally, the vast majority of PDMS waveguides are step-index and operate in a highly multimode regime. Access and more research in the few- and single-mode regimes and within the near-infrared region of the spectrum could spur new applications of PDMS waveguides in optical communications and interconnects where those regimes are most useful.

Their use has been mostly directed to applications that require short distances, e.g., short-reach interconnects, optical sensing and optogenetics, because of their considerable optical attenuation. The lowest propagation losses found in the literature are still four to five orders of magnitude higher than silica-based optical waveguides. Attenuation can be minimized to a certain extent by reducing mold roughness, removing impurities, and providing efficient light coupling. In this sense, the graded-index architecture could be further exploited to reduce optical attenuation and increase bandwidth by means of fabrication techniques such as the Mosquito method. In addition to optical attenuation, factors such as high thermal expansion coefficient, mechanical hysteresis, stress-softening, and strain-hardening must be considered for accurate long-term performance and reliability assessments. Despite current limitations, PDMS waveguides exhibit vast potential for impactful applications across various fields notably in optical sensing, phototherapy, photochemistry, integrated circuits, and others.

Supporting Information

Supporting Information is available from the Wiley Online Library or from the author.

Acknowledgements

This research was funded by Fonds de Recherche du Québec-Nature et Technologies (grant number 304946), and ÉTS Research Chair in Engineering Marcelle-Gauvreau. All authors read and approved the final

manuscript. C.A.Z. would like to acknowledge the use of the perceptually uniform scientific colormaps by Crameri, F. (2019). Scientific Colour Maps. Zenodo. Retrieved from https://zenodo.org/record/1243862.

Conflict of Interest

The authors declare no conflict of interest.

Keywords

applications, poly(dimethylsiloxane), polymer optical waveguides, processing, properties

Received: July 24, 2024
Revised: September 26, 2024
Published online:

[1] Emergen Research, **2020**, https://www.emergenresearch.com/industry-report/optical-waveguide-market, (accessed: September 2022).
[2] M. Lebby, Polymer Materials, Integrated Photonic Systems Roadmap - International (IPSR-I) **2024**, https://photonicsmanufacturing.org/sites/default/files/documents/polymer_ipsr-i_2024_0.pdf (accessed: June 2024).
[3] H. Bai, S. Li, J. Barreiros, Y. Tu, C. R. Pollock, R. F. Shepherd, *Science* **2020**, *370*, 848.
[4] J. Guo, K. Zhao, B. Zhou, W. Ning, K. Jiang, C. Yang, L. Kong, Q. Dai, *Adv. Opt. Mater.* **2019**, *7*, 1.
[5] C. K. Harnett, H. Zhao, R. F. Shepherd, *Adv. Mater. Technol.* **2017**, *2*, 1700087.
[6] D. Wang, B. Sheng, L. Peng, Y. Huang, Z. Ni, *Polymers* **2019**, *11*, 1433.
[7] J. Guo, M. Niu, C. Yang, *Optica* **2017**, *4*, 1285.
[8] J. Guo, B. Zhou, C. Yang, Q. Dai, L. Kong, *Adv. Funct. Mater.* **2019**, *29*, 1.
[9] K. N. Amouzou, A. A. Romero, D. Sengupta, S. K. Mishra, A. Richard-Denis, J.-M. Mac-Thiong, Y. Petit, J.-M. Lina, B. Ung, *Photonics* **2022**, *9*, 557.
[10] A. T. Stadler, B. Wiesmayr, M. Krieger, W. Baumgartner, *Sensoren Messsyst.* **2018**, 442.
[11] H. Zhao, K. O'Brien, S. Li, R. F. Shepherd, *Sci. Robot.* **2016**, *1*, 1.
[12] A. Ersen, M. Sahin, *J. Biomed. Opt.* **2017**, *22*, 055005.
[13] S. J. J. Kwok, M. Kim, H. H. Lin, T. G. Seiler, E. Beck, P. Shao, I. E. Kochevar, T. Seiler, S.-H. Yun, *Invest. Ophthalmol. Visual Sci.* **2017**, *58*, 2596.
[14] V. Prajzler, M. Neruda, P. Nekvindová, *J. Mater. Sci. Mater. Electron.* **2018**, *29*, 5878.
[15] J. Guo, C. Yang, Q. Dai, L. Kong, *Sens. Switz.* **2019**, *19*, 1.
[16] B. M. Quandt, L. J. Scherer, L. F. Boesel, M. Wolf, G.-L. Bona, R. M. Rossi, *Adv. Healthcare Mater.* **2015**, *4*, 330.
[17] Y. Koike, K. Koike, *J. Polym. Sci. Part B Polym. Phys.* **2011**, *49*, 2.
[18] J. T. M. Pinto, K. J. Amaral, S. Hartard, P. R. Janissek, K. Helling, *J. Clean. Prod.* **2017**, *165*, 762.
[19] M. A. Andersen, J. Schouenborg, *Sci. Rep.* **2023**, *13*, 16090.
[20] Y. Cao, S. Pan, M. Yan, C. Sun, J. Huang, C. Zhong, L. Wang, L. Yi, *BMC Biol.* **2021**, *19*, 1.
[21] O. Podrazký, P. Peterka, I. Kašík, S. Vytykáčová, J. Proboštová, J. Mrázek, M. Kuneš, V. Závalová, V. Radochová, O. Lyutakov, E. Ceci-Ginistrelli, D. Pugliese, N. G. Boetti, D. Janner, D. Milanese, *J. Biophotonics* **2019**, *12*, 1.
[22] E. Arrospide, I. Bikandi, I. García, G. Durana, G. Aldabaldetreku, J. Zubia, in *Polym. Opt. Fibres Fibre Types Mater. Fabr. Characterisation Appl*, (Eds: C.-A. Bunge, T. Gries, M. Beckers), Woodhead Publishing, Sawston, UK **2017**, pp. 201–216.
[23] D. Zaremba, R. Evert, in *Polym. Opt. Fibres* (Eds: C.-A. Bunge, T. Gries, M. Beckers), Woodhead Publishing, Sawston, UK **2017**, pp. 153–186.
[24] W. D. Callister Jr., D. G. Rethwisch, *Materials Science and Engineering: An Introduction*, John Wiley & Sons, Hoboken, NJ **2010**.
[25] S. H. Kim, J.-H. Moon, J. H. Kim, S. M. Jeong, S.-H. Lee, *Biomed. Eng. Lett.* **2011**, *1*, 199.
[26] J. E. Mark, D. W. Schaefer, G. Lin, *The Polysiloxanes*, Oxford University Press, New York, USA **2015**.
[27] M. J. Owen, P. R. Dvornic (Eds.), *Silicone Surface Science*, Springer, Netherlands, Dordrecht **2012**.
[28] A. R. L. Colas, J. Curtis, in *Biomater. Sci. Introd. Mater. Med.*, Elsevier Academic Press, California, USA, **2005**, pp. 697–707.
[29] F. O. Stark, J. R. Falender, A. P. Wright, in *Compr. Organomet. Chem.*, Pergamon, Oxford, UK **1982**, Vol. *2*, pp. 305–363.
[30] D. Wang, J. Klein, E. Mejía, *Chem. – Asian J.* **2017**, *12*, 1180.
[31] G. C. Lisensky, D. J. Campbell, K. J. Beckman, C. E. Calderon, P. W. Doolan, R. M. Ottosen, A. B. Ellis, *J. Chem. Educ.* **1999**, *76*, 537.
[32] S. Venkatachalam, D. Hourlier, *Ceram. Int.* **2019**, *45*, 6255.
[33] P. Mazurek, S. Vudayagiri, A. L. Skov, *Chem. Soc. Rev.* **2019**, *48*, 1448.
[34] J. N. Lee, C. Park, G. M. Whitesides, *Anal. Chem.* **2003**, *75*, 6544.
[35] E. Ogliani, L. Yu, P. Mazurek, A. L. Skov, *Polym. Degrad. Stab.* **2018**, *157*, 175.
[36] C. M. Roland, C. A. Aronson, *Polym. Bull.* **2000**, *45*, 439.
[37] X. Shi, *The Crystalline Structure of Polydimethylsiloxane: Additional Results and Additional Questions*, Université Paris-Saclay, Paris, France, **2021**.
[38] H. Zhang, C. Cai, W. Liu, D. Li, J. Zhang, N. Zhao, J. Xu, *Sci. Rep.* **2017**, *7*, 11833.
[39] S. Krpovic, K. Dam-Johansen, A. L. Skov, *J. Appl. Polym. Sci.* **2021**, *138*, 50380.
[40] M. Y. Tang, A. Letton, J. E. Mark, *Colloid Polym. Sci.* **1984**, *262*, 990.
[41] S. Park, K. Mondal, R. M. Treadway, V. Kumar, S. Ma, J. D. Holbery, M. D. Dickey, *ACS Appl. Mater. Interfaces* **2018**, *10*, 11261.
[42] T. Bardelli, C. Marano, F. Briatico Vangosa, *eXPRESS Polym. Lett.* **2022**, *16*, 924.
[43] T. Arends, H. P. Huinink, L. Pel, *Polymer* **2019**, *164*, 8.
[44] J. Heiner, B. Stenberg, M. Persson, *Polym. Test.* **2003**, *22*, 253.
[45] D. Cai, H. M. Heise, in *Mol. Spectrosc. Theory Chall. Adv. Comput. Chem. Phys*, (Eds: A. Koleżyński, M. Król), Springer, Berlin **2019**, pp. 401–425.
[46] M. R. Ramli, M. B. H. Othman, A. Arifin, Z. Ahmad, *Polym. Degrad. Stab.* **2011**, *96*, 2064.
[47] S. Tazawa, A. Shimojima, T. Maeda, A. Hotta, *J. Appl. Polym. Sci.* **2018**, *135*, 45419.
[48] P. Zheng, T. J. McCarthy, *J. Am. Chem. Soc.* **2012**, *134*, 2024.
[49] A. S. Fawcett, M. A. Brook, *Macromolecules* **2014**, *47*, 1656.
[50] B. Yi, S. Wang, C. Hou, X. Huang, J. Cui, X. Yao, *Chem. Eng. J.* **2021**, *405*, 127023.
[51] M. Krehel, R. M. Rossi, G.-L. Bona, L. J. Scherer, *Sensors* **2013**, *13*, 11956.
[52] B. M. Quandt, R. Hufenus, B. Weisse, F. Braun, M. Wolf, A. Scheel-Sailer, G.-L. Bona, R. M. Rossi, L. F. Boesel, *Eur. Polym. J.* **2017**, *88*, 44.
[53] M. Rothmaier, M. P. Luong, F. Clemens, *Sensors* **2008**, *8*, 4318.
[54] Wacker Chemie AG, *Safety Data Sheet: Elastosil R 401/40 S (Version 2.10 US)*, Wacker Chemie AG, München, Germany **2023**.
[55] N. E. Stankova, P. A. Atanasov, Ru. G. Nikov, R. G. Nikov, N. N. Nedyalkov, T. R. Stoyanchov, N. Fukata, K. N. Kolev, E. I. Valova, J. S. Georgieva, St. A. Armyanov, *Appl. Surf. Sci.* **2016**, *374*, 96.

[56] V. Prajzler, P. Nekvindova, J. Spirkova, M. Novotny, *J. Mater. Sci. Mater. Electron.* **2017**, *28*, 7951.
[57] D. Cai, A. Neyer, R. Kuckuk, H. M. Heise, *J. Mol. Struct.* **2010**, *976*, 274.
[58] M.-H. Wu, K. E. Paul, G. M. Whitesides, *Appl. Opt.* **2002**, *41*, 2575.
[59] A. S. Cruz-Félix, A. Santiago-Alvarado, J. Márquez-García, J. González-García, *Heliyon* **2019**, *5*, e03064.
[60] K. Su, J. V. DeGroot Jr., A. W. Norris, P. Y. Lo, in *Proc. SPIE 6029 ICO20 Mater. Nanostructures 60291C* (Eds: W. Lu, J. Young), SPIE, Changchun, China **2006**, p. 60291C, https://doi.org/10.1117/12.667752.
[61] K. Keshmiri, H. Huang, N. Nazemifard, *SN Appl. Sci.* **2019**, *1*, 1.
[62] A. Mata, A. J. Fleischman, S. Roy, *Biomed. Microdevices* **2005**, *7*, 281.
[63] M. J. Owen, *Macromol. Rapid Commun.* **2021**, *42*, 2000360.
[64] R. Seghir, S. Arscott, *Sens. Actuators Phys.* **2015**, *230*, 33.
[65] S. Varaprath, C. L. Frye, J. Hamelink, *Environ. Toxicol. Chem.* **1996**, *15*, 1263.
[66] P. D. Riggs, P. Kinchesh, M. Braden, M. P. Patel, *Biomaterials* **2001**, *22*, 419.
[67] J. A. Barrie, D. Machin, *J. Macromol. Sci. Part B* **1969**, *3*, 673.
[68] B. Balakrisnan, S. Patil, E. Smela, *J. Micromechanics Microengineering* **2009**, *19*, 047002.
[69] R. Dahiya, G. Gottardi, N. Laidani, *Microelectron. Eng.* **2015**, *136*, 57.
[70] J. E. Mark (Ed.), *Polymer Data Handbook*, Oxford University Press, Oxford, UK **1999**.
[71] X. Su, B. Shi, L. Wang, *J. Macromol. Sci. Part B* **2015**, *54*, 1248.
[72] C. V. Rumens, M. A. Ziai, K. E. Belsey, J. C. Batchelor, S. J. Holder, *J. Mater. Chem. C* **2015**, *3*, 10091.
[73] E. Favre, *Eur. Polym. J.* **1996**, *32*, 1183.
[74] W. Chen, J. E. Saunders, J. A. Barnes, S. S.-H. Yam, H.-P. Loock, *Opt. Lett.* **2013**, *38*, 365.
[75] D. Kacik, I. Martincek, *Opt. Fiber Technol.* **2017**, *34*, 70.
[76] O. R. Ranjbar Naeini, A. Barandak, M. M. Tahmasebi, H. Latifi, in *Proc. SPIE 11056, Optical Measurement Systems for Industrial Inspection XI* (Eds: P. Lehmann, W. Osten, A. Albertazzi Gonçalves), SPIE, Munich, Germany **2019**, p. 1105630.
[77] F. Schneider, J. Draheim, R. Kamberger, U. Wallrabe, *Sens. Actuators Phys.* **2009**, *151*, 95.
[78] A. Camenzind, T. Schweizer, M. Sztucki, S. E. Pratsinis, *Polymer* **2010**, *51*, 1796.
[79] A. Zahid, B. Dai, R. Hong, D. Zhang, *Mater. Res. Express* **2017**, *4*, 105301.
[80] J. Liu, G. Zong, L. He, Y. Zhang, C. Liu, L. Wang, *Micromachines* **2015**, *6*, 855.
[81] J. E. Mark, H. R. Allcock, R. West, in *Inorganic Polymers*, Oxford University Press, Oxford, **2005**, pp. 154–199.
[82] G. S. Rajan, G. S. Sur, J. E. Mark, D. W. Schaefer, G. Beaucage, *J. Polym. Sci. Part B Polym. Phys.* **2003**, *41*, 1897.
[83] S. Lee, H. J. Shin, S. M. Yoon, D. K. Yi, J. Y. Choi, U. Paik, *J. Mater. Chem.* **2008**, *18*, 1751.
[84] J.-S. Boisvert, A. Hlil, I. Hassan, J. Thomas, P. Lorre, W. Correr, Y. Ledemi, Y. Messaddeq, R. Kashyap, *OSA Contin.* **2020**, *3*, 1334.
[85] J.-S. Boisvert, A. Hlil, S. Loranger, A. Riaz, Y. Ledemi, Y. Messaddeq, R. Kashyap, *Sci. Rep.* **2022**, *12*, 1623.
[86] F. Sales, A. Souza, R. Ariati, V. Noronha, E. Giovanetti, R. Lima, J. Ribeiro, *J. Compos. Sci.* **2021**, *5*, 1.
[87] Y. Shi, M. Hu, Y. Xing, Y. Li, *Mater. Des.* **2020**, *185*, 108219.
[88] A. Piruska, I. Nikcevic, S. H. Lee, C. Ahn, W. R. Heineman, P. A. Limbach, C. J. Seliskar, *Lab Chip* **2005**, *5*, 1348.
[89] D. W. Van Krevelen, K. Te Nijenhuis, *Properties of Polymers*, Elsevier, Amsterdam **2009**.
[90] X. Zhang, J. Qiu, J. Zhao, X. Li, L. Liu, *J. Quant. Spectrosc. Radiat. Transf.* **2020**, *252*, 107063.
[91] X. Zhang, J. Qiu, X. Li, J. Zhao, L. Liu, *Appl. Opt.* **2020**, *59*, 2337.
[92] Z. Cai, W. Qiu, G. Shao, W. Wang, *Sens. Actuators Phys.* **2013**, *204*, 44.
[93] B. E. A. Saleh, M. C. Teich, *Fundamentals of Photonics*, John Wiley & Sons, Inc, Hoboken, NJ, USA **2019**.
[94] K. Sharma, E. Morlec, S. Valet, M. Camenzind, B. Weisse, R. M. Rossi, F. Sorin, L. F. Boesel, *Mater. Des.* **2023**, *232*, 112115.
[95] J. Feng, Y. Zheng, Q. Jiang, M. K. Włodarczyk-Biegun, S. Pearson, A. del Campo, *Adv. Mater. Technol.* **2022**, *7*, 2101539.
[96] C. A. Zimmermann, K. N. Amouzou, D. Sengupta, A. Kumar, N. R. Demarquette, B. Ung, *Front. Optoelectron.* **2024**, *17*, 21.
[97] D. Jandura, D. Pudis, A. Kuzma, *Optik* **2016**, *127*, 2848.
[98] J. S. Kee, D. P. Poenar, P. Neuzil, L. Yobas, *Opt. Express* **2009**, *17*, 11739.
[99] J. S. Kee, D. P. Poenar, P. Neuzil, L. Yobas, *Sens. Actuators, B* **2008**, *134*, 532.
[100] D. A. Chang-Yen, R. K. Eich, B. K. Gale, *J. Light. Technol.* **2005**, *23*, 2088.
[101] D. Pérez-Calixto, D. Zamarrón-Hernández, A. Cruz-Ramírez, M. Hautefeuille, J. Hérnandez-Cordero, V. Velázquez, M. Grether, *Opt. Mater. Express* **2017**, *7*, 1343.
[102] R. K. Parajuli, R. Saruya, N. Akutzu, S. Miura, W. Kada, S. Kawabata, Y. Matsubara, T. Satoh, M. Koka, N. Yamada, T. Kamiya, K. Miura, O. Hanaizumi, *Jpn. J. Appl. Phys.* **2016**, *55*, 06GD01.
[103] J. A. Singer, T. Stramm, J. Fasel, O. Schween, A. Gelaeschus, A. Bahr, M. Kuhl, in *2023 IEEE 36th International Conference on Micro Electro Mechanical Systems (MEMS)*, IEEE, Munich, Germany **2023**, p. 370.
[104] M. Okoshi, J. Li, P. R. Herman, *Opt. Lett.* **2005**, *30*, 2730.
[105] I. Martincek, D. Pudis, M. Chalupova, *IEEE Photonics Technol. Lett.* **2014**, *26*, 1446.
[106] J. Missinne, G. Van Steenberge, B. Van Hoe, K. Van Coillie, T. Van Gijseghem, P. Dubruel, J. Vanfleteren, P. Van Daele, in *Proc. SPIE 7221, Photonics Packaging, Integration, and Interconnects IX* (Eds: A.L. Glebov, R.T. Chen), SPIE, California, USA **2009**, p. 722105.
[107] V. Prajzler, V. Chlupaty, M. Neruda, *Optik* **2022**, *250*, 168348.
[108] A. W. Norris, J. V. DeGroot, T. Ogawa, T. Watanabe, T. C. Kowalczyk, A. Baugher, R. Blum, in *Proc. SPIE Vol. 5212 Linear and Nonlinear Optics of Organic Materials III* (Eds: M. G. Kuzyk, M. Eich, R. A. Norwood), San Diego, California, USA **2003**, pp. 76–82.
[109] Z. Zhu, L. Liu, Z. Liu, Y. Zhang, Y. Zhang, *Opt. Lett.* **2017**, *42*, 2948.
[110] L. Liu, Z. Liu, Y. Zhang, S. Liu, *Opt. Lett.* **2019**, *44*, 5093.
[111] H. Gao, H. Hu, Y. Zhao, J. Li, M. Lei, Y. Zhang, *Sens. Actuators Phys.* **2018**, *284*, 22.
[112] D. Poudereux, M. Caño-García, J. F. Algorri, B. García-Cámara, J. M. Sánchez-Pena, X. Quintana, M. A. Geday, J. M. Otón, *Opt. Express* **2015**, *23*, 28935.
[113] A. Neyer, S. Kopetz, E. Rabe, W. J. Kang, S. Tombrink, in *Proceedings Electronic Components and Technology 2005 ECTC '05*, IEEE, Florida, USA **2005**, pp. 246–250.
[114] S. Kopetz, D. Cai, E. Rabe, A. Neyer, *AEU – Int. J. Electron. Commun.* **2007**, *61*, 163.
[115] D. K. Cai, A. Neyer, *Microelectron. Eng.* **2010**, *87*, 2268.
[116] J. S. Park, R. Cabosky, Z. Ye, I. (Isaac) Kim, *Opt. Mater.* **2018**, *85*, 153.
[117] I. Turek, N. Tarjányi, I. Martinček, D. Káčik, *Opt. Mater.* **2014**, *36*, 965.
[118] P. Gutruf, E. Zeller, S. Walia, S. Sriram, M. Bhaskaran, *Adv. Opt. Mater.* **2015**, *3*, 1565.
[119] P. R. Subramanian, V. Galiatsatos, *Makromol. Chem. Macromol. Symp.* **1993**, *76*, 233.
[120] N. Tarjányi, I. Turek, I. Martinček, *Opt. Mater.* **2014**, *37*, 798.
[121] T. Farrell, C. I. Smith, A. L. Schofield, R. L. Williams, P. Weightman, *J. Phys. Appl. Phys.* **2010**, *43*, 245301.

[122] B. D. Viers, J. E. Mark, *J. Inorg. Organomet. Polym. Mater.* **2007**, *17*, 283.
[123] M. I. Aranguren, *Polymer* **1998**, *39*, 4897.
[124] N. Bosq, N. Guigo, J. Persello, N. Sbirrazzuoli, *Phys. Chem. Chem. Phys.* **2014**, *16*, 7830.
[125] A. Ručigaj, M. Krajnc, U. Šebenik, *Polym. Sci.* **2017**, *03*, 6.
[126] N. Grassie, I. G. Macfarlane, *Eur. Polym. J.* **1978**, *14*, 875.
[127] T. Dollase, H. W. Spiess, M. Gottlieb, R. Yerushalmi-Rozen, *Europhys. Lett.* **2002**, *60*, 390.
[128] B. Julián, C. Gervais, E. Cordoncillo, P. Escribano, F. Babonneau, C. Sanchez, *Chem. Mater.* **2003**, *15*, 3026.
[129] A. R. Hlil, J.-S. Boisvert, H. M. Titi, Y. Garcia-Puente, W. Correr, S. Loranger, J. Thomas, A. Riaz, Y. Messaddeq, R. Kashyap, *ACS Omega* **2023**, *8*, 32340.
[130] T. Wright, Y. Petel, C. O. Zellman, E. R. Sauvé, Z. M. Hudson, C. A. Michal, M. O. Wolf, *Chem. Sci.* **2020**, *11*, 3081.
[131] N. S. Gupta, K.-S. Lee, A. Labouriau, *Polymers* **2021**, *13*, 1141.
[132] S. Zakaria, F. B. Madsen, A. L. Skov, *Polym.-Plast. Technol. Eng.* **2017**, *56*, 83.
[133] S. Zakaria, P. H. F. Morshuis, M. Y. Benslimane, K. V. Gernaey, A. L. Skov, in *Proc. SPIE EAPAD 2014 Electroact. Polym. Actuators Devices* (Ed.: Y. Bar-Cohen), SPIE, California, USA **2014**, p. 90562V, https://doi.org/10.1117/12.2037292.
[134] S. D. Burnside, E. P. Giannelis, *Chem. Mater.* **1995**, *7*, 1597.
[135] J. D. Jovanovic, M. N. Govedarica, P. R. Dvornic, I. G. Popovic, *Polym. Degrad. Stab.* **1998**, *61*, 87.
[136] R. T. Johnson, R. M. Biefeld, J. A. Sayre, *Polym. Eng. Sci.* **1984**, *24*, 435.
[137] D. Yang, W. Zhang, R. Yao, B. Jiang, *Polym. Degrad. Stab.* **2013**, *98*, 109.
[138] J. Wang, G. Li, Z. Zhang, Q. Huang, B. Niu, Y. Zhang, D. Long, *Chem. Eng. J.* **2024**, *488*, 150728.
[139] K. Xiang, G. Huang, J. Zheng, X. Wang, G. xian Li, J. Huang, *J. Polym. Res.* **2012**, *19*, 9869.
[140] Dow Corning Corporation, *Information about Dow Corning Brand Silicone Encapsulants*, Dow Corning Corporation, Midland, MI **2005**.
[141] A. Müller, M. C. Wapler, U. Wallrabe, *Soft Matter* **2019**, *15*, 779.
[142] G. Zhang, Y. Sun, B. Qian, H. Gao, D. Zuo, *Polym. Test.* **2020**, *90*, 106670.
[143] Xuefeng Li, Shuo Lin, Jinxing Liang, Yupeng Zhang, H. Oigawa, T. Ueda, *IEEE Photonics J.* **2012**, *4*, 155.
[144] F. Gaudière, I. Masson, S. Morin-Grognet, O. Thoumire, J.-P. Vannier, H. Atmani, G. Ladam, B. Labat, *Soft Matter* **2012**, *8*, 8327.
[145] X. Q. Brown, K. Ookawa, J. Y. Wong, *Biomaterials* **2005**, *26*, 3123.
[146] M. Cui, W. Wang, *Chin. Sci. Bull.* **2007**, *52*, 2048.
[147] I. D. Johnston, D. K. McCluskey, C. K. L. Tan, M. C. Tracey, *J. Micromechanics Microengineering* **2014**, *24*, 035017.
[148] T. K. Kim, J. K. Kim, O. C. Jeong, *Microelectron. Eng.* **2011**, *88*, 1982.
[149] F. Schneider, T. Fellner, J. Wilde, U. Wallrabe, *J. Micromechanics Microengineering* **2008**, *18*, 065008.
[150] M. Liu, J. Sun, Q. Chen, *Sens. Actuators Phys.* **2009**, *151*, 42.
[151] A. Ghosh, R. S. Rajeev, A. K. Bhattacharya, A. K. Bhowmick, S. K. De, *Polym. Eng. Sci.* **2003**, *43*, 279.
[152] M. Liu, J. Sun, Y. Sun, C. Bock, Q. Chen, *J. Micromechanics Microengineering* **2009**, *19*.
[153] J. Missinne, S. Kalathimekkad, B. Van Hoe, E. Bosman, J. Vanfleteren, G. Van Steenberge, *Opt. Express* **2014**, *22*, 4168.
[154] F. C. P. Sales, R. M. Ariati, V. T. Noronha, J. E. Ribeiro, *Procedia Struct. Integr.* **2022**, *37*, 383.
[155] S. Zhang, C. Ge, R. Liu, *Sens. Actuators Phys.* **2022**, *341*, 113580.
[156] M. A. Brook, H.-U. Saier, J. Schnabel, K. Town, M. Maloney, *Ind. Eng. Chem. Res.* **2007**, *46*, 8796.
[157] H. Hocheng, C. M. Chen, Y. C. Chou, C. H. Lin, *Microsyst. Technol.* **2010**, *16*, 423.
[158] R. Hopf, L. Bernardi, J. Menze, M. Zündel, E. Mazza, A. E. Ehret, *J. Mech. Behav. Biomed. Mater.* **2016**, *60*, 425.
[159] K. Khanafer, A. Duprey, M. Schlicht, R. Berguer, *Biomed. Microdevices* **2009**, *11*, 503.
[160] E. Rubino, T. Ioppolo, *J. Polym. Sci. Part B Polym. Phys.* **2016**, *54*, 747.
[161] K. Song, N.-K. Cho, K. Park, C.-S. Kim, *Polymers* **2022**, *14*, 2373.
[162] H. S. Cho, H.-Y. Moon, H. S. Lee, Y. T. Kim, S. C. Jeoung, *Bull. Korean Chem. Soc.* **2021**, *42*, 1225.
[163] J. C. Lötters, W. Olthuis, P. H. Veltink, P. Bergveld, *J. Micromechanics Microengineering* **1997**, *7*, 145.
[164] W. S. Lee, K. S. Yeo, A. Andriyana, Y. G. Shee, F. R. Mahamd Adikan, *Mater. Des.* **2016**, *96*, 470.
[165] A. T. Miller, D. L. Safranski, K. E. Smith, R. E. Guldberg, K. Gall, *J. Mech. Behav. Biomed. Mater.* **2016**, *54*, 268.
[166] P. Xu, J. E. Mark, *J. Polym. Sci. Part B Polym. Phys.* **1991**, *29*, 355.
[167] Z. Wang, A. A. Volinsky, N. D. Gallant, *J. Appl. Polym. Sci.* **2014**, *131*, 1.
[168] S. Stassi, G. Canavese, *J. Polym. Sci. Part B Polym. Phys.* **2012**, *50*, 984.
[169] A. Sharfeddin, A. A. Volinsky, G. Mohan, N. D. Gallant, *J. Appl. Polym. Sci.* **2015**, *132*, 42680.
[170] R. H. Pritchard, P. Lava, D. Debruyne, E. M. Terentjev, *Soft Matter* **2013**, *9*, 6037.
[171] G. B. Shah, R. W. Winter, *Macromol. Chem. Phys.* **1996**, *197*, 2201.
[172] G. B. Shah, *J. Appl. Polym. Sci.* **2016**, *133*, n/a.
[173] L. Bernardi, R. Hopf, D. Sibilio, A. Ferrari, A. E. Ehret, E. Mazza, *Polym. Test.* **2017**, *60*, 117.
[174] R. Shanks, I. Kong, in *Thermoplast. Elastomers*, InTech, London, UK **2012**, p. 416.
[175] ASTM D638-14, **2014**, 1.
[176] S. Zakaria, L. Yu, G. Kofod, A. L. Skov, *Mater. Today Commun.* **2015**, *4*, 204.
[177] D. Fuard, T. Tzvetkova-Chevolleau, S. Decossas, P. Tracqui, P. Schiavone, *Microelectron. Eng.* **2008**, *85*, 1289.
[178] V. Placet, P. Delobelle, *J. Micromechanics Microengineering* **2015**, *25*, 035009.
[179] J. M. Kim, F. Wolf, S. K. Baier, *Tribol. Int.* **2015**, *89*, 46.
[180] A. L. Larsen, K. Hansen, P. Sommer-Larsen, O. Hassager, A. Bach, S. Ndoni, M. Jørgensen, *Macromolecules* **2003**, *36*, 10063.
[181] D. Armani, C. Liu, N. Aluru, in *Tech. Dig. IEEE Int. MEMS 99 Conf. Twelfth IEEE Int. Conf. Micro Electro Mech. Syst. Cat No99CH36291*, Florida, USA **1999**, pp. 222–227.
[182] F. Carrillo, S. Gupta, M. Balooch, S. J. Marshall, G. W. Marshall, L. Pruitt, C. M. Puttlitz, *J. Mater. Res.* **2005**, *20*, 2820.
[183] F. Clément, L. Bokobza, L. Monnerie, *Rubber Chem. Technol.* **2001**, *74*, 847.
[184] J. E. Mark, *J. Chem. Educ.* **1981**, *58*, 898.
[185] W. Xu, N. Chahine, T. Sulchek, G. W. Woodruff, **2011**, *27*, 8470.
[186] J. Wen, J. E. Mark, *Polym. J.* **1995**, *27*, 492.
[187] Y. Yue, H. Zhang, Z. Zhang, Y. Chen, *Compos. Part Appl. Sci. Manuf.* **2013**, *54*, 20.
[188] L. C. Yanyo, F. N. Kelley, *Rubber Chem. Technol.* **1987**, *60*, 78.
[189] G. B. Shah, *J. Appl. Polym. Sci.* **2004**, *94*, 1719.
[190] D. E. Hanson, M. Hawley, R. Houlton, K. Chitanvis, P. Rae, E. B. Orler, D. A. Wrobleski, *Polymer* **2005**, *46*, 10989.
[191] L. Yan, D. A. Dillard, R. L. West, L. D. Lower, G. V. Gordon, *J Polym Sci Part B Polym Phys* **2010**, *48*, 2207.
[192] S. Cantournet, R. Desmorat, J. Besson, *Int. J. Solids Struct.* **2009**, *46*, 2255.
[193] V. A. Beloshenko, Ya. E. Beigel'zimer, V. N. Varyukhin, Y. V. Voznyak, *Dokl. Phys. Chem.* **2006**, *409*, 207.
[194] K. A. Grosch, J. A. C. Harwood, A. R. Payne, *Rubber Chem. Technol.* **1968**, *41*, 1157.

[195] B. J. Carey, P. K. Patra, L. Ci, G. G. Silva, P. M. Ajayan, *ACS Nano* **2011**, *5*, 2715.
[196] S. Proj. M. Lucas, *Medical Device Material Performance Study Siloxane Safety Profile*, ECRI, USA, **2020**.
[197] B. Nair, A. R. Elmore, *Int. J. Toxicol.* **2003**, *22*, 10.
[198] Report No 26: Linear Polydimethylsiloxanes (Viscosity 10–100,000 Centistokes) CAS No. 63148-62-9, *European Centre For Ecotoxicology And Toxicology Of Chemicals (ECETOC)*, Brussels, **1994**.
[199] Report No 55: Linear Polydimethylsiloxanes CAS No. 63148-62-9, *European Centre For Ecotoxicology And Toxicology Of Chemicals (ECETOC)*, Brussels, **2011**.
[200] P. H. Howard, P. R. Durkin, A. Hanchett, *Environmental Hazard Assesment of Liquid Siloxanes (Silicones), Office Of Toxic Substances*, US Environmental Protection Agency, Washington, DC, **1974**.
[201] E. Pedraza, A. C. Brady, C. A. Fraker, C. L. Stabler, *J. Biomater. Sci., Polym. Ed.* **2013**, *24*, 1041.
[202] B. H. Shin, B. H. Kim, S. Kim, K. Lee, Y. B. Choy, C. Y. Heo, *Biomater. Res.* **2018**, *22*, 37.
[203] J. C. Doloff, O. Veiseh, R. de Mezerville, M. Sforza, T. A. Perry, J. Haupt, M. Jamiel, C. Chambers, A. Nash, S. Aghlara-Fotovat, J. L. Stelzel, S. J. Bauer, S. Y. Neshat, J. Hancock, N. A. Romero, Y. E. Hidalgo, I. M. Leiva, A. M. Munhoz, A. Bayat, B. M. Kinney, H. C. Hodges, R. N. Miranda, M. W. Clemens, R. Langer, *Nat. Biomed. Eng.* **2021**, *5*, 1115.
[204] M. Younes, G. Aquilina, L. Castle, K.-H. Engel, P. Fowler, M. J. Frutos Fernandez, P. Fürst, R. Gürtler, U. Gundert-Remy, T. Husøy, M. Manco, W. Mennes, S. Passamonti, R. Shah, D. H. Waalkens-Berendsen, D. Wölfle, M. Wright, P. Boon, P. Tobback, A. Giarola, A. M. Rincon, A. Tard, P. Moldeus, *EFSA J.* **2020**, *18*, e06107.
[205] V. Borba, A. Malkova, N. Basantsova, G. Halpert, L. Andreoli, A. Tincani, H. Amital, Y. Shoenfeld, *Biomolecules* **2020**, *10*, 1.
[206] *Dow Chemical Canada ULC, Safety Data Sheet: SYLGARD™ 184 Silicone Elastomer Base*, Dow Chemical Canada ULC, Calgary, Canada, **2022**.
[207] Wacker Chemie AG, *Safety data sheet: ELASTOSIL RT 601 A (v. 2.7 US)*, Wacker Chemie AG, München, Germany, **2023**.
[208] L. J. Jara, G. García-Collinot, G. Medina, M. del P. Cruz-Dominguez, O. Vera-Lastra, R. A. Carranza-Muleiro, M. A. Saavedra, *Immunol. Res.* **2017**, *65*, 8.
[209] NuSil Technology LLC, *Safety Data Sheet: MED-4860 Part A & B (v. 3.0)*, NuSil Technology LLC, California, USA, **2018**.
[210] Dow Chemical Canada ULC, *Safety Data Sheet: SYLGARD™ 184 Silicone Elastomer Base*, Dow Chemical Canada ULC, Calgary, Canada, **2019**.
[211] J. L. Torgunrud, A. M. Reverón Pérez, E. B. Spitzberg, S. A. Miller, *Macromolecules* **2023**, *56*, 3668.
[212] A. R. L. Colas, Silicones : Preparation, Properties and Performance, Dow Corning, Life Sciences **2005**.
[213] E. F. C. Griessbach, R. G. Lehmann, *Chemosphere* **1999**, *38*, 1461.
[214] R. G. Lehmann, S. Varaprath, R. B. Annelin, J. L. Arndt, *Environ. Toxicol. Chem.* **1995**, *14*, 1299.
[215] D. Graiver, K. W. Farminer, R. Narayan, *J. Polym. Environ.* **2003**, *11*, 129.
[216] C. Stevens, D. E. Powell, P. Mäkelä, C. Karman, *Mar. Pollut. Bull.* **2001**, *42*, 536.
[217] E. J. Hobbs, M. L. Keplinger, J. C. Calandra, *Environ. Res.* **1975**, *10*, 397.
[218] F. Rocha, V. Homem, J. Castro-Jiménez, N. Ratola, *Sci. Total Environ.* **2019**, *650*, 2364.
[219] Y. Zhang, M. Shen, Y. Tian, G. Zeng, *J. Soils Sediments* **2018**, *18*, 2063.
[220] W. Błaszczyk, A. Siatecka, P. Tlustoš, P. Oleszczuk, *Sci. Total Environ.* **2024**, *945*, 173517.
[221] C. Côté-Beaulieu, F. Chain, J. G. Menzies, S. D. Kinrade, R. R. Bélanger, *Environ. Exp. Bot.* **2009**, *65*, 155.
[222] J. Sanchís, M. Llorca, Y. Picó, M. Farré, D. Barceló, *Sci. Total Environ.* **2016**, *545–546*, 236.
[223] J. Sanchís, A. Cabrerizo, C. Galbán-Malagón, D. Barceló, M. Farré, J. Dachs, *Environ. Sci. Technol.* **2015**, *49*, 4415.
[224] A. A. Werkneh, *Heliyon* **2022**, *8*, e10929.
[225] B. R. Bzdek, A. J. Horan, M. R. Pennington, N. J. Janechek, J. Baek, C. O. Stanier, M. V. Johnston, *Environ. Sci. Technol.* **2014**, *48*, 11137.
[226] R. Hajj, R. Brunel, R. Sonnier, C. Longuet, F. Ganachaud, *Polym. Degrad. Stab.* **2022**, *200*, 109947.
[227] N. Duc Vu, A. Boulègue-Mondière, N. Durand, J. Raynaud, V. Monteil, *Green Chem.* **2023**, *25*, 3869.
[228] I. V. Elmanovich, V. E. Sizov, V. V. Zefirov, A. A. Kalinina, M. O. Gallyamov, V. S. Papkov, A. M. Muzafarov, *Polymers* **2022**, *14*, 5170.
[229] B. Rupasinghe, J. C. Furgal, *ACS Appl. Polym. Mater.* **2021**, *3*, 1828.
[230] T. Feix, A. A. Fadhil, D. Troegel, *Hydrometallurgy* **2024**, *225*, 106283.
[231] S. K. Lahiri, Z. Azimi Dijvejin, K. Golovin, *Nat. Sustain.* **2023**, *6*, 559.
[232] Y. Qian, P. Cui, J. Zhang, S. Wang, X. Duan, G. Li, *Environ. Pollut.* **2023**, *335*, 122356.
[233] Z. Shentu, J. Kang, Z. Zhu, L. Wang, Y. Guo, T. Xu, C. Zhao, *Opt. Fiber Technol.* **2021**, *63*, 102531.
[234] W. Kada, K. Miura, H. Kato, R. Saruya, A. Kubota, T. Satoh, M. Koka, Y. Ishii, T. Kamiya, H. Nishikawa, O. Hanaizumi, *Nucl. Instrum. Methods Phys. Res. Sect. B Beam Interact. Mater. At.* **2015**, *348*, 218.
[235] S. Z. Szilasi, J. Budai, Z. Pápa, R. Huszank, Z. Tóth, I. Rajta, *Mater. Chem. Phys.* **2011**, *131*, 370.
[236] C. N. B. Udalagama, S. F. Chan, S. Homhuan, A. A. Bettiol, T. Wohland, F. Watt, in *Proc. SPIE 6882, Micromach. Microfabr. Process Technol. XII* (Eds: M.-A. Maher, J.-C. Chiao, P.J. Resnick), SPIE, California,USA **2008**, p. 68820D, https://doi.org/10.1117/12.762885.
[237] S. Valouch, H. Sieber, S. Kettlitz, C. Eschenbaum, U. Hollenbach, U. Lemmer, *Opt. Express* **2012**, *20*, 28855.
[238] J. Paek, J. Kim, *Nat. Commun.* **2014**, *5*, 3324.
[239] I. Martincek, D. Pudis, P. Gaso, *IEEE Photonics Technol. Lett.* **2013**, *25*, 2066.
[240] J. Lee, J. Kim, *J. Micromechanics Microengineering* **2011**, *21*, 085016.
[241] K. Nakakubo, H. Inoue, H. Yoshioka, K. Morita, T. Kotani, Y. Oki, in *Proc. SPIE 11682,* Opt. Compon. Mater. XVIII, SPIE, Online (Eds: M.J. Digonnet, S. Jiang) **2021**, p. 116820J, https://doi.org/10.1117/12.2582700.
[242] M. Ramuz, B. C. K. Tee, J. B. H. Tok, Z. Bao, *Adv. Mater.* **2012**, *24*, 3223.
[243] M. Novak, J. Nedoma, M. Fajkus, J. Jargus, V. Vasinek, in *Proc. SPIE 10232, Micro-Struct. Spec. Opt. Fibres V* (Eds: K. Kalli, J. Kanka, A. Mendez, P. Peterka), SPIE, Prague, Czech Republic **2017**, p. 1023200, https://doi.org/10.1117/12.2257064.
[244] *The Dow Chemical Company, Technical Data Sheet: SYLGARD™ 184 Silicone Elastomer*, The Dow Chemical Company **2017**.
[245] T. Bardelli, C. Marano, F. Briatico Vangosa, *J. Appl. Polym. Sci.* **2021**, *138*, 51013.
[246] M. H. Madsen, N. A. Feidenhans'l, P.-E. E. Hansen, J. Garnæs, K. Dirscherl, N. A. Feidenhans'l, P.-E. E. Hansen, J. Garnæs, K. Dirscherl, *J. Micromechanics Microengineering* **2014**, *24*, 2.
[247] K. Soma, T. Ishigure, *IEEE J. Sel. Top. Quantum Electron.* **2013**, *19*, 3600310.
[248] G. Giovannini, K. Sharma, L. F. Boesel, R. M. Rossi, *Adv. Healthcare Mater.* **2024**, *13*, 2302603.
[249] L. Rudmann, D. Scholz, M. T. Alt, A. Dieter, E. Fiedler, T. Moser, T. Stieglitz, *Adv. Healthcare Mater.* **2024**, *13*, 2304513.
[250] I. Dominguez, I. D. Villar, J. Montoya-Cardona, O. Fuentes, N. D. Gomez-Cardona, J. M. Corres, I. R. Matias, *IEEE Access* **2021**, *9*, 31627.
[251] J. Guo, B. Zhou, C. Yang, Q. Dai, L. Kong, *Opt. Lett.* **2019**, *44*, 5747.

[252] A. Leal-Junior, J. Guo, R. Min, A. J. Fernandes, A. Frizera, C. Marques, *Photonics Res.* **2021**, *9*, 272.
[253] S. Han, G. Shin, *Coatings* **2020**, *10*, 1153.
[254] I. Martincek, I. Turek, N. Tarjányi, *Opt. Mater. Express* **2014**, *4*, 1997.
[255] J. C. McDonald, G. M. Whitesides, *Acc. Chem. Res.* **2002**, *35*, 491.
[256] J. Friend, L. Yeo, *Biomicrofluidics* **2010**, *4*, 026502.
[257] C.-S. Huang, E. Y.-B. Pun, W.-C. Wang, *JOSA B* **2009**, *26*, 1256.
[258] V. Lien, Kai Zhao, Y. Berdichevsky, Yu-Hwa Lo, *IEEE J. Sel. Top. Quantum Electron.* **2005**, *11*, 827.
[259] S. H. Cho, J. Godin, C. H. Chen, F. S. Tsai, Y.-H. Lo, in *Proc. SPIE 7135, Optoelectronic Materials and Devices III* (Eds: Y. Luo, J. Buus, F. Koyama, Y.-H. Lo), SPIE, Hangzhou, China, **2008**, p. 71350M.
[260] H. Y. Chen, A. A. McClelland, Z. Chen, J. Lahann, *Anal. Chem.* **2008**, *80*, 4119.
[261] M. A. Eddings, M. A. Johnson, B. K. Gale, *J. Micromechanics Microengineering* **2008**, *18*, 067001.
[262] H. Herzog, A. Klein, H. Bleckmann, P. Holik, S. Schmitz, G. Siebke, S. Tätzner, M. Lacher, S. Steltenkamp, *Bioinspir. Biomim.* **2015**, *10*, 036001.
[263] E. Zgraggen, I. M. Soganci, F. Horst, A. L. Porta, R. Dangel, B. J. Offrein, S. A. Snow, J. K. Young, B. W. Swatowski, C. M. Amb, O. Scholder, R. Broennimann, U. Sennhauser, G. L. Bona, *J. Light. Technol.* **2014**, *32*, 3036.
[264] A. Ryabchun, O. Sakhno, M. Wegener, *RSC Adv.* **2016**, *6*, 51791.
[265] H. Takao, M. Okoshi, N. Inoue, *Appl. Phys. Mater. Sci. Process.* **2004**, *79*, 1571.
[266] M. Okoshi, T. Kimura, H. Takao, N. Inoue, T. Yamashita, *Jpn. J. Appl. Phys. Part 1 Regul. Pap. Short Notes Rev. Pap.* **2004**, *43*, 3438.
[267] V.-M. Graubner, R. Jordan, O. Nuyken, T. Lippert, M. Hauer, B. Schnyder, A. Wokaun, *Appl. Surf. Sci.* **2002**, *197–198*, 786.
[268] S. S. Zakariyah, P. P. Conway, D. A. Hutt, D. R. Selviah, K. Wang, H. Baghsiahi, J. Rygate, J. Calver, W. Kandulski, in *Proc. IEEE, 11th Electron. Packag. Technol. Conf*, IEEE, Singapore, **2009**, pp. 936–941, https://doi.org/10.1109/EPTC.2009.5416408.
[269] K. Kruse, C. Middlebrook, *Photonics Nanostructures – Fundam. Appl.* **2015**, *13*, 66.
[270] G. Panusa, Y. Pu, J. Wang, C. Moser, D. Psaltis, *Opt. Mater. Express* **2019**, *9*, 128.
[271] R. Woods, S. Feldbacher, D. Zidar, G. Langer, V. Satzinger, V. Schmidt, N. Pucher, R. Liska, W. Kern, *Opt. Mater. Express* **2014**, *4*, 486.
[272] R. Huszank, S. Z. Szilasi, D. Szikra, *J. Phys. Chem. C* **2013**, *117*, 25884.
[273] S. Z. Szilasi, J. Kokavecz, R. Huszank, I. Rajta, *Appl. Surf. Sci.* **2011**, *257*, 4612.
[274] A. A. Bettiol, S. Y. Chiam, E. J. Teo, C. Udalagama, S. F. Chan, S. K. Hoi, J. A. van Kan, M. B. H. Breese, F. Watt, *Nucl. Instrum. Methods Phys. Res. Sect. B Beam Interact. Mater. At.* **2009**, *267*, 2280.
[275] S. Z. Szilasi, R. Huszank, A. Csik, C. Cserháti, I. Rajta, *Nucl. Instrum. Methods Phys. Res. Sect. B Beam Interact. Mater. At.* **2009**, *267*, 2296.
[276] R. Huszank, D. Szikra, A. Simon, S. Z. Szilasi, I. P. Nagy, *Langmuir* **2011**, *27*, 3842.
[277] W. Ding, J. Sun, G. Chen, L. Zhou, J. Wang, X. Gu, J. Wan, X. Pu, B. Tang, Z. L. Wang, *J. Mater. Chem. C* **2019**, *7*, 10769.
[278] J. H. Lee, T. Lim, K. Seo, J. Park, J. Yang, S.-M. Jeong, S. Ju, *NPG Asia Mater.* **2022**, *14*, 1.
[279] Y. Kobayashi, Y. Sakaguchi, K. Yasuhara, T. Ishigure, *Opt. Express* **2021**, *29*, 9513.
[280] K. Yasuhara, F. Yu, T. Ishigure, *Opt. Express* **2017**, *25*, 8524.
[281] Y. Li, B. Li, *Oxf. Open Mater. Sci.* **2022**, *2*, itac008.
[282] P. Calcagnile, G. Cacciatore, C. Demitri, F. Montagna, C. Esposito Corcione, *Materials* **2018**, *11*, 1578.
[283] F. C. Krebs, *Sol. Energy Mater. Sol. Cells* **2009**, *93*, 394.
[284] S. M. Azmayesh-Fard, E. Flaim, J. N. McMullin, *J. Micromechanics Microengineering* **2010**, *20*, 087002.
[285] F. Shi, *Flexible Polymer Waveguides for High-Speed Short-Reach Links*, University of Cambridge, Cambridge, UK **2019**.
[286] M. D. Tyona, *Adv. Mater. Res.* **2013**, *2*, 195.
[287] V.-M. Graubner, D. Clemens, T. Gutberlet, R. Kötz, T. Lippert, O. Nuyken, B. Schnyder, A. Wokaun, *Langmuir* **2005**, *21*, 8940.
[288] M. Krehel, M. Schmid, R. M. Rossi, L. F. Boesel, G. L. Bona, L. J. Scherer, *Sens. Switz.* **2014**, *14*, 13088.
[289] D. Kim, S.-H. Kim, J. Y. Park, *Polymers* **2019**, *11*, 1264.
[290] J. Sun, C. Yun, B. Cui, P. Li, G. Liu, X. Wang, F. Chu, *Polymers* **2018**, *10*, 1209.
[291] V. Prajzler, V. Chlupaty, P. Kulha, M. Neruda, S. Kopp, M. Mühlberger, *Nanomaterials* **2021**, *11*, 1.
[292] Y. Huang, N. Bu, Y. Duan, Y. Pan, H. Liu, Z. Yin, Y. Xiong, *Nanoscale* **2013**, *5*, 12007.
[293] G. Hochleitner, E. Fürsattel, R. Giesa, J. Groll, H.-W. Schmidt, P. D. Dalton, *Macromol. Rapid Commun.* **2018**, *39*, 1800055.
[294] H. Niu, H. Wang, H. Zhou, T. Lin, *RSC Adv.* **2014**, *4*, 11782.
[295] J. R. L. Little, *Tunable and High Refractive Index Polydimethylsiloxane Polymers for Label-Free Optical Sensing*, Queen's University Kingston, Ontario, Canada **2013**.
[296] M. Odeh, B. Voort, A. Anjum, B. Paredes, C. Dimas, M. S. Dahlem, *Appl. Opt.* **2017**, *56*, 1202.
[297] I. Uba, K. Ghebreyessus, D. Geddis, U. Hommerich, in *SoutheastCon 2021*, IEEE, Atlanta, GA, USA **2021**, pp. 1–5.
[298] N. Yamada, I. Yoshinaga, S. Katayama, *J. Sol-Gel Sci. Technol.* **2000**, *17*, 123.
[299] S. Motakef, T. Suratwala, R. L. Roncome, J. M. Boulton, G. Teowee, D. R. Uhlmann, *J. Non-Cryst. Solids* **1994**, *178*, 37.
[300] S. Kohjiya, K. Maeda, S. Yamashita, Y. Shibata, *J. Mater. Sci.* **1990**, *25*, 3368.
[301] S. Vudayagiri, S. Zakaria, L. Yu, S. S. Hassouneh, M. Benslimane, A. L. Skov, *Smart Mater. Struct.* **2014**, *23*, 105017.
[302] A. L. Larsen, P. Sommer-Larsen, O. Hassager, in *Proc. SPIE 5385, Smart Struct. Mater. 2004 Electroact. Polym. Actuators Devices EAPAD* (Ed: Y. Bar-Cohen), SPIE, California, USA **2004**, p. 108, https://doi.org/10.1117/12.538057.
[303] I. Uba, D. Geddis, K. Ghebreyessus, U. Hömmerich, J. Dumas, *Polymers* **2022**, *14*, 896.
[304] A. Ryabchun, M. Wegener, Y. Gritsai, O. Sakhno, *Adv. Opt. Mater.* **2016**, *4*, 169.
[305] K. Raman, T. R. Srinivasa Murthy, G. M. Hegde, *Phys. Procedia* **2011**, *19*, 146.
[306] C. M. Whang, C. S. Yeo, Y. H. Kim, *Bull. Korean Chem. Soc.* **2001**, *22*, 1366.
[307] A. Goyal, M. Mohl, A. Kumar, R. Puskas, A. Kukovecz, Z. Konya, I. Kiricsi, P. M. Ajayan, *Compos. Sci. Technol.* **2011**, *71*, 129.
[308] A. Goyal, A. Kumar, P. K. Patra, S. Mahendra, S. Tabatabaei, P. J. J. Alvarez, G. John, P. M. Ajayan, *Macromol. Rapid Commun.* **2009**, *30*, 1116.
[309] J. F. Algorri, D. Poudereux, B. García-Cámara, V. Urruchi, J. M. Sánchez-Pena, R. Vergaz, M. Caño-García, X. Quintana, M. A. Geday, J. M. Otón, *Opt. Data Process. Storage* **2016**, *2*, 1.
[310] D. T. Eddington, J. P. Puccinelli, D. J. Beebe, *Sens. Actuators, B* **2006**, *114*, 170.
[311] J. Roth, V. Albrecht, M. Nitschke, C. Bellmann, F. Simons, S. Zschoche, S. Michel, C. Luhmann, K. Grundke, B. Voit, *Langmuir* **2008**, *24*, 12603.
[312] J. A. Vickers, M. M. Caulum, C. S. Henry, *Anal. Chem.* **2006**, *78*, 7446.
[313] A. Tóth, I. Bertóti, M. Blazsó, G. Bánhegyi, A. Bognar, P. Szaplonczay, *J. Appl. Polym. Sci.* **1994**, *52*, 1293.
[314] Z. Almutairi, C. L. Ren, L. Simon, *Colloids Surf. Physicochem. Eng. Asp.* **2012**, *415*, 406.

[315] Q. Tu, J.-C. Wang, Y. Zhang, R. Liu, W. Liu, L. Ren, S. Shen, J. Xu, L. Zhao, J. Wang, *Rev. Anal. Chem.* **2012**, *31*, 177.
[316] J. Zhou, D. A. Khodakov, A. V. Ellis, N. H. Voelcker, *Electrophoresis* **2012**, *33*, 89.
[317] A. Gokaltun, M. L. Yarmush, A. Asatekin, O. B. Usta, *Technology* **2017**, *05*, 1.
[318] L. B. Neves, I. S. Afonso, G. Nobrega, L. G. Barbosa, R. A. Lima, J. E. Ribeiro, *Micromachines* **2024**, *15*, 670.
[319] A. Papra, A. Bernard, D. Juncker, N. B. Larsen, B. Michel, E. Delamarche, *Langmuir* **2001**, *17*, 4090.
[320] C. Donzel, M. Geissler, A. Bernard, H. Wolf, B. Michel, J. Hilborn, E. Delamarche, *Adv. Mater.* **2001**, *13*, 1164.
[321] M. Morra, E. Occhiello, R. Marola, F. Garbassi, P. Humphrey, D. Johnson, *J. Colloid Interface Sci.* **1990**, *137*, 11.
[322] M. J. Owen, P. J. Smith, *J. Adhes. Sci. Technol.* **1994**, *8*, 1063.
[323] H. Hillborg, J. F. Ankner, U. W. Gedde, G. D. Smith, H. K. Yasuda, K. Wikström, *Polymer* **2000**, *41*, 6851.
[324] Y. Berdichevsky, J. Khandurina, A. Guttman, Y. H. Lo, *Sens. Actuators, B* **2004**, *97*, 402.
[325] H. Hillborg, N. Tomczak, A. Olàh, H. Schönherr, G. J. Vancso, *Langmuir* **2004**, *20*, 785.
[326] A. E. Özçam, K. Efimenko, J. Genzer, *Polymer* **2014**, *55*, 3107.
[327] H. Hillborg, M. Sandelin, U. W. Gedde, *Polymer* **2001**, *42*, 7349.
[328] K. Efimenko, W. E. Wallace, J. Genzer, *J. Colloid Interface Sci.* **2002**, *254*, 306.
[329] K. L. Mills, X. Zhu, S. Takayama, M. D. Thouless, *J. Mater. Res.* **2008**, *23*, 37.
[330] F. Jahangiri, T. Hakala, V. Jokinen, *Microfluid. Nanofluidics* **2020**, *24*, 2.
[331] B. Miller, A. M. Agarwal, A. Agrahari, *Spectroscopy and Refractive Index Sensing, Integrated Photonic Systems Roadmap - International (IPSR-I)* **2024**.
[332] B. E. Slentz, N. A. Penner, F. E. Regnier, *J. Chromatogr. A* **2002**, *948*, 225.
[333] S. Hu, X. Ren, M. Bachman, C. E. Sims, G. P. Li, N. Allbritton, *Anal. Chem.* **2002**, *74*, 4117.
[334] J. Lahann, M. Balcells, H. Lu, T. Rodon, K. F. Jensen, R. Langer, *Anal. Chem.* **2003**, *75*, 2117.
[335] T. Trantidou, Y. Elani, E. Parsons, O. Ces, *Microsyst. Nanoeng.* **2017**, *3*, 1.
[336] J. Li, M. Wang, Y. Shen, *Surf. Coat. Technol.* **2012**, *206*, 2161.
[337] M. Dabaghi, S. Shahriari, N. Saraei, K. Da, A. Chandiramohan, P. R. Selvaganapathy, J. A. Hirota, *Micromachines* **2021**, *12*, 132.
[338] G. T. Roman, C. T. Culbertson, *Langmuir* **2006**, *22*, 4445.
[339] G. J. Kookootsedes, H. H. Reese, B. I. Gutek, G. H. Pretzer, *US4701017A*, **1987**.
[340] Y. Shibata, A. Nishimura, S. Niwa, Y. Osawa, T. Uemiya, *US4750796A*, **1988**.
[341] L. Fliegans, J. Troughton, V. Divay, S. Blayac, M. Ramuz, *Sensors* **2022**, *23*, 114.
[342] A. Levi, M. Piovanelli, S. Furlan, B. Mazzolai, L. Beccai, *Sensors* **2013**, *13*, 6578.
[343] C. To, T. Hellebrekers, J. Jung, S. J. Yoon, Y.-L. Park, *IEEE Robot. Autom. Lett.* **2018**, *3*, 3821.
[344] C. Guignier, B. Camillieri, M. Schmid, R. M. Rossi, M.-A. Bueno, *Sensors* **2019**, *19*, 3011.
[345] I. Martincek, D. Pudis, P. Gaso, in *Proc. SPIE 8816, Nanoengineering: Fabrication, Properties, Optics, and Devices X* (Eds: E.M. Campo, E.A. Dobisz, L.A. Eldada), SPIE, San Diego, California, USA **2013**, p. 88161D.
[346] Q. She, P. Wu, W. Lin, Y. Huang, F. Wang, Z. Ye, in *Proc. SPIE 12595, Adv. Fiber Laser Conf. AFL2022*, SPIE, Changsha, China **2023**, pp. 560–566, https://doi.org/10.1117/12.2669085.
[347] W.-C. Wang, C.-T. Ho, Y.-R. Lian, W.-C. Chuang, *Appl. Opt.* **2006**, *45*, 1893.
[348] J. D. Sandt, M. Moudio, J. K. Clark, J. Hardin, C. Argenti, M. Carty, J. A. Lewis, M. Kolle, *Adv. Healthcare Mater.* **2018**, *7*, 1.
[349] W. Peng, Q. Liao, H. Song, *Nanoscale Res. Lett.* **2021**, *16*, 23.
[350] C. To, T. L. Hellebrekers, Y. L. Park, *IEEE Int. Conf. Intell. Robots Syst.* **2015**, *2015*, 5898.
[351] W.-C. Wang, W. R. Ledoux, C.-Y. Huang, C.-S. Huang, G. K. Klute, P. G. Reinhall, *IEEE Trans. Biomed. Eng.* **2008**, *55*, 614.
[352] H. Liang, Y. He, M. Chen, L. Jiang, Z. Zhang, X. Heng, L. Yang, Y. Hao, X. Wei, J. Gan, Z. Yang, *Adv. Intell. Syst.* **2021**, *3*, 2100035.
[353] A. Llobera, V. J. Cadarso, K. Zinoviev, C. Dominguez, S. Buttgenbach, J. Vila, J. A. Plaza, S. Biittgenbach, *IEEE Photonics Technol. Lett.* **2009**, *21*, 79.
[354] C.-H. Mak, Y. Li, K. Wang, M. Wu, J. D.-L. Ho, Q. Dou, K.-Y. Sze, K. Althoefer, K.-W. Kwok, *Adv. Intell. Syst.* **2024**, *6*, 2300082.
[355] R. Koeppe, P. Bartu, S. Bauer, N. S. Sariciftci, *Adv. Mater.* **2009**, *21*, 3510.
[356] O. R. Ranjbar-Naeini, F. Jafari, H. Latifi, in *26th International Conference on Optical Fiber Sensors, OSA Technical Digest*, Optica Publishing Group, Lausanne, Switzerland **2018**, p. WF92.
[357] A. Klein, H. Bleckmann, *Beilstein J. Nanotechnol.* **2011**, *2*, 276.
[358] B. Wiesmayr, M. Höglinger, M. Krieger, P. Lindner, W. Baumgartner, A. Stadler, *Sensors* **2019**, *19*, 925.
[359] A. T. Stadler, P. Pavlicek, W. Baumgartner, Istanbul (Turkey), **2015**.
[360] A. Massaro, F. Spano, R. Cingolani, A. Athanassiou, *IEEE Sens. J.* **2011**, *11*, 1780.
[361] K. Deisseroth, *Nat. Neurosci.* **2015**, *18*, 1213.
[362] S. I. Park, D. S. Brenner, G. Shin, C. D. Morgan, B. A. Copits, H. U. Chung, M. Y. Pullen, K. N. Noh, S. Davidson, S. J. Oh, J. Yoon, K.-I. Jang, V. K. Samineni, M. Norman, J. G. Grajales-Reyes, S. K. Vogt, S. S. Sundaram, K. M. Wilson, J. S. Ha, R. Xu, T. Pan, T. Kim, Y. Huang, M. C. Montana, J. P. Golden, M. R. Bruchas, R. W. Gereau, J. A. Rogers, *Nat. Biotechnol.* **2015**, *33*, 1280.
[363] A. Ersen, M. Sahin, in *2016 38th Annu. Int. Conf. IEEE Eng. Med. Biol. Soc. EMBC*, IEEE, Orlando, FL, USA **2016**, pp. 4475–4478.
[364] Y. Zhao, K. Wang, S. Li, P. Zhang, Y. Shen, Y. Fu, Y. Zhang, J. Zhou, C. Wang, *J. Biomed. Nanotechnol.* **2018**, *14*, 1099.
[365] F. Saleheen, J. Goldstein, R. Rajan, D. Caroline, S. Pascarella, C. Won, in *2018 40th Annu. Int. Conf. IEEEEng. Med. Biol. Soc. EMBC*, IEEE, Honolulu, HI **2018**, pp. 4969–4972.
[366] D. Wang, M. L. Kuzma, X. Tan, T.-C. He, C. Dong, Z. Liu, J. Yang, *Adv. Drug Delivery Rev.* **2021**, *179*, 114036.
[367] M. Jablonski, F. Bossuyt, J. Vanfleteren, T. Vervust, H. De Smet, in *Proc. SPIE 9129, Biophotonics: Photonic Solutions for Better Health Care IV* (Eds: J. Popp, V.V. Tuchin, D.L. Matthews, F.S. Pavone, P. Garside), SPIE, Brussels, Belgium **2014**, p. 912921.
[368] D. E. J. G. J. Dolmans, D. Fukumura, R. K. Jain, *Nat. Rev. Cancer* **2003**, *3*, 380.
[369] Ł. Bijoch, U. Włodkowska, R. Kasztelanic, M. Pawłowska, D. Pysz, L. Kaczmarek, R. Lapkiewicz, R. Buczyński, R. Czajkowski, *ACS Appl. Mater. Interfaces* **2023**, *15*, 12831.
[370] S. Ohayon, A. Caravaca-Aguirre, R. Piestun, J. J. DiCarlo, *Biomed. Opt. Express* **2018**, *9*, 1492.
[371] S. Nizamoglu, M. C. Gather, M. Humar, M. Choi, S. Kim, K. S. Kim, S. K. Hahn, G. Scarcelli, M. Randolph, R. W. Redmond, S. H. Yun, *Nat. Commun.* **2016**, *7*, 10374.
[372] A. K. Yetisen, N. Jiang, A. Fallahi, Y. Montelongo, G. U. Ruiz-Esparza, A. Tamayol, Y. S. Zhang, I. Mahmood, S.-A. Yang, K. S. Kim, H. Butt, A. Khademhosseini, S.-H. Yun, *Adv. Mater.* **2017**, *29*, 1606380.
[373] M. Choi, M. Humar, S. Kim, S.-H. Yun, *Adv. Mater.* **2015**, *27*, 4081.
[374] M. Haurylau, G. Chen, H. Chen, J. Zhang, N. A. Nelson, D. H. Albonesi, E. G. Friedman, P. M. Fauchet, *IEEE J. Sel. Top. Quantum Electron.* **2006**, *12*, 1699.

[375] M. Lebby, A. Haile-Mariam, A. Evans, *Transceivers and Interconnects*, Integrated Photonic Systems Roadmap – International (IPSR-I), **2023**.
[376] N. Bamiedakis, Jian Chen, P. Westbergh, J. S. Gustavsson, A. Larsson, R. V. Penty, I. H. White, *J. Light. Technol.* **2015**, *33*, 882.
[377] R. Dangel, F. Horst, D. Jubin, N. Meier, J. Weiss, B. J. Offrein, B. W. Swatowski, C. M. Amb, D. J. DeShazer, W. K. Weidner, *J. Light. Technol.* **2013**, *31*, 3915.
[378] S. Yang, L. Yang, B. Li, F. Luo, X. Wang, Y. Du, *Opt. Express* **2020**, *28*, 14605.
[379] V. Prajzler, M. Neruda, M. Květoň, *J. Mater. Sci. Mater. Electron.* **2019**, *30*, 16983.
[380] X. Gan, N. Pervez, I. Kymissis, F. Hatami, D. Englund, *Appl. Phys. Lett.* **2012**, *100*, 231104.
[381] C. L. Bliss, J. N. McMullin, C. J. Backhouse, *Lab Chip* **2007**, *7*, 1280.
[382] V. Lien, Y. Berdichevsky, Y.-H. Lo, *IEEE Photonics Technol. Lett.* **2004**, *16*, 1525.
[383] J. W. Parks, H. Schmidt, *Sci. Rep.* **2016**, *6*, 33008.
[384] C.-H. Chou, M.-H. Hsu, F.-C. Chen, *Nano Energy* **2015**, *15*, 729.
[385] S. Sadeghi, H. Bahmani Jalali, S. B. Srivastava, R. Melikov, I. Baylam, A. Sennaroglu, S. Nizamoglu, *iScience* **2020**, *23*, 101272.
[386] C.-S. Huang, X. Kang, R. M. Rossi, M. V. Kovalenko, X. Sun, H. Peng, L. F. Boesel, *J. Mater. Chem. A* **2021**, *9*, 25974.
[387] D. Cambié, F. Zhao, V. Hessel, M. G. Debije, T. Noël, *Angew. Chem., Int. Ed.* **2017**, *56*, 1050.
[388] D. Cambié, F. Zhao, V. Hessel, M. G. Debije, T. Noël, *React. Chem. Eng.* **2017**, *2*, 561.

Camila A. Zimmermann is currently pursuing her Ph.D. in applied engineering at the Department of Electrical Engineering, École de Technologie Supérieure, Canada. She holds a bachelor's degree in Chemical Engineering from the University of the Joinville Region and a master's degree in Materials Science and Engineering from the Federal University of Santa Catarina, Brazil, where her research focused on electrically conductive polymer-based anticorrosion coatings. With over 8 years of industrial experience in polymer testing and characterization, her research interests encompass polymer optical waveguides, polymer science, stimuli-chromic materials, and optical sensing.

Koffi N. Amouzou holds a Master's in physics from the University of Lome, Togo and a Master's in mathematical sciences from the African Institute for Mathematical Sciences, Senegal. He completed a second Master's in physics at the University of Moncton and is currently pursuing a Ph.D. in electrical engineering at École de Technologie Supérieure, Canada. His research focuses on elastomeric pressure/shear devices for biomedical applications. His interests include optics, photonic sensors, multifunctional fibers, polymer materials, nanostructured thin films, and solar energy.

Bora Ung, Ph.D. in physical engineering from Polytechnique Montreal (2012), is a professor in the electrical engineering department of École de Technologie Supérieure, Canada, since 2014 where he heads the PHotonic Innovations Lab (Φ-lab). His research interests are in the design of specialty optical fibers and the development of novel photonic devices for applications in optical sensing and telecommunications. His research is supported by a NSERC Discovery Grant and the Marcelle-Gauvreau ÉTS Research Chair in multimaterial and multifunctional photonic devices.